Cell signaling guides morphogenesis: Roles for Eph-Ephrin signaling in sea urchin morphogenesis.

by

Oliver A. Krupke
MSc, Brock University, 2000
BSc, Brock University, 1997

A Dissertation Submitted in Partial Fulfillment
of the Requirements for the Degree of

DOCTOR OF PHILOSOPHY

in the Department of Biochemistry and Microbiology

© Oliver Krupke, 2015
University of Victoria

All rights reserved. This dissertation may not be reproduced in whole or in part, by photocopy or other means, without the permission of the author.

Supervisory Committee

Cell signaling guides morphogenesis: Roles for Eph-Ephrin signaling in cell migration and shape change during sea urchin embryogenesis.

by

Oliver Krupke
MSc, Brock University, 2000
BSc, Brock University, 1997

Supervisory Committee

Robert D. Burke, Department of Biochemistry and Microbiology
Supervisor

Caren C. Helbing, Department of Biochemistry and Microbiology
Departmental Member

Perry Howard, Department of Biochemistry and Microbiology
Departmental Member

Bob Chow, Biology Department
Outside Member

Abstract

Supervisory Committee
Robert D. Burke, Department of Biochemistry and Microbiology
Supervisor
Caren C. Helbing, Department of Biochemistry and Microbiology
Departmental Member
Perry Howard, Department of Biochemistry and Microbiology
Departmental Member
Bob Chow, Biology Department
Outside Member

The role that signaling molecules play during morphogenesis and their interactions is a field of intense study and the sea urchin represents a facile system to study these aspects of development in the early embryo. In many instances, the *S. purpuratus* genome contains relatively simple receptor-ligand signaling systems compared to vertebrate counterparts and this provides interesting opportunities to study their diversity of function during the morphogenetic events that shape the embryo. The Eph-Ephrin signaling components are an excellent example of this and they are represented by dozens of members in the vertebrate system with developmental functions that include axon guidance, cell migration and tissue segregation. In contrast, the sea urchin genome contains a single Eph receptor and a single Ephrin ligand and by interacting with different effectors of signal transduction, this simple, bipartite system can fulfill a variety of functional roles during morphogenesis. Studying the function of Eph-Ephrin signaling in the sea urchin embryo, I have revealed two distinct morphogenetic movements in which Eph-Ephrin signaling is necessary; apical constriction of ciliary band cells and pigment cell migration. In both examples, a functionally relevant Ephrin gradient establishes spatial information in the developing tissues, producing a reaction from cells expressing the Eph receptor. In the case of pigment cells, the distribution of migrating cells is affected and in the case of ciliary band cells, apical constriction occurs. The different outcomes of Eph-Ephrin signaling in these two tissues exemplifies signaling components communicating spatial information and initiating morphogenetic programs with outcomes dependent on cellular context. Furthermore, I have identified downstream components of Eph-Ephrin signaling that have necessary functions in both models, illustrating how different cellular programs can be induced by the same signaling

components. My research contributes to understanding fundamental aspects of how complex 3 dimensional tissues arise from the genes and regulatory elements encoded in metazoan genomes.

Table of Contents

Supervisory Committee ii
Abstract iii
Table of Contents v
List of Abbreviations Used vii
List of Figures viii
List of Tables ix
Acknowledgments x
Dedication xi
Introduction 1
References 18
Chapter 1: Eph-Ephrin Signaling and Focal Adhesion Kinase Regulate Actomyosin-dependent Apical Constriction of Ciliary Band Cells 20
Summary 20
Introduction 21
Methods 23
Embryo culture and injection 23
Plasmids and reagents 23
Antibody production 23
Immunofluorescence microscopy 24
Cell surface area calculations 25
Relative intensity measurements 25
Statistical Analyses 26
Protein Affinity 26
Results 26
Apical surface area of ciliary band cells 26
Change in surface area in the absence of cell division 27
Actin cytoskeleton of the Ciliary Band 27
Ectodermal expression of Sp-Eph and Sp-Ephrin and interaction with FAK 34
Eph-Ephrin signaling is necessary for apical constriction 35
Ciliary-band-specific accumulation of $pY^{397}FAK$ is regulated by Eph-Ephrin signaling 42
Apical constriction requires Eph-Ephrin signaling and Phosphorylation of FAK 42
Planar Cell Polarity in Ciliary Band Cells 42
Discussion 50
References 51
Chapter 2: Eph-Ephrin and Semaphorin-Plexin-Rap1A are required for Mesenchyme to Epithelial Transition during innate immune cell development in the sea urchin larva. ... 55
Summary 55
Introduction 56
Methods 58
Results 60
Discussion 81

Supplementary Figures 85
References 91
Chapter 3: Future Directions 96
Chapter 4: Prospectus 102
Appendix 1: Imaging Neural Development in Embryonic and Larval Urchins 104
Summary 104
Introduction 104
Materials 106
Blastomere injection and double injection components 106
Immunological methods: Fixatives and components 109
Methods 110
Blastomere injections; double injections procedures 110
Procedures for combined in situ hybridization and immunofluorescence 112
Immunological Localization Methods 114
References 126

List of Abbreviations Used

aPKC – Atypical Protein Kinase C

BMP – Bone Morphogenetic Protein

EdU – 5-ethynyl-2'-deoxyuridine

EMT – Epithelial Mesenchymal Transition

FAK – Focal Adhesion Kinase

GPI – Glycophosphatidylinositol

Hnf – Hepatocyte Nuclear Factor

JNK – c-Jun N-terminal Kinase

MASO – Mopholino Antisense Oligonucleotide

MET – Mesenchymal Epithelial Transition

MLC – Myosin Light Chain

PEM – PIPES-EGTA-MgCl

PMC – Primary Mesenchyme Cell

SMC – Secondary Mesenchyme Cell

TGFβ - Transforming Growth Factor Beta

List of Figures

Figure 1 6
Figure 2 7
Figure 3 10
Figure 4 13
Figure 1.1 19
Figure 1.2 21
Figure 1.3 23
Figure 1.4 27
Figure 1.5 29
Figure 1.6 31
Figure 1.7 35
Figure 1.8 37
Figure 1.9 39
Figure 2.1 53
Figure 2.2 55
Figure 2.3 59
Figure 2.4 63
Figure 2.5 65
Figure 2.6 69
Figure 5 97
Figure 6 98

List of Tables

Table 1 17

Acknowledgments

I would like to thank the following people: My supervisor, Dr. Robert Burke for his guidance throughout this thesis and the creative environment he provides. My committee members, Dr.'s Robert Burke, Bob Chow, Caren Helbing and Perry Howard for their input and critique. Dr. Caroline Cameron for access to equipment. Dr. Andy Ransick for providing reagents, data and advice. All current and past members of the Burke lab for their help and support.

Dedication

To Kyla and Sophia:

For helping me experience the beauty of
human development.

Introduction

Combined with the control of cell growth and cellular differentiation, morphogenesis is one of the three fundamental aspects of developmental biology. Morphogenetic programs guide cell shape changes and movements that take place during embryogenesis and the successful embryo passes through these early growth stages in a perfectly orchestrated manner. Developmental biology studies these patterned processes to gain understanding of the cellular mechanisms used to move cells and cell sheets in an embryo and change their shape to form tissues and other specialized structures. Although the major movements that typify gastrulation involve folding and bending of cell sheets, particularly ectoderm and endoderm, all the three germ layers undergo massive cellular movements that help form the target tissues and these movements are generated by changes within individual cells.

The sea urchin provides perhaps the most facile model for producing and observing early embryos. In fact, much of our knowledge regarding the biochemical events of fertilization and fate specification during early cleavage has developed from observations made in the sea urchin (Rothschild and Swan, 1949; Cameron et al., 1987; Davidson et al., 1998). The simplicity of the sea urchin model has also provided an effective tool for studying the morphogenetic processes that shape the early embryo and some of the most detailed explanations of cellular and molecular processes driving basic morphogenetic movements have come from studies in urchin embryos (Rhumbler, 1902; Piston et al., 1998; Beane et al., 2006; Wu and McClay, 2007; Krupke and Burke, 2014). Furthermore, elaboration of the sea urchin gene regulatory network over the past decade has provided a detailed explanation of the genetic controls behind progression of

specification and spatial organisation of the sea urchin embryo and how these genetic elements interact with one another at specific developmental stages (Hinman and Davidson, 2007; Peter and Davidson, 2010; Ettensohn, 2013). Thus, the sea urchin model remains one of the most facile and tractable post-genomic models for early embryonic development.

The cellular movements that occur during embryogenesis can be categorized into those where movement or shape changes take place in a sheets of cells, as occurs during invagination, involution and convergent extension or those types where the movement or shape change may be seen in a single cell, as occurs during ingression. Although the latter typically involves single cells it is important to note that tens or even hundreds of cells in the embryo may synchronously undergo a specific type of movement such as ingression, producing a large population of cells destined for a particular fate. Revealing the communication and signaling mechanisms driving these synchronous cell shape changes and movements has been one of the major focuses of modern developmental biology and a number of well-characterized models have been put forward.

Among the most widely studied morphogenetic cues are receptor tyrosine kinase-based Eph-Ephrin signaling pathways. Often observed as a repulsion mechanism that serves to guide migrating cells, axons and to segregate cells in adjacent tissue domains (Poliakov et al., 2004), Eph-Ephrin signaling can also provide attractant cues to neurons (Kao et al., 2012). Furthermore, signaling can be bidirectional, with intracellular signaling pathways being activated downstream of the Eph receptor (forward signaling) or the Ephrin ligand (reverse signaling) (Kullander and Klein, 2002). In classic models where Eph-Ephrin signaling drives axon guidance and growth cone response, the Ephrin ligand typically

provides a repulsive cue to Eph-expressing neurons, signaling growth cone collapse in pathfinding axons (Sahin et al., 2005). In tissues that fit the model, graded expression of Ephrin is a feature of the extracellular matrix and neurons respond differentially to the morphogen gradient based on their Eph receptor complement (Klein, 2004). In these examples, cellular response to activation by Ephrin is typically achieved through tyrosine phosphorylation of effector proteins by the intracellular kinase domain of Eph. These effector proteins then modulate the activity of Rho family GTPases, thereby regulating cytoskeletal dynamics (Noren and Pasquale, 2004).

While axon guidance is the classic model for repulsion via Eph-Ephrin signaling, development of the vertebrate hindbrain provides a well-characterized example where repulsion and adhesion are simultaneously signalled by Eph-Ephrin interactions in differential cell populations. Eph and Ephrin can interact with other receptor ligand systems directly through *cis* interactions and indirectly through downstream effector interactions, adding a layer of complexity to transduction of Ephrin signals during morphogenesis (Klein, 2012). In the zebrafish model, reciprocal expression of Eph and Ephrin drives the segregation of progenitors that form rhombomeres and somites of the developing hindbrain (Batlle and Wilkinson, 2012). Interestingly, Eph-Ephrin signaling also functions in an adhesive role in this model; cells of the same cohort are stimulated by Eph-Ephrin signals to form adhesive contacts at boundaries. Combined with the repulsive cues provided by adjacent cohorts of cells, these Eph-Ephrin mediated signals are necessary in maintaining a tight cellular architecture and sharp borders during hindbrain development (Cooke et al., 2005).

In vertebrates, Eph-Ephrin signaling components have expanded and diversified and fulfill a range of specialized developmental roles (Mellott and Burke, 2008). Eph receptors are the largest subgroup of receptor tyrosine kinases and are subdivided into two subclasses, termed EphA and EphB based on their preference for binding the two Ephrin subclasses. Ephrin ligands have an extracellular binding domain, allowing them to bind and activate Eph receptors. In addition to activating Eph receptors to facilitate forward signaling, the Ephrin ligands are capable of reverse signaling. EphrinA ligands are GPI-anchored and lack intracellular domains, however their extracellular domains can interact with other trans-membrane co-receptors in *cis* to facilitate reverse signaling (Bonanomi et al., 2012). Ephrin B ligands have a transmembrane domain with intracellular domains that facilitate reverse signaling more directly using conserved tyrosine residues that are phosphorylated upon Eph-binding, and a C-terminal PDZ-binding domain that recruits proteins containing PDZ domains (Xu and Henkemeyer, 2012; Klein, 2012).

The complexity of Eph and Ephrin in the vertebrate genome contrasts starkly with their representation in the sea urchin genome, where we observe a single Eph receptor and a single Ephrin (Sodergren, 2006) and the simplicity of this model presents interesting opportunities. Binding of Ephrins to their respective Eph receptors is known to be promiscuous, with cross-reactivity reported (Himanen, 2004; Pasquale, 2008) and we now know that signaling through Eph-Ephrin requires the formation of receptor clusters containing other Eph receptors and other receptor ligand pairs (Himanen et al., 2010). The urchin embryo provides a simplified system where Ephrin can only interact with a single Eph receptor, possibly allowing more direct interpretation when dissecting the

contribution of Eph-Ephrin signaling to developmental roles. In vertebrates there exist both A-type and B-type Ephrins, categorized by their ability to bind to A or B type Eph receptors. A types Ephrins typically…. B type Ephrins are similar to A-type however they lack the extracellulardomains and instead possess a GPI (add abbreviation) anchor which links them to the cellular membrane (Kullander and Klein, 2002). are linked to the In the sea urchin both Eph and Ephrin (Figure 1) are classified as B type (Mellott and Burke, 2008). The Eph-Ephrin signaling pathway is well-described in vertebrates, with downstream influences that include but are not limited to effects on cellular proliferation, boundary formation, cytoskeletal dynamics and adhesion (Figure 2), however a role in echinoderms has not been described.

With the abundance of gene regulatory network information available in the sea urchin model, we now have the opportunity to link gene regulatory information to cell signaling pathways and observe downstream cytoskeletal and morphogenetic effects. Methods to visualize the actin cytoskeleton in the sea urchin are available, however the resolution and clarity of preservation provided by the fixation methods currently in use can be improved. An improved fixation procedure has been developed for visualizing cytoskeletal features in T51B rat liver cells using immunofluorescence and these appear amenable to sea urchin embryos and larvae (Vielkind and Swierenga, 1989). Developing these methods would benefit the sea urchin community, where visualization of cytoskeletal features by immunofluorescence is widely used in eggs up until fully developed larval stages (Bachman and McClay, 1995; Morris et al., 2006; Bonder et al., 2009; Krupke and Burke, 2014)

Eph and Ephrin in the urchin

Human	C. elegans	Drosophila	Urchin
14 Eph & 9 Ephrin	2 Eph & 4 Ephrin	4 Eph & 1 Ephrin	1 Eph & 1 Ephrin
A and B types	A and B types	B type only	B type only

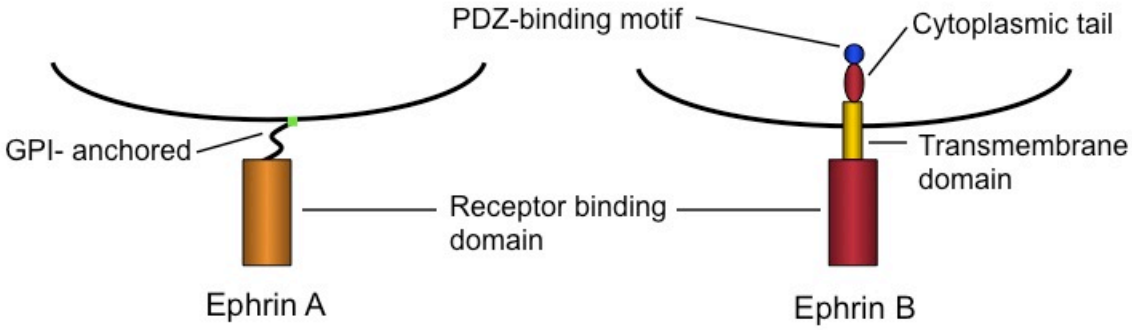

Figure 1: Sea urchin Eph and Ephrin in comparison to other model organisms and the domain structure of Ephrin A and B.

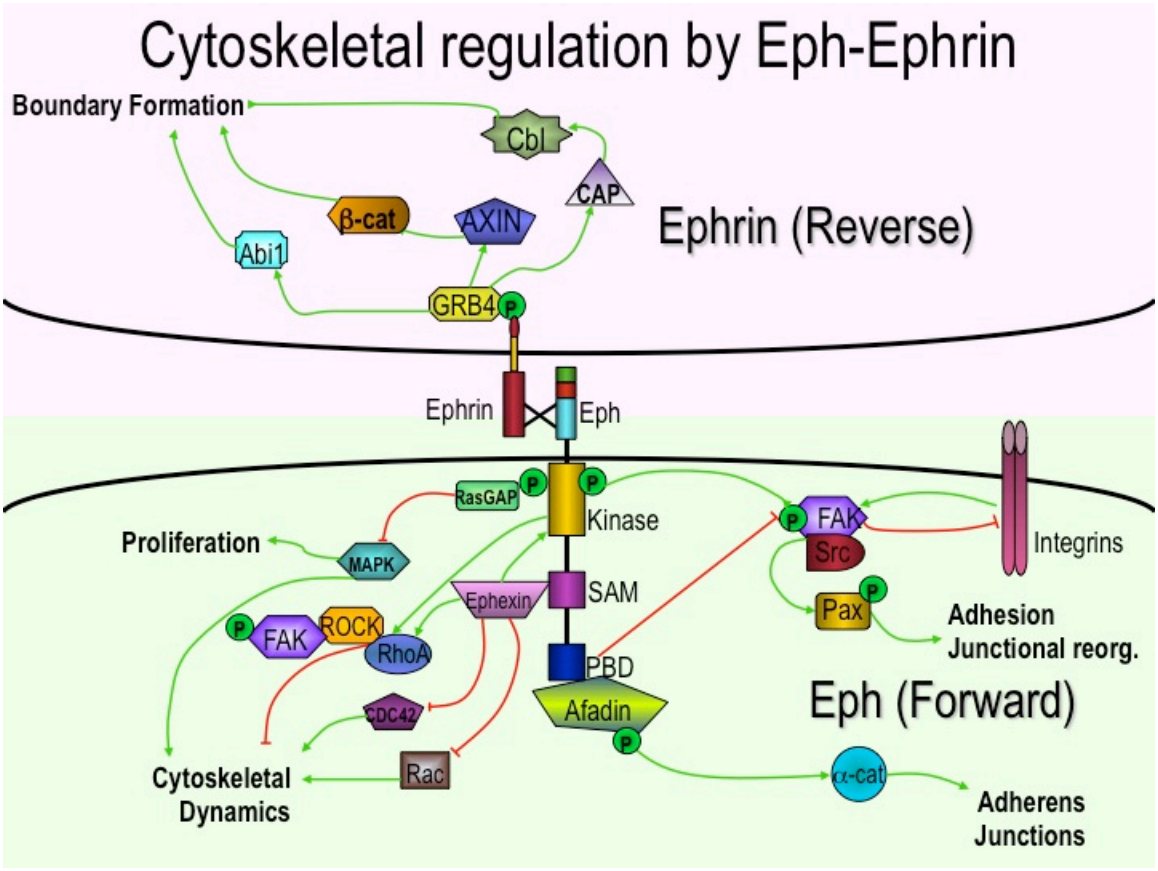

Figure 2: Signaling pathways described for Eph-Ephrin signaling in both forward and reverse directionalities.

Reverse signaling through EphrinA is known to occur via interactions with other transmembrane receptors, however there is a paucity of information regarding the developmental relevance and downstream effectors of these interactions (Holmberg et al., 2005; Coate et al., 2009; Bonanomi et al., 2012). The simplicity of the Eph-Ephrin signaling in the sea urchin model and ease with which embryos can be manipulated will allow exploration into the role of reverse EphrinA signaling during the shape changes that drive early embryogenesis.

Cell adhesion and linkage of the cytoskeleton to the cell membrane is tightly regulated during embryogenesis. Afadin is a scaffolding protein that has known signaling roles and studies have revealed the afadin/nectin complex as a strong candidate in mediating the linkage between the actin cytoskeleton and adherens junctions (Sawyer et al., 2009). Nectins bind to Afadin and these are members of the immunoglobulin superfamily and are a major component of adherens junctions (Takahashi et al., 1999). Afadin, also known as AF-6, is a large protein (>250kDa) containing actin binding, Ras association (RA), PDZ, dilute (DIL) and forkhead-associated (FHA) domains (Figure 3). Afadin can bind Nectin, β-catenin, ZO-1, Guanidine exchange factors, GTPase activating proteins, the small GTPases Ras and Rap1 and has recently been shown to bind Jagged-1; a Delta/Serrate/LAG-2 (DSL) protein (Ikeda et al., 1999; Radziwill et al., 2003; Su et al., 2003; Wei et al., 2005; Miyata et al., 2009; Ooshio et al, 2010). One of the more intriguing features of this large protein are two regions (FHA and DIL) that share homology with kinesin and myosin motor domains (Ponting, 1995). Aside from Afadin homologues in other species, the region spanning amino acids 365-452 of SpAfadin shows homology to kinesin motor domains, particularly the U104 domain found in to

UNC104 subfamily, suggesting that this functional domain is involved in protein-protein interactions regulated by phosphorylation (Westerholm-Parvinen et al., 2000). The DIL region shares homology to class-Va Myosins although the significance of this domain and its function are unknown.

All of these features of Afadin indicate it as a useful marker for cell-cell junctions that has both structural and regulatory roles. Studies of the Drosophila Afadin homologue, Canoe have led to significant discoveries in the field of cytoskeletal regulation highlighting the important role Afadin has in linking the plasma membrane and actin cytoskeleton (Sawyer et al., 2009a) during cell shape changes and movements. The main binding partner for the two RA domains is Rap1; a highly conserved regulator of cell polarity, adhesion and matrix interactions that has been shown to act through other effector molecules to influence the actin cytoskeleton and adhesion molecules (Knox and Brown, 2002; Boerrner et al., 2003; Boettner and VanAelst, 2009). Recent work by Sawyer et al. (2009a) describes a regulatory role for Canoe in linking adherens junctions to the actin cytoskeleton during apical constriction. In this work, Canoe mutant embryos are shown to improperly internalise mesoderm precursor cells through a failure in apical constriction during ventral furrow formation. Microscopic investigation illustrates that the actomyosin network is not contiguous with the apical surfaces of ventral furrow cells in mutant embryos and these cells fail to undergo apical constriction properly. As a result, mesodermal cells do not internalise, leading to disruption of the ventral epithelium and mortality.

For over 100 years the sea urchin embryo has been a primary tool in studying signaling phenomena that result in cell remodeling, the initiation of primary invagination

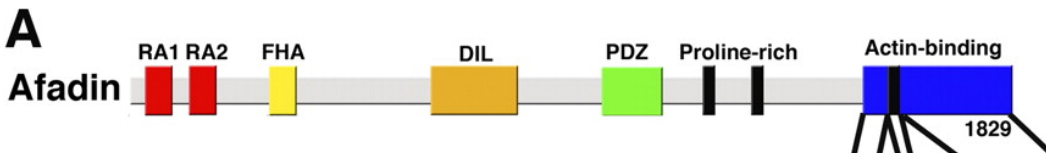

Figure 3: Domain structure of Afadin

and subsequent formation of the archenteron (Rhumbler, 1902; Hörstadius, 1937). Apical constriction has also been studied using the sea urchin larva. Bottle cells undergo apical constriction and these cells are likely derivatives of the mesenchyme cells and their loss delays initiation of primary invagination (Keller, 1981; Kimberly and Hardin, 1998). Signaling by micromeres occurs at least in part through the expression of paired-class micromere anti-repressor 1 (pmar1), a transcription factor that is thought to represses a repressor of genes required for the EMT pathway (Oliveri et al., 2002). The most well-studied gene in this gene regulatory network (GRN) is delta. The Delta protein is a membrane-bound ligand for that activates Notch signaling. The dynamics of this signaling in specifying cell fate in the vegetal plate are being revealed in the sea urchin (Smith and Davidson, 2008; Croce and McClay, 2010). Delta knockdown experiments illustrate that this protein has significant roles in apical constriction, ingression of mesenchyme cells and in primary invagination, however the effect of this signaling pathway on Afadin function at the onset of AC in bottle cells has not been explored.

A distinguishing characteristic gastrulation in the urchin embryo is the formation of bottle cells, marking the first visible occurrence of significant and dramatic changes in cell shape during development. This phenotype is a direct consequence of AC and the transparent, easily cultured, manipulated and observed sea urchin embryo provides a wonderful opportunity to study the regulation of this phenomenon. Afadin is found in the apical complex during a variety of cellular movements and is thought to act through transient, weak interactions with many adherens junction proteins (Takai et al., 2008). Recent work suggests Afadin couples AJs to the cytoskeleton (Sawyer et al., 2009a), regulates Ras-like GTPases during cellular movements (Miyata et al., 2009, Severson et

al., 2009) and binds signaling components (Ooshio et al., 2010) that are present at the vegetal pole during bottle cell formation (Sweet et al., 2002), with important roles in apical constriction and other cell movements, including EMT.

Epithelial mesenchymal transitions (EMTs) are widely used throughout life and widely studied for their roles in early embryogenesis. The sea urchin embryo is has proven an excellent model for dissecting details of epithelial mesenchyme transition during primary and secondary mesenchyme cell specification and more recently, abundant GRN information is detailing the genetic expression dynamics that drive this complex developmental process (Saunders and McClay, 2014). Although it was first described in early embryogenesis, EMTs are widely used throughout life are critical to organogenesis, cancer metastasis and wound healing (Yang and Weinberg, 2008). While complex, the three dimensional cellular shape changes that occur during morphogenesis are produced using a limited number of established cellular processes including: Loss of apical polarity, apical constriction, breaking of adherens junctions, remodelling of cytoskeleton, loss of cell adhesion and increased motility (Shook and Keller, 2003; Pilot and Lecuit, 2005; Levayer and Lecuit, 2008; Thiery et al., 2009).

Compared to the widely studied field of EMT, the reversal of these cellular traits that occurs during mesenchymal epithelial transition (MET) has not been well defined (Figure 4). It is clear that MET has an important role in organ development and the best examples are provided by nephrogenesis (Davies, 1996; Boyle et al., 2011), although MET is also critical in somitogenesis (Nakaya et al., 2004), cardiogenesis (Nakajima et al., 2000), and hepatogenesis (Li et al., 2011). These examples of MET involve a closely associated group of mesenchyme cells that give rise to an epithelium. However, there is

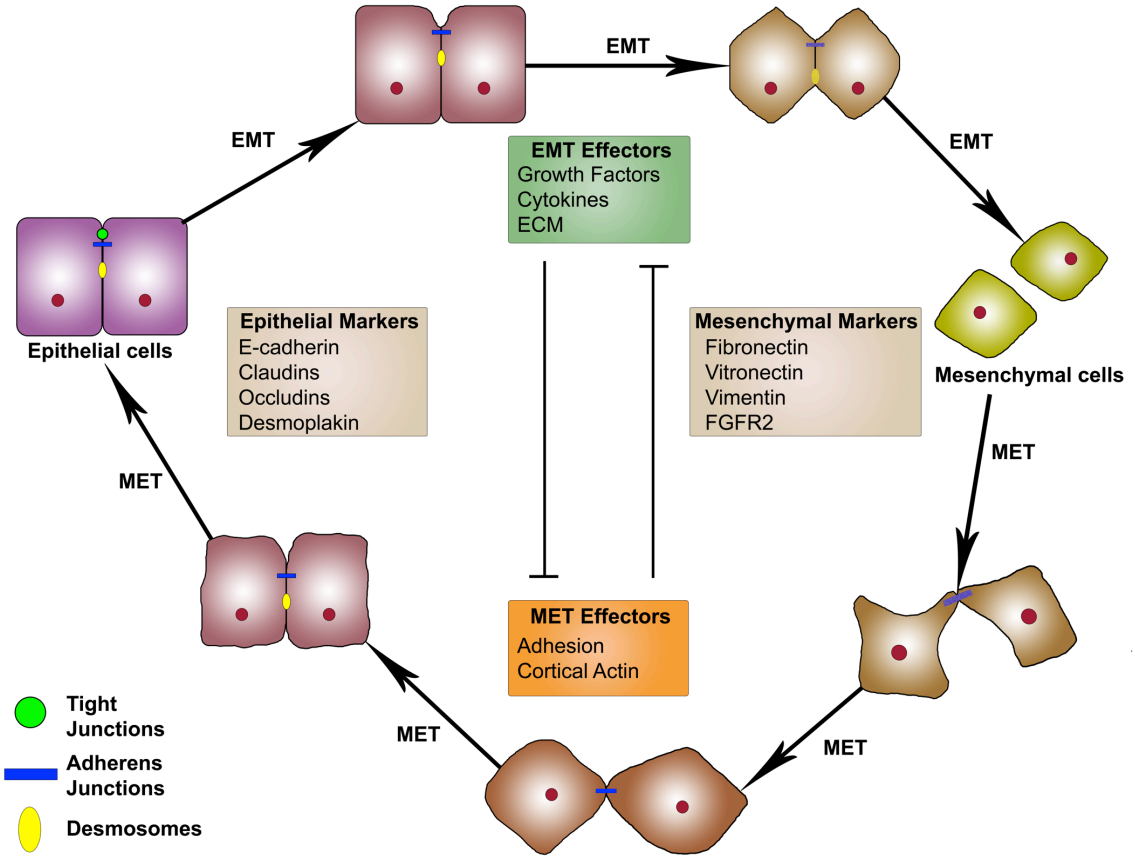

Figure 4: Mechanisms, effectors, and markers described for both EMT and MET.

another category of MET, wherein single cells undergo MET to join an already existing epithelium and although this type of MET is far less studied, it is an important in the development of many neural crest derivatives including stem cells (Pinnamaneni and Funderburgh, 2012; Høffding and Hyttel, 2015), mesenchyme-derived pigment cells/melanocytes (Gibson and Burke, 1983; Cichorek et al., 2013), lymphocytes (Hieronymus et al., 2014), and metastatic cells (Thiery and Sleeman, 2006).. Although there are some tissue-specific differences, the physical changes observed in cells undergoing MET typically involve enrichment or activation of epithelial-specific genes and downregulation of mesenchyme-specific genes (Rowton et al., 2013). These changes revert the cell to an epithelial morphology, however our current understanding of the molecular signals that drive MET indicate that the process is not simply a reversal of the signals that guide EMT and that the signaling events driving MET are often tissue-specific (Chaffer et al., 2007). One consistent feature is the role of signals from epithelial neighbours and epithelial-mesenchymal communication and interactions appear to drive local changes, allowing mesenchyme cells to enter the epithelium (Campbell et al., 2010).

Beginning just prior to gastrulation, the first examples of EMT in *S. purpuratus* involve specified cells of the vegetal plate, the primary and secondary mesenchyme cells, that ingress into the blastocoel in a stereotypic manner. The primary mesenchyme cells (PMCs) ingress first and are often referred to as skeletogenic mesenchyme since they are the exclusive progenitors of cells that eventually secrete the larval skeleton (Decker and Lennarz, 1988). The secondary mesenchyme cells (SMCs) ingress after the PMCs and many of these remain in the blastocoel to take on a variety of immune and fibroblast-like roles (Tamboline and Burke, 1992). A subpopulation of SMCs, the pigment cells, has a

different immune fate; they re-enter the embryonic epithelium, undergoing MET as they invade and intercalate with aboral ectoderm (Gibson and Burke, 1983). These cells are of particular interest because they may provide a tractable model to study the mechanisms that accompany MET when a single cell joins an existing epithelium.

In addition to providing insight into developmental mechanisms, the study of MET has an important application to the study of cancer metastasis. Accumulating evidence illustrates an EMT-like process as one of the main mechansisms whereby cancer cells metastasize and move to other locations in the body and more recently, the reverse process of MET has been shown as a mechanisms for the formation of secondary tumours and metastatic colonisation in breast cancer (Gunasinghe et al., 2012). This highlights the importance of understanding the mechanisms involved during this process, particularly when a single cell joins an epithelium, as seen in cancer metastasis and the sea urchin embryo provides an excellent model to study this.

In this thesis, I attempt to characterise the role of Eph-Ephrin signaling in early sea urchin development using immunofluorescent (see Table 1 for a list of antibodies) confocal microscopy and image analysis. Chapter 1 focuses on Eph-Ephrin signaling during ciliary band formation, identifying downstream effectors in this signaling cascade and how they impinge on the cytoskeleton to effect shape changes. The overall aim of Chapter 1 is to developing a model describing the signaling mechanisms that are critical to ciliary band formation. Chapter 2 focuses on the role of Eph-Ephrin signaling during pigment cell development, from post-EMT migration to differentiation in the ectoderm. The overall aim of Chapter 2 is to develop a model describing the signaling mechanisms necessary for guiding pigment cells to the ectoderm and for initiating MET. Appendix 1

focuses on developing methods for improved visualization of cytoskeletal components of cells in the developing urchin embryo.

Oliver A. Krupke developed materials, concepts and approaches, performed experiments, analyzed data, and prepared thesis. Robert D. Burke developed concepts, approaches, analyzed data and edited thesis. For Chapter 2, Jenna Reis developed Sema1A antibody, DNA constructs for microinjection and helped prepare images.

Table 1: List of Antibodies used

Antigen	Host Species	Source	Dilution	Fixative
Eph	Rat	In house	1:500	MeOH
pEph	Mouse	Abcam Ab62256	1:2000	MeOH
Ephrin	Mouse MAb sup	In house	1:2	PEM
pFAK	Rabbit MAb	Santa Cruz sc1176	1:2000	MeOH
Afadin	Rat PAs	In house	1:1000	MeOH
Rap1A	Rabbit MAb	Abcam ab75871	1:200	MeOH
Rap1A-GTP	Mouse MAb	NewEast 26912	1:200	PFA
Sp1	Mouse MAb asc	In house	1:1000	MeOH
Semaphorin	Rat PAs	In house	1:800	MeOH
Plexin	Rat PAs	In house	1:300	MeOH
Hnf6	Rat PAs	In house	1:800	PEM
Caspase-3	Rabbit MAb	Cell Signal 9661	1:300	MeOH
aPKC	Rabbit MAb	SantaCruz sc216	1:250	MeOH
pMyo	Mouse MAb	Cell Signal 3675	1:200	PEM

References

Boyle, S.C., Kim, M., Valerius, M.T., McMahon, A.P., and Kopan, R. (2011). Notch pathway activation can replace the requirement for Wnt4 and Wnt9b in mesenchymal-to-epithelial transition of nephron stem cells. Development **138**: 4245-54.

Campbell, K., Casanova, J., and Skaer, H. (2010). Mesenchymal-to-epithelial transition of intercalating cells in Drosophila renal tubules depends on polarity cues from epithelial neighbours. Mech. Dev. **127**:345-57.

Chaffer, C.L., Thompson, E.W., and Williams, E.D. (2007). Mesenchymal to epithelial transition in development and disease. Cells Tissues Organs. **185**:7-19.

Cichorek, M., Wachulska, M., Stasiewicz, A., and Tymińska, A. (2013). Skin melanocytes: biology and development. Postepy Dermatol Alergol. **30**(1): 30-41..

Chiu, S.T., Chang, K.J., Ting, C.H., Shen, H.C., Li, H., and Hsieh, F.J. (2009). Over-expression of EphB3 enhances cell-cell contacts and suppresses tumor growth in HT-29 human colon cancer cells. Carcinogenesis **30**: 1475-86.

Davies, J.A. (1996). Mesenchyme to epithelium transition during development of the mammalian kidney tubule. Acta Anat. **156**: 187–201.

Decker, G.L., and Lennarz, W.J. (1988). Skeletogenesis in the sea urchin embryo. Development **103**(2): 231–247.

Gunasinghe, N.P., Wells, A., Thompson, E.W., and Hugo H.J. (2012). Mesenchymal-epithelial transition (MET) as a mechanism for metastatic colonisation in breast cancer. Cancer Metastasis Rev. 31: 469-78.

Høffding, M.K., and Hyttel, P. (2015). Ultrastructural visualization of the Mesenchymal-to-Epithelial Transition during reprogramming of human fibroblasts to induced pluripotent stem cells. Stem Cell Res. 2015 **14**(1): 39-53.

Li, B., Zheng, Y.W., Sano, Y., and Taniguchi, H. (2011). Evidence for mesenchymal-epithelial transition associated with mouse hepatic stem cell differentiation. PLoS ONE **6**: e17092.

Nakaya, Y., Kuroda, S., Katagiri, Y.T., Kaibuchi, K., and Takahashi, Y. (2004). Mesenchymal-epithelial transition during somitic segmentation is regulated by differential roles of Cdc42 and Rac1. Dev. Cell **7**: 425–38.

Nakajima, Y., Yamagishi, T., Hokari, S., and Nakamura, H. (2000). Mechanisms involved in valvuloseptal endocardial cushion formation in early cardiogenesis: roles of

transforming growth factor (TGF)-beta and bone morphogenetic protein (BMP). Anat. Rec. **258**: 119–27.

Pinnamaneni, N., and Funderburgh, J.L. (2012). Concise review: Stem cells in the corneal stroma. Stem Cells **30**(6):1059-63.

Piston, D.W., Summers, R.G., Knobel, S.M., and Morrill, J.B. (1998). Characterization of Involution during Sea Urchin Gastrulation Using Two-Photon Excited Photorelease and Confocal Microscopy. Microsc. Microanal. **4**(4):404-414.

Rowton, M., Ramos, P., Anderson, D.M., Rhee, J.M., Cunliffe, H.E., and Rawls, A. (2013). Regulation of mesenchymal-to-epithelial transition by PARAXIS during somitogenesis. Dev. Dyn. **242**: 1332-44.

Thiery, J.P., and Sleeman, J.P. (2006). Complex networks orchestrate epithelial-mesenchymal transitions. Nat. Rev. Mol. Cell Biol. **7**:131-42.

Chapter 1: Eph-Ephrin Signaling and Focal Adhesion Kinase Regulate Actomyosin-dependent Apical Constriction of Ciliary Band Cells.

Krupke OA, Burke RD. (2014). Eph-Ephrin signaling and focal adhesion kinase regulate actomyosin-dependent apical constriction of ciliary band cells. Development **141**: 1075-84.

Summary

Apical constriction typically accompanies inward folding of an epithelial sheet. In recent years there has been progress in understanding mechanisms of apical constriction and their contribution to morphogenetic processes. Sea urchin embryos form a specialized region of ectoderm, the ciliary band, which is a strip of epithelium, 3-5 cells wide, encircling the oral ectoderm and functioning in larval swimming and feeding. Ciliary band cells exhibit distinctive apical-basal elongation, have narrow apices bearing a cilium, and are planar polarized, so that cilia beat away from the mouth. Here we show filamentous actin and phosphorylated myosin light chain are uniquely distributed in ciliary band cells. Inhibition of myosin phosphorylation or actin polymerization perturbes this distribution and blocks apical constriction. During ciliary band formation, Sp-Ephrin and Sp-Eph expression overlap in the presumptive ciliary band. Knockdown of Sp-Eph or Sp-Ephrin, or treatment with an Eph kinase inhibitor interferes with actomyosin networks, accumulation of pY^{397}FAK, and apical constriction. The cytoplasmic domain of Sp-Eph, fused to GST and containing a single amino acid substitution reported as kinase dead, will pull down pY^{397}FAK from embryo lysates. As well, pY^{397}FAK colocalizes with Sp-Eph in a JNK-dependent, planar polarized manner on latitudinal apical junctions of the ciliary band and this polarization is dissociable from apical constriction. We propose Sp-Eph and pY^{397}FAK function together in an apical complex that is necessary for remodelling actomyosin to produce centripetal forces causing apical constriction. Morphogenesis of ciliary band cells is a unique example of apical constriction where receptor-mediated cell shape change produces a strip of specialized tissue without an accompanying folding of epithelium.

Introduction

Apical constriction is a cellular shape change that reduces apical surface area, producing bottle-shaped cells. This process is fundamental to morphogenetic movements of cells and cellular sheets that are integral to embryogenesis. It occurs co-ordinately in specific cell groups and is critical to events such as gastrulation (Sweeton et al., 1991), neurulation (Nagele and Lee, 1987), or formation of specialized epithelia (Pilot and Lecuit, 2005; Sawyer et al., 2010). The mechanisms for achieving apical constriction appear to vary between organisms and even cell types within an organism (Sawyer et al. 2010), therefore characterizing these complex regulatory mechanisms is critical in developing a generalized understanding of morphogenesis.

It is widely accepted that actin filaments interact with myosin II motor units to provide mechanical force for apical constriction and live imaging reveals concomitant organizational changes of actomyosin networks in apically constricting cells (Hildebrand, 2005; Lee and Harland, 2007). One of the most elaborate models for apical constriction occurs during *Drosophila* ventral furrow formation where the process is coordinated by a subcellular, ratcheting mechanism that produces a series of local, pulsed contractions in the supracellular, actomyosin meshwork; incrementally reducing apical surface area (Martin et al., 2009). While constriction of the apical surface occurs in pulses, contraction and cortical tension within the actomyosin network occur prior to, and in the absence of, apical surface area reduction. This implies a regulatory mechanism controlling transient linkage of tensioned actomyosin networks to contact zones on the membrane surface (Roh-Johnson et al., 2012).

Echinoderm embryos have a distinctive ectodermal structure, the ciliary band. This region is a continuous, 3-5 cell wide, band of cells encircling the oral field and forming a boundary between oral and aboral ectoderm. The ciliary band, like most ectoderm, is specified in late cleavage as a consequence of TGFβ signaling (Angerer et al., 2000; Duboc et al., 2004). Nodal is expressed ventrally and establishes oral ectoderm while BMP2/4, also expressed ventrally, acts with BMP5/8 to specify aboral ectoderm (Lapraz et al., 2009; Ben-Tabou de Leon et al. 2013). A band of cells between the major ectoderm domains is protected from this signaling and adopts the default state of becoming ciliary band ectoderm (Saudemont et al. 2010; Bradham et al. 2009; Yaguchi et

al. 2010). The presumptive ciliary band cells are distinguished by expression of Hnf6, a putative core element of the gene regulatory network that specifies ciliary band cells (Otim et al. 2009; Poustka et al. 2009). Each ciliary band cell bears a cilium and their coordinated action provides feeding and locomotory functions for the larva (Strathmann, 1971; Strathmann et al., 1972). The cilia normally beat with their power stroke directed away from the oral field (Strathmann, 2007) and are functionally polarized in the plane of the epithelium. In *S. purpuratus*, the ciliary band is first apparent at ~60 hours of development (Strathmann, 1971) when cells apparently reduce their apical surface area and become bottle-shaped (Burke, 1978). The mechanism of this shape change has not been explored.

The Eph receptor tyrosine kinases and their Ephrin ligands constitute the largest class of receptor tyrosine kinases in vertebrates. They are cell-surface molecules with roles in diverse biological processes, though they typically function at the interface of patterning and morphogenesis. Eph and Ephrin function in adhesion and regulate cytoskeletal organization by influencing regulatory protein complexes (Wilkinson, 2000; Klein, 2012). These include interaction with focal adhesion kinase (FAK) (Carter et al., 2002), a non-receptor tyrosine kinase that regulates many cellular functions that has long been identified as a cytoskeletal regulator (Arold, 2011). Recent data describes FAK as an effector of Eph-Ephrin signaling, remodelling cytoskeleton through recruitment and activation of Src-family kinases (Thomas, 1998; Parri et al., 2007; Shi et al., 2009; Darie et al., 2011).

Here, we describe ciliary band morphogenesis in the developing sea urchin embryo. The ciliary band forms in the embryonic region where ectodermal expression domains of Eph and Ephrin overlap. We show apical constriction is independent of cell division and loss-of-function experiments indicate that actin, myosin, Eph-Ephrin, and FAK, are necessary for apical constriction. We propose that Eph-Ephrin signaling in the ciliary band provides a proximate cue initiating formation of a planar polarized, FAK-containing complex that regulates of apical constriction in ciliary band cells. Apical constriction of ciliary band cells is a distinctive model in which there is no inward folding of epithelium.

Methods

Embryo culture and injection

Eggs and sperm were collected from *S. purpuratus* adults induced to spawn with 0.55 M KCl or by shaking and/or gentle prodding. Sperm was diluted 1:1000 in filtered seawater prior to fertilization and embryos were grown at 14°C. Unless otherwise mentioned, inhibitors were added 48 hours post fertilization. Eggs were prepared for microinjection as described previously (Krupke et al., 2013). Injection solutions containing 22.5% glycerol, either RhodamineB-dextran (Sigma, R9379) or Fluorescein isothiocyanate-dextran (Sigma, 46945) and RNA were microfiltered at 5,000 X G for 1 minute using 0.22 μm Ultrafree centrifugal filters (Millepore). Morpholino antisense oligonucleotides were obtained from GeneTools and injected as previously described (Krupke et al., 2013).

Plasmids and reagents

Oligonucleotide DNA primers were obtained from Operon. Sequences encoding full-length Sp-Ephrin and Sp-Eph were obtained via PCR from cDNA isolated from 72 hour *S. purpuratus* embryos and cloned using standard methods. Morpholino antisense oligonucleotides were obtained from GeneTools. EphrinMO1: 5'-AAATTTAGTCCTGGAAAGATGAGAC-3'. EphrinMO2: 5'CTCCAGGGTCAAAGTGCTCAGGTAT-3'. EphMO1: 5'ATTGGAAAGAGTAAATCCGAGATGT-3'. EphMO2: 5'AAATAAGTCATTCTCTCCTCTCCGT-3'. ControlMO: 5'GAATGAAACTGTCCTTATCCATCA-3'. Inhibitors (Tocris Biosciences) were used as follows: 50 mM c-Jun peptide (Cat. No. 1989), 20 μM cytochalasin D (Cat. No. 1233), 5 μM ML 7 (Cat. No. 4310), 1.75 μM NVP BHG 712 (NVP, Cat. No. 4405), 10 μM PF 573228 (PF573, Cat. No. 3239).

Antibody production

Proteins were produced using pET28a vector (Novagen) for expression of 6XHis tagged proteins. The C-terminal half of Sp-Eph (aa 447-746) and the N-terminus of Sp-Ephrin (aa 28-169) were amplified by PCR, cloned into pET28a and protein expression was induced in *E. coli* using standard protocols. Bacterial lysate was prepared using

BugBuster (Novagen) and protein was solubilized in binding buffer (6 M guanidine HCl, 0.5 M NaCl, 100 mM Na_2HPO_4, 100mM NaH_2PO_4, 10 mM imidazole, 10 mM Tris, 1 mM 2-mercaptoethanol, pH 8.0) prior to affinity purification by immobilized metal ion affinity chromatography (IMAC) using Chelex 100 Resin (Bio-Rad). Proteins were purified by size exclusion on Hi Load 16/60 Superdex 75 prep grade column (GE Healthcare, Mississauga, Ontario, Canada) using the ÄKTA prime plus system (GE Healthcare, Mississauga, Ontario, Canada). Purified protein was concentrated and dialyzed in PBS and mixed with Freund's complete adjuvant (Sigma) for initial immunization or with Freund's incomplete adjuvant (Sigma) for booster immunizations at a 1:1 ratio. Animals were immunized and housed at the University of Victoria Animal Care Facility. Immunization via subcutaneous injection included 100 µg antigen in 250 µl total volume at 0 days, 21 days and 42 days. Terminal bleed via cardiac puncture was performed at 52-56 days. Blood samples were incubated for 45 minutes at 37°C and placed at 4°C overnight. Clots were centrifuged at 1,000 X G, serum collected and sodium azide (Sigma) added to a final concentration of 0.02% w/v. Antibody specificity was confirmed by western blot against antigen and subsequently against an embryonic lysate. Anti-Sp-Ephrin mouse serum recognized a doublet typical of Ephrin antibody at 38 and 42 kDa, corresponding to the approximate weight of native Ephrin protein. Mice were then used to produce an Sp-Ephrin monoclonal antibody (4D2) according to previous methods (Loveless et al. 2011) and this recognises bands at approximately 38 and 42 kDa. Anti-Sp-Eph rat serum recognizes a single band at approximately 110kDa, corresponding to the predicted molecular weight of native Sp-Eph protein.

Immunofluorescence microscopy

S. purpuratus embryos were fixed for 5 minutes in PEM buffer (Vielkind and Swierenga, 1989) or ice-cold methanol. Embryos were washed with PBS and probed with primary antibody diluted in SuperBlock (Thermo). Primary antibodies: atypical protein kinase C ζ (aPKC, 1:300, Santa Cruz), Sp-Ephrin (1:2, 4D2 supernatant), Sp-Eph (1:500, serum), Sp-Hnf6 (Yaguchi et al. 2010) (1:700, serum), pY^{397}FAK (1:2000, Invitrogen), pY^{379}Eph (1:3000, Abcam), Phalloidin-Alexa633 (1:300, Invitrogen), pS^{19}myosin light chain II (pS^{19}MLC, 1:200, Cell Signaling Technology). Embryos were washed three times with PBS and visualized with Alexa Fluor secondary

antibodies (Invitrogen) on a Zeiss 700 LSM (Carl Zeiss) confocal microscope.

Contribution of cell division to apical constriction in ciliary band ectoderm was assessed by adding DMSO or 0.6 μM aphidicolin (Sigma, A0781) with 1 μM EdU (5-ethynyl-2´-deoxyuridine) to sea water at 60 h. Following fixation, EdU incorporation was detected using Click-IT detection kit (Life Technologies, C10340) according to manufacturers direction.

All immunofluorescent images are maximum intensity projections of whole mounted, sea urchin larvae oriented with oral ectoderm at top and aboral ectoderm at bottom. Insets were chosen randomly in an area of ciliary band ectoderm or chosen to highlight typical defects observed with treatments. Images used for data analyses are maximum intensity projections that extend from the cell surface to a 3-4 μm depth for cell shape (anti-aPKC) and 7 μm for all cytoskeleton (pSer^{19}Myosin and Phalloidin). Optimal gain, pinhole diameter and laser intensity settings were established for each antibody/ fluorophore combination and settings were re-used consistently. Imaging and analysis was conducted using ZEN software (Carl Zeiss). Adobe Photoshop was used for cropping and assembling figures and to adjust image contrast and brightness.

Cell surface area calculations

For surface area measurements, anti-aPKC was used to visualize apical cell membranes and ciliary band cells were identified using the ciliary-band-specific marker, anti-Hnf6. Apical membranes were outlined and cell surface area was calculated using ZEN software. Surface area values were exported to Microsoft Excel for further analysis.

Relative intensity measurements

Images were quantified using ZEN software and areas of interest selected by encircling them (when comparing intensity in ciliary band and aboral ectoderm) or by drawing a 5 pixel width line along the structure of interest (when comparing latitudinal and longitudinal expression). Dark pixels and saturated pixels were excluded in relative intensity measurements. Data sets were collected as intensity values per pixel within or along the region of interest and exported into Microsoft Excel for further analysis.

Statistical Analyses

Grouped data were analyzed using a one-way ANOVA and the p-value for each comparison is reported.

Protein Affinity

Ectodermal cells were isolated from embryos at 72 hours (McClay and Marchase, 1979) for preparation of ectodermal cell lysate. Lysate was clarified by ultracentrifugation (4°C, 10 minutes, 100,000 X G) and protein quantified by Bradford analysis. Full-length Sp-Eph and the cytoplasmic portion (aa 322-762) of a kinase-dead Sp-Eph, SpEphKD[K445R], were cloned into pGEX4T-1 to create GST fusions and transformed into *E. coli* BL21 for expression using standard protocols. Cells were harvested by centrifugation (4 °C, 15 minutes, 12,000 X G), resuspended in ice-cold lysis buffer (25 mM Tris-HCl pH 7.6, 150 mM NaCl, 1 mM EDTA, 1% v/v Triton X-100, 5% v/v glycerol, 0.03% w/v SDS, 1 mM DTT, 1 mM NaF, 1 mM sodium orthovanadate, 1 mM PMSF, 8 μM leupeptin, 1.5 μM pepstatin, 0.3 μM aprotinin) and lysed by sonication at 4 °C. Lysate was clarified by ultracentrifugation (4 °C, 10 minutes, 100,000 X G) and protein was quantified by Bradford analysis. Fusion protein lysate was incubated for 30 min. at 4 °C with glutathione-agarose at a rate of 35 mg/ml wet resin. Resin was washed with 3 volumes lysis buffer and ectodermal lysate was added at 35 mg/ml wet beads and incubated at 4 °C for 1 hour with rocking. Beads were washed with 3 volumes lysis buffer and proteins eluted with two 0.5 volume additions of elution buffer (5 mM reduced glutathione, 50 mM Tris-HCl, pH 9.0).

SDS-PAGE used 12% polyacrylamide resolving gels with 5% stacking gel in Mini-protean TetraCell (Bio-Rad, Mississauga, Ontario, Canada) for 50 min. at 200 V in standard running buffer. Proteins were blotted onto PVDF membrane in standard transfer buffer for 1 hour using Genie Blotter (Idea Scientific, Minneapolis, Minnesota, U.S.A.). Blots were probed with anti-GST (1:5000, Cedarlane) and anti-pFAK[pY397] (1:1000, Invitrogen). Infrared detection of secondary antibodies (Rockland) was done on an Odyssey Imager (Li-Cor Biosciences, Lincoln, Nebraska, U.S.A.) and images were adjusted for brightness and contrast using Photoshop.

Results

Apical surface area of ciliary band cells

The shape of ciliary band cells suggests apical constriction may be a feature of

their development and we asked whether apical surface area of ciliary band cells decreases during ciliary band formation. Between 48 and 96 hours the ectoderm is transformed from a uniform sheet of cells into clearly defined regions of oral, aboral and ciliary band (Fig. 1). At 48 hours there is no measureable difference in surface area between ciliary band cells and non-ciliary band cells (Fig 1A'',E). At 55 hours, Hnf6 positive cells have a noticeable reduction in their surface area (not shown). Over the next 17 hours the surface area of ciliary band cells is reduced by roughly one half; the majority of this occurring between 60 and 72 hours (Fig. 1A'',B'', Fig. 1E). Reduction in surface area is largely completed after 96 hours (Fig. 1D''). When viewed in cross-section, ciliary band cells change their shape from having almost equal width and depth (Fig. 1F) to bottle-shaped (Fig. 1F'). This shape change appears to be an important event in ciliary band formation and we focused on identifying the underlying mechanism.

Change in surface area in the absence of cell division

To assess whether reduction in apical surface area of ciliary band cells is due to localized cytokinesis, we inhibited DNA polymerase at 60 hours using aphidicolin and cultured embryos in the presence of EdU to label newly synthesized DNA and confirm inhibition of cytokinesis as an indirect effect. After 72 hours development, ciliary band cells in control embryos reduce their apical surface area (Fig 2A') and incorporate EdU into their nuclei (Fig. 2A), indicating DNA synthesis and subsequent cell division. Although aphidicolin completely blocks DNA synthesis (Fig. 2B) and indirectly prevents cytokinesis, ciliary band cells in treated embryos also appear to apically constrict (Fig. 2B'). Apical surface area measurements of ciliary band cells in embryos with cell division blocked and control embryos are not significantly different ($p= 0.062$) (Fig. 2C), indicating that reduction of apical surface area occurs independently of cytokinesis.

Actin cytoskeleton of the Ciliary Band

At 35 hours, actin and $pS^{19}MLC$ are distributed uniformly around the apical margin of ciliary band cells and colocalize with apical junction components (Fig. 3A-A'''). Beginning at about 40 hours, actin and $pS^{19}MLC$ are not associated solely with cell junctions (Fig. 3B-B'') but are distributed throughout the apical cortex of ciliary band cells. At 72 hours, $pS^{19}MLC$ is in discontinuous patches at the cell periphery and actin is dispersed in strands and patches in the apical cortex of ciliary band cells (Fig. 3C-C''), suggesting a role during apical surface area reduction of ciliary band cells.

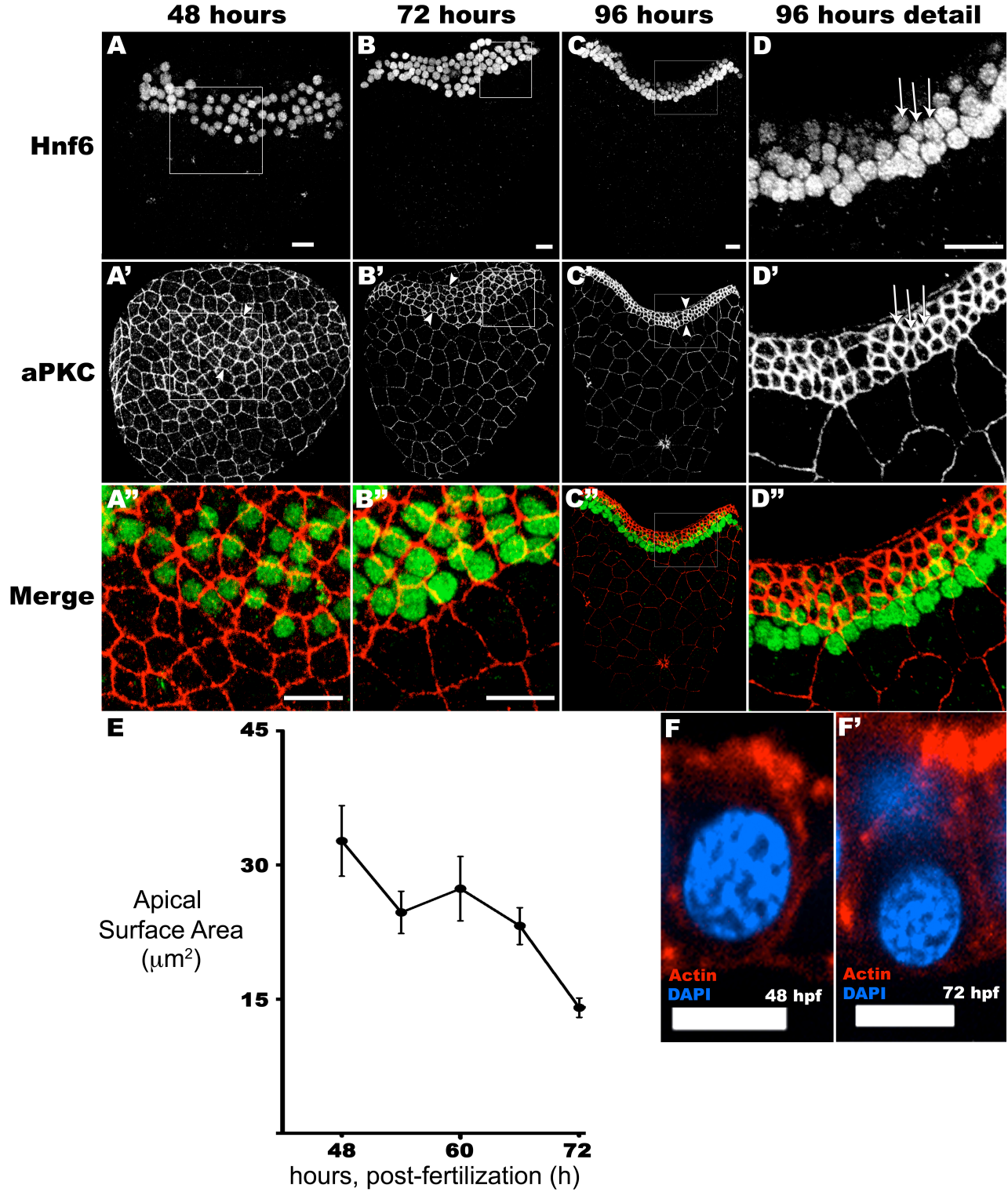
48 hours
72 hours
96 hours
96 hours detail
Hnf6
aPKC
Merge
A
B
C
D
A'
B'
C'
D'
A''
B''
C''
D''
E
45
30
15
Apical
Surface Area
(μm²)
48
60
72
hours, post-fertilization (h)
F
F'
Actin
DAPI
48 hpf
Actin
DAPI
72 hpf

Figure 1.1

Apical constriction of ciliary band cells in *S. purpuratus* during early embryonic development. (A-A'') At 48 hours, cells expressing the ciliary band marker, Hnf6 are not apically constricted compared to non-Hnf6 cells. (B-B'') At 72 hours, Hnf6 expressing cells appear constricted compared to non-ciliary band cells and there is a noticeable boundary (B', arrowheads and B'') between the ciliary band, aboral and oral ectoderm. (C-C'' and D-D'') At 96 hours, Hnf6 expressing cells form a band of tissue (arrowheads) with cells arranged in compact rows (arrows) that encircle the oral field. (E) Apical surface area of ciliary band cells measured from 50 to 72 hours, illustrating apical constriction. (50h, n= 1292 cells from 19 embryos; 55h, n= 1032 cells from 16 embryos; 60h, n= 1196 cells from 16 embryos; 65h, n= 724 cells in 10 embryos; 72h, n=1045 cells in 12 embryos). (F and F') Constriction of apical cell surface (top of image) causes ciliary band cells to change their cross-sectional shape from oval at 48 hours (F) to bottle-shaped at 72 hours (F'). Scale bars A-D = 10μm, F and F'= 5μm.

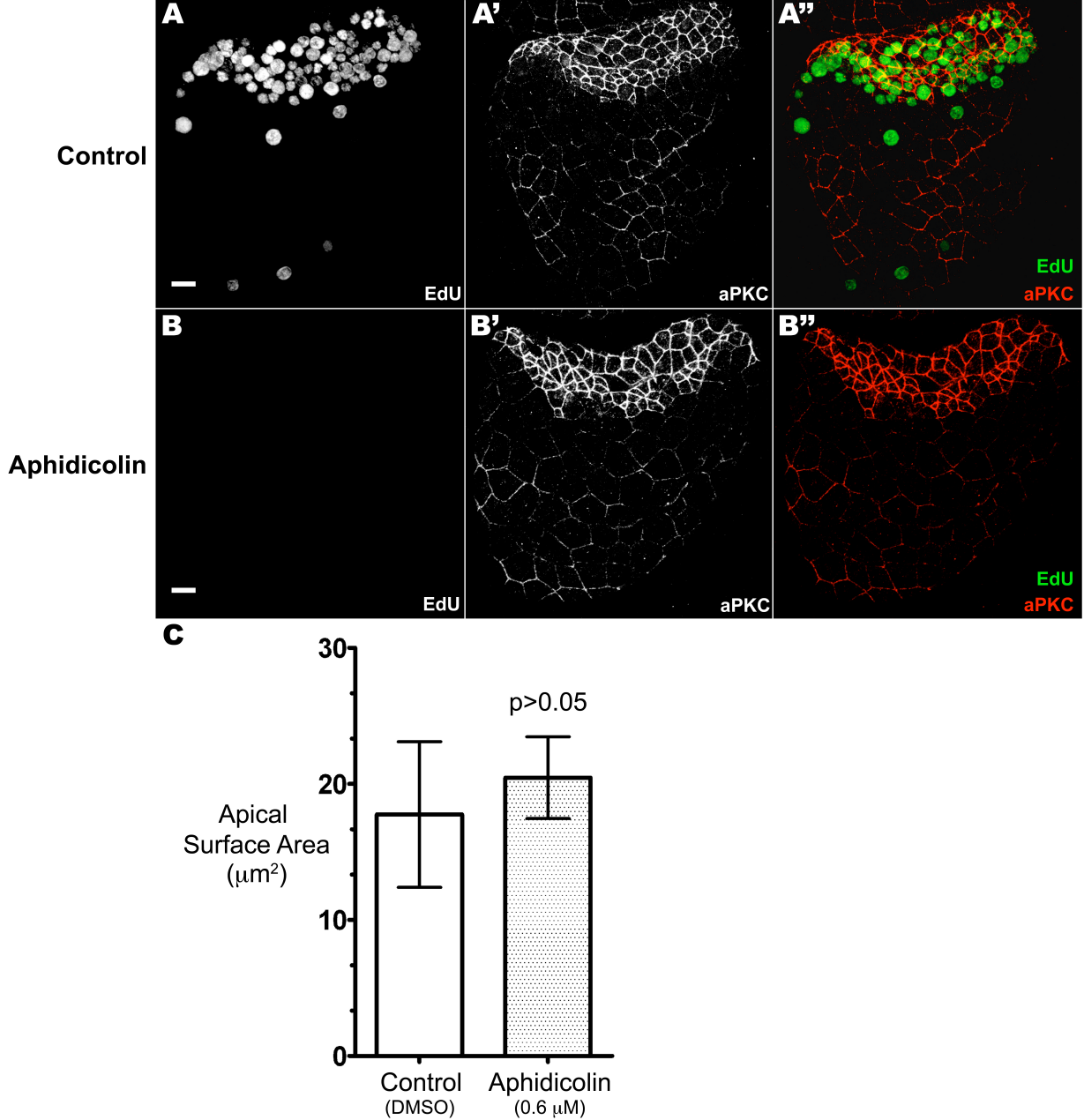
Control
Aphidicolin
A
A'
A"
B
B'
B"
EdU
aPKC
EdU
aPKC
C
30
20
10
0
Apical
Surface Area
(μm²)
p>0.05
Control
(DMSO)
Aphidicolin
(0.6 μM)

Figure 1.2

Apical constriction is independent of cell division. 72 hours. (A) Incorporation of EdU from 60-72 hours illustrates many ciliary band cells are in S-phase during this interval. (A') Apical constriction is evident in untreated embryos. (B) Incorporation of EdU from 60-72 hours is blocked by adding 0.6 μM aphidicolin at 60 hours. (B' and B'') Apical constriction is evident in treated embryos. (C) Blocking cell division from 60-72 hours has no significant effect on apical constriction in ciliary band cells (Aphidicolin, n= 570 cells in 12 embryos; Control, 1551 cells in 19 embryos). Scale bars = 10μm.

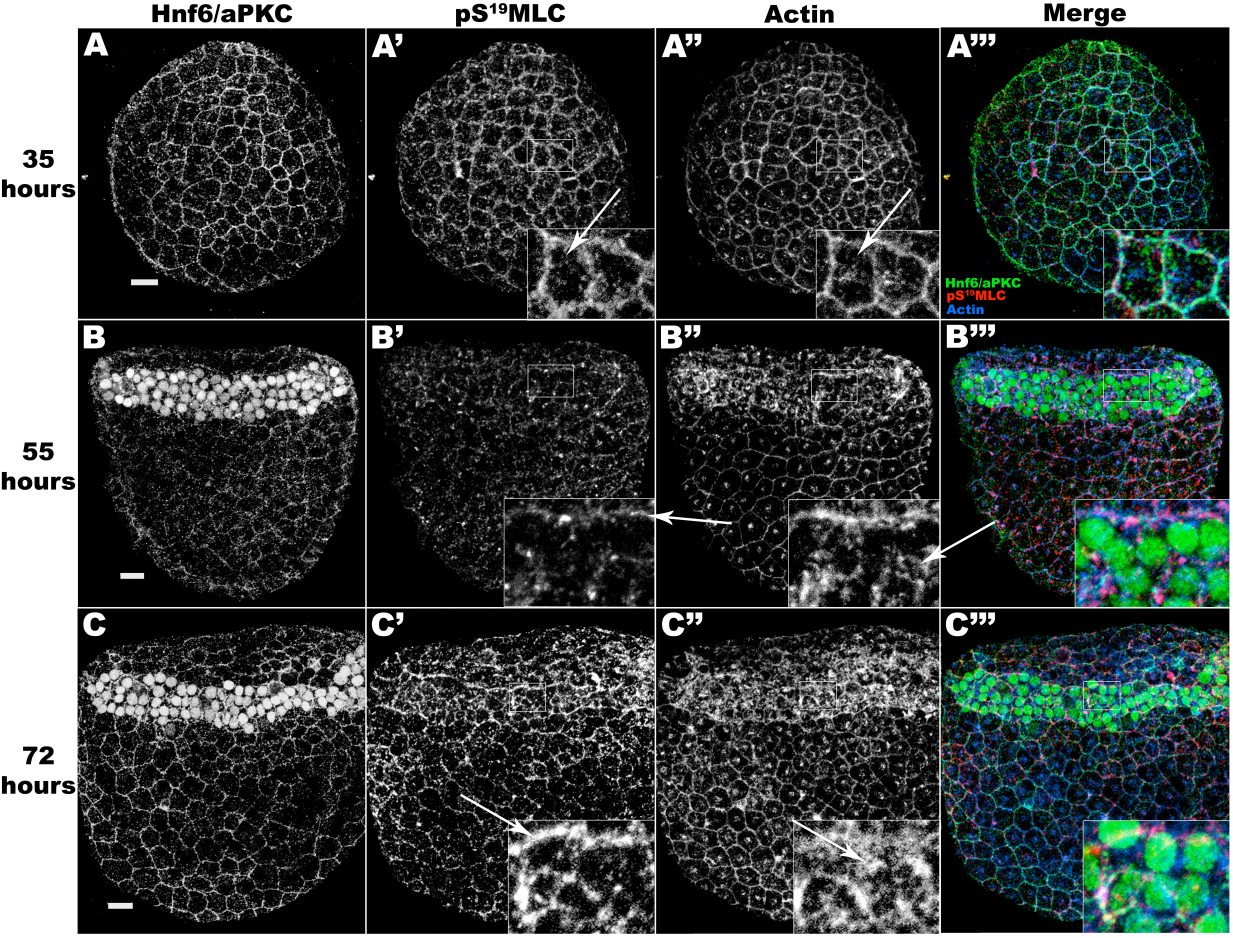
Hnf6/aPKC
pS19MLC
Actin
Merge
35 hours
55 hours
72 hours
A
A'
A''
A'''
B
B'
B''
B'''
C
C'
C''
C'''
Hnf6/aPKC
pS19MLC
Actin

Figure 1.3

Cytoskeletal networks of actin and phospho-myosin ($pS^{19}MLC$) undergo remodelling in ciliary band cells during apical constriction with no apparent changes in actomyosin of non-ciliary band cells. (A) 35 hours, cell junctions are clear and Hnf6 is not yet expressed. (A' and A'') $pS^{19}MLC$ and actin localize primarily to apical, junctions with minimal amounts in the apical cortex (inset, arrows). (B) 55 hours, presumptive ciliary band cells express Hnf6 and cell junctions are indicated with anti-aPKC antibody. (B') Polarized distribution of $pS^{19}MLC$ is evident on latitudinal membranes of the ciliary band (inset, arrow). (B'') Ciliary band specific remodelling of actin is evident in the apical cortex (inset, arrow). (C) 72 hours, ciliary band cells have apically constricted. (C') A continuous, supracellular network of $pS^{19}MLC$ in the ciliary band characterized by polarized expression on latitudinal junctions (inset, arrow). (C'') Continuous actin filaments form a supracellular network in the ciliary band accompanied by formation of dense actin networks in apical cortices of ciliary band cells (inset, arrow). Scale bars = 10μm

We hypothesized that the actomyosin network provides some of the mechanical force that contributes to apical constriction and that interfering with actomyosin contractility would lead to a loss of apical constriction in ciliary band cells. We tested this using cytochalasin D (Miyoshi et al., 2006) to disrupt actin filaments (Fig. 4A-A''), or ML 7 (Uehara et al., 2008) to inhibit myosin light chain kinase (Fig. 4B-B''). Cytochalasin D treated embryos are rounded and exhibit loosely packed cells expressing Hnf6 (Fig. 4A) and distribution of actin and pS^{19}Myo are perturbed (Fig. 4A', A''). Specifically, circular structures of pS^{19}Myo are present in the ciliary band (Fig. 4A', arrows and inset). Similarly, actin networks in the ciliary band are discontinuous and appear as hollow circles (Fig. 4A'', arrows and inset). Embryos treated with ML 7 are rounded and Hnf6 expressing cells are loosely packed (Fig. 4B). Latitudinal distribution of pS^{19}Myo is irregular (Fig. 4B', arrowheads and inset). Similarly, actin networks are irregular and discontinuous in these embryos (Fig. 4B'') and apical cortices often lack actin accumulation. (Fig. 4C) Ciliary band cells in embryos treated with ML 7 (dashed line) or cytochalasin D (dotted line) are less apically constricted than control embryos (solid line). This indicates polymerization of actin filaments and phosphorylation of myosin light chain are necessary for apical constriction of ciliary band cells.

Ectodermal expression of Sp-Eph and Sp-Ephrin and interaction with FAK

Preliminary data indicated that Sp-Eph and Sp-Ephrin were expressed in ectoderm beginning at gastrulation. In further analysis, antibodies against pY^{379}Eph and Sp-Eph indicate that Sp-Eph is expressed throughout the oral and ciliary band ectoderm (Fig. 5E, F) and becomes phosphorylated in the ciliary band during apical constriction (Fig. 5A'-A'', B'-B''; ciliary band boundary to oral ectoderm marked by arrowheads, boundary to aboral ectoderm marked by arrows). In the ciliary band, beginning at 48 hours, Sp-Eph is polarized in its distribution; it is most abundant on latitudinal membranes (Fig. 5E, F, arrows). This contrasts with the expression in the oral ectoderm, where Sp-Eph is expressed uniformly around the periphery of cells (Fig. 4F, asterisks). Antibodies against Sp-Ephrin indicate that the protein is expressed on aboral ectoderm and the ciliary band (Fig. 5A-A', B-B'). Expression of Sp-Ephrin could not be detected in the oral ectoderm during ciliary band formation (Fig. 5B-B'). The overlapping expression of Sp-Eph and Sp-Ephrin in the region in which the ciliary band is forming and the detection of

phosphorylated form of the Sp-Eph receptor suggests that Sp-Eph is signaling in presumptive ciliary band cells. A ciliary band expression pattern similar to Sp-Eph is observed using pY^{397}FAK antibody (Fig. 5C, 5E', F'), and these colocalize during apical constriction (Fig. 5E'', F'') suggesting an interaction.

Following these observations, we investigated interactions between Sp-Eph and pY^{397}FAK in vitro using a GST-tagged, cytoplasmic domain (322-762) of native Sp-Eph (Fig. 5D). This protein failed to reliably pulldown pY^{397}FAK in epithelial cell lysate from 72h embryos (Fig. 5D, lower panel). Since kinase domains often bind substrates transiently, releasing them upon phosphorylation, we created a kinase-dead form of this construct as a substrate trap (Roose et al., 2005) and we find it pulls down pY^{397}FAK (Fig. 5D, top panel). This indicates a potential physical interaction between Sp-Eph and pY^{397}FAK in ciliary band cells.

Eph-Ephrin signaling is necessary for apical constriction

To assess the role of Eph-Ephrin signaling during apical constriction, we blocked translation of Sp-Eph or Sp-Ephrin in the embryo by MASO injection (Fig. 6). For each protein, we injected two, non-overlapping oligonucleotides to knock down expression with 42.4% (+/- 16.4% S.E.) mean knockdown based on fluorescence intensity. When we knockdown Sp-Eph or Sp-Ephrin, a distinct ciliary band fails to form after 72 hours and embryos are ovoid in shape (Fig. 6A,A',B,B'). At 72 hours, actin and pS^{19}MLC in Sp-Eph knockdown embryos appear in circular or crescent-shaped patches throughout the ciliary band (Fig. 6C-C'''). These patches appear restricted to individual cells for pS^{19}MLC (Fig. 6C', arrow and inset) and for actin (Fig. 6C'', arrow and inset) and do not form an interconnected, supracellular network as seen in untreated embryos (Fig. 3), indicating Sp-Eph is necessary for actomyosin reorganization during ciliary band formation. Furthermore, ciliary band cells in MASO injected embryos appear larger than in control embryos (Fig. 6D-F) and when we quantify apical surface area, we find apical constriction is significantly reduced in knockdown embryos ($p < 0.0001$) (Fig. 6G), indicating Sp-Eph and Sp-Ephrin are necessary for apical constriction of ciliary band cells.

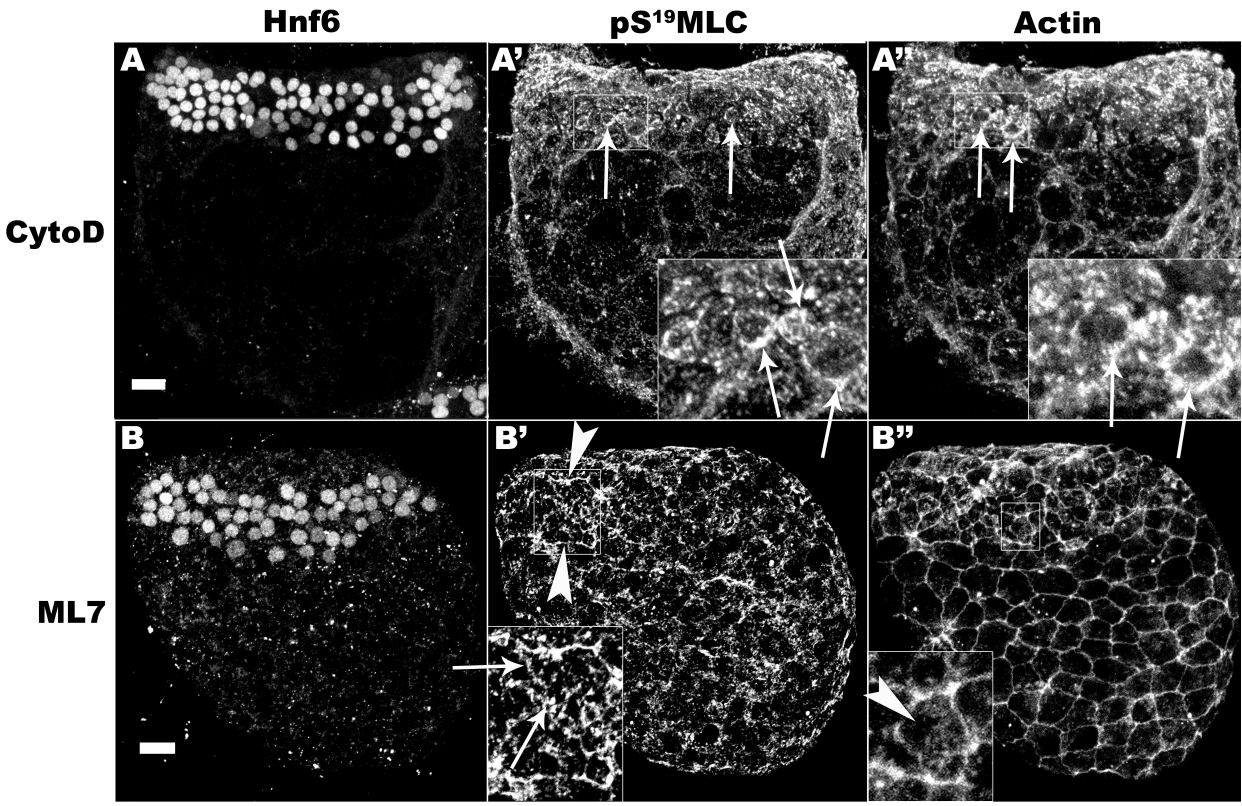
Hnf6
pS19MLC
Actin
CytoD
ML7
A
A'
A''
B
B'
B''

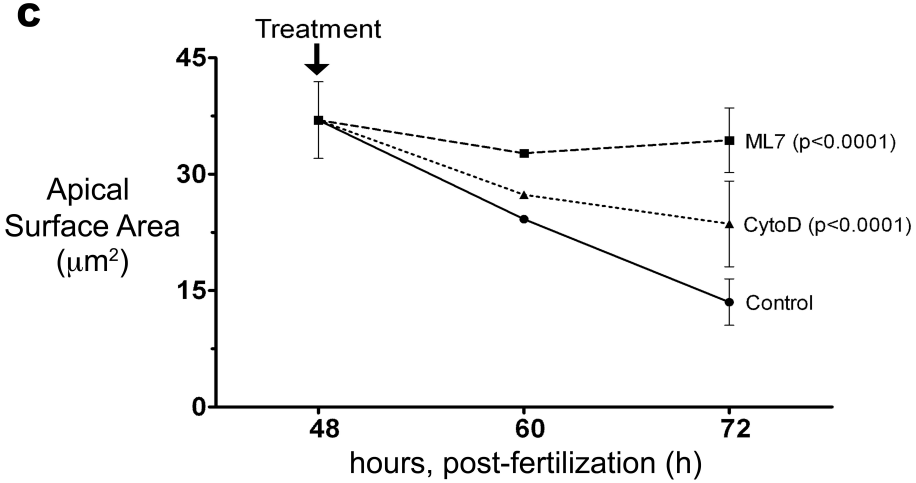
C
Treatment
45
30
15
0
Apical Surface Area (μm2)
48
60
72
hours, post-fertilization (h)
ML7 (p<0.0001)
CytoD (p<0.0001)
Control

Figure 1.4

Treatment with cytochalasin D or ML 7 disrupts cytoskeletal networks of actin and phospho-myosin ($pS^{19}MLC$) and inhibits apical constriction. 72 hours. (A-A'') Embryos exposed to 20 μM cytochalasin D at 48 hours fail to form a ciliary band and form rounded embryos that lack a clearly defined ciliary band. (A) Ciliary band cells are loosely packed. (A') Random accumulations of $pS^{19}MLC$ appear on apical junctions of ciliary band cells (inset, arrows). (A'') Patchy actin distributed randomly on all cell junctions throughout the ciliary band (inset, arrows). (B –B'') Treatment with 5 μM ML 7 at 48 hours disrupts ciliary band formation. (B) Embryos are ovoid and lack a clearly defined ciliary band. (B') Distribution of $pS^{19}MLC$ is polarized to latitudinal membranes in some areas of the ciliary band (arrowheads). Aberrant, $pS^{19}MLC$-containing structures form in the apical cortices of cells (inset, arrow). (B'') Dense actin networks in only some areas of the ciliary band and actin does not accumulate in apical cortices (inset, arrowhead). (C) Inhibitors of actin polymerization and myosin light chain kinase block apical constriction of ciliary band cells. Apical surface area of ciliary band cells in control embryos reduces more than 50% from 48 to 72 hours (solid line, 48h, n=625 cells in 10 embryos; 60h, n=747 cells in 10 embryos; 72h, n=788 cells in 10 embryos). Apical constriction is significantly reduced in ciliary band cells of embryos treated with cytoskeletal inhibitor cytochalasin D (dashed line, 48h, n=625 cells in 10 embryos; 60h, n=637 cells in 10 embryos; 72h, n=639 cells in 10 embryos) or ML-7 (dotted line, 48h, n=625 cells in 10 embryos; 60h, n=654 cells in 10 embryos; 72h, n=597 cells in 10 embryos). Scale bars = 10μm.

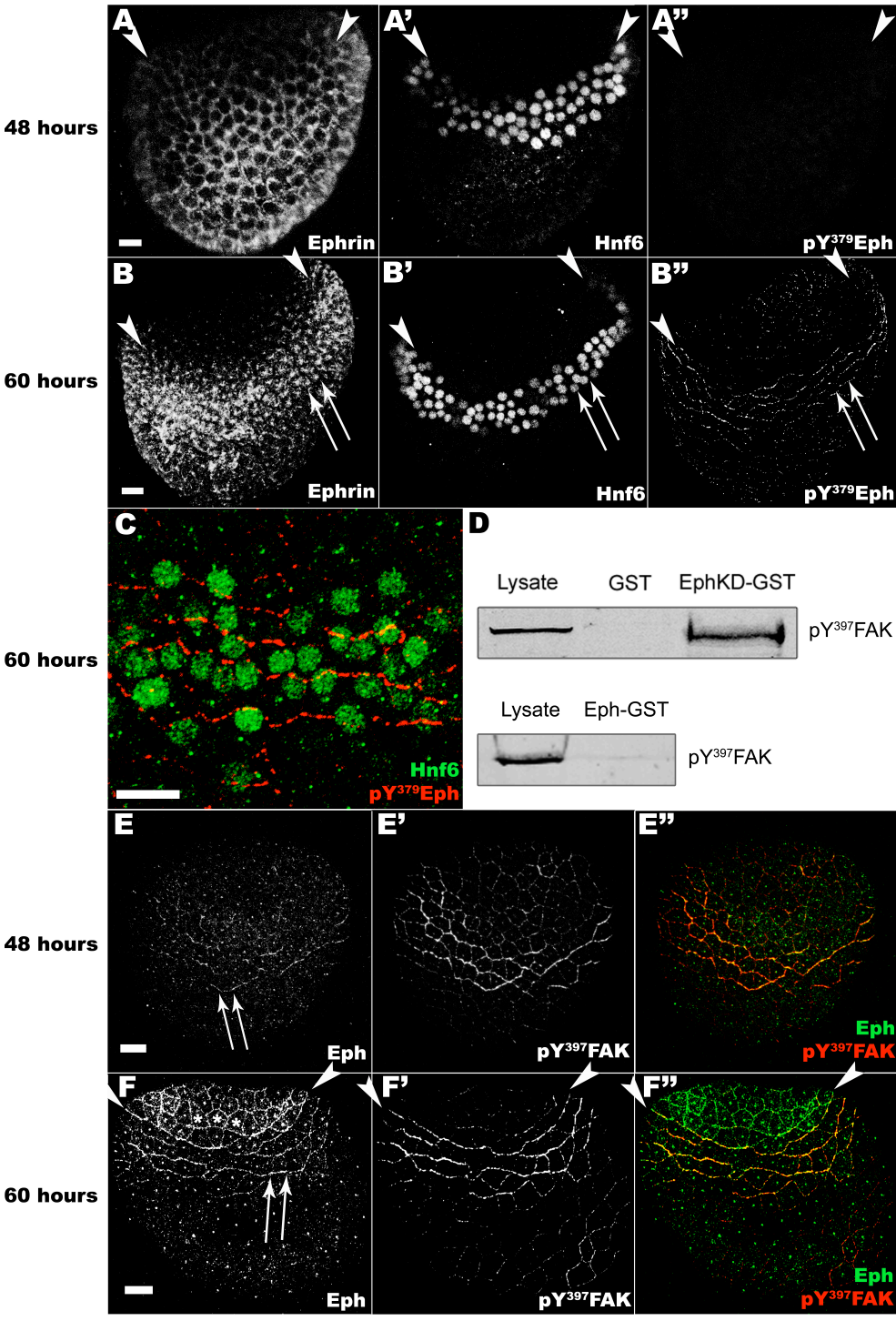
48 hours
A
Ephrin
A'
Hnf6
A''
pY379Eph
60 hours
B
Ephrin
B'
Hnf6
B''
pY379Eph
60 hours
C
Hnf6
pY379Eph
D
Lysate
GST
EphKD-GST
pY397FAK
Lysate
Eph-GST
pY397FAK
48 hours
E
Eph
E'
pY397FAK
E''
Eph
pY397FAK
60 hours
F
Eph
F'
pY397FAK
F''
Eph
pY397FAK

Figure 1.5

During apical constriction, Eph and Ephrin expression overlap in the ciliary band and Eph becomes phosphorylated along latitudinal membranes where it colocalizes with pY^{397}FAK. Antigens and developmental stages indicated. Arrowheads mark oral ectoderm-ciliary band boundary. Arrows mark aboral ectoderm-ciliary band boundary. (A-A') Region-specific expression of Ephrin prior to apical constriction. (A) Ephrin is primarily on aboral and ciliary band ectoderm. (A') Expression of Hnf6 marks the ciliary band. (A'') Prior to apical constriction, pY^{379}Eph is undetected. (B-B'') Ciliary band specific colocalization of pY^{379}Eph and Ephrin during apical constriction (B) Ephrin expression is restricted to aboral and ciliary band ectoderm. (B') Hnf6 expression indicates ciliary band cells are forming a tightly packed band of tissue. (B'') pY^{379}Eph is detected on junctions in the ciliary band and largely absent from oral and aboral ectoderm. (C) During apical constriction, pY^{379}Eph is polarized to latitudinal membrane junctions of ciliary band cells. (D) Eph cytoplasmic domain and pY^{397}FAK interact physically. (Top panel) A GST fusion protein of kinase-dead SpEph (EphKD) cytoplasmic domain acts as a substrate trap, showing a specific interaction with pY^{397}FAK in an ectodermal cell lysate from *S. purpuratus* embryos, 72 hours. (Bottom panel) A native form of Eph cytoplasmic domain does not reliably pull down detectable quantities pY^{397}FAK from an ectodermal lysate. (E-E'') Prior to apical constriction, Eph and pY^{397}FAK are apparent in the presumptive ciliary band. (E) Eph is apparent on apical junctions within oral and ciliary band ectoderm, and latitudinal polarization is evident on junctions bordering the aboral ectoderm (arrows). (E') pY^{397}FAK becomes abundant on apical junctions in the ciliary band where it colocalizes (E'') with Eph. (F-F'') Distinct latitudinal polarization of Eph and pY^{397}FAK during apical constriction of ciliary band cells. (F) Eph distribution is polarized in the ciliary band and does not extend into aboral ectoderm (arrows). Uniformly distributed on junctions of oral ectoderm (asterisks). (F') Polarized expression of pY^{397}FAK is restricted to the ciliary band where it colocalizes with Eph (F''). Puncta in E and F represent recognition of material in ciliary basal bodies. Scale bars = 10μm.

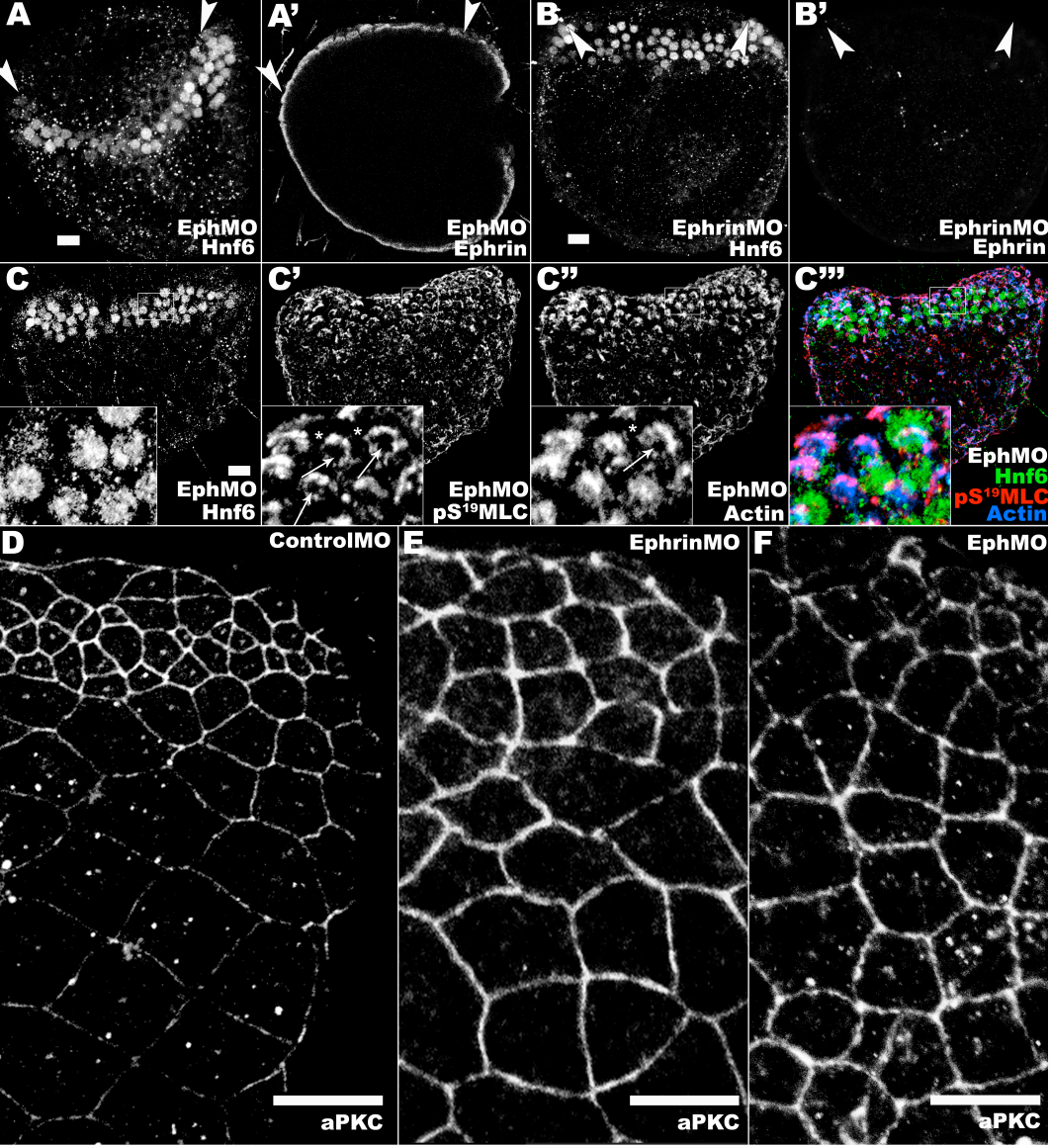
A
EphMO
Hnf6
A'
EphMO
Ephrin
B
EphrinMO
Hnf6
B'
EphrinMO
Ephrin
C
EphMO
Hnf6
C'
EphMO
pS19MLC
C''
EphMO
Actin
C'''
EphMO
Hnf6
pS19MLC
Actin
D
ControlMO
aPKC
E
EphrinMO
aPKC
F
EphMO
aPKC

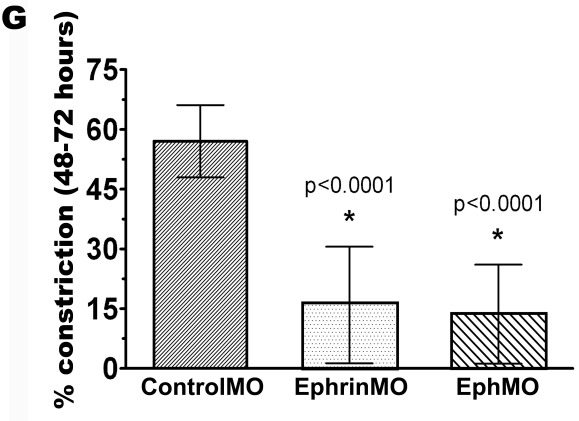
G
% constriction (48-72 hours)
75
60
45
30
15
0
ControlMO
EphrinMO
EphMO
p<0.0001
*
p<0.0001
*

Figure 1.6

Blocking Eph-Ephrin signaling prevents apical constriction and formation of supracellular networks in the ciliary band. Arrowheads mark the boundary between oral and ciliary band ectoderm. 72 hours. Knockdown of Eph expression by MASO injection (EphMO – 250μM solution) produces embryos with a rounded appearance (A-A'). (A) Hnf6 expression indicates loosely packed ciliary band cells. (A') Ephrin expression extends into the oral ectoderm. Knockdown of Ephrin expression by morpholino injection (EphrinMO – 200 μM solution) produces embryos with a rounded appearance (B-B'); (B) Hnf6 expression indicates loosely packed ciliary band cells. (B') Ephrin expression is faint in aboral ectoderm and absent in oral ectoderm. (C-C''') Eph knockdown disrupts the supracellular actomyosin network in the ciliary band. (C) The ciliary band is loosely packed and Hnf6 marks individual cells. (C'and C'') pS^{19}MLC and actin in the ciliary band form discrete, hollow circles (inset, arrows), closely associated with apical membranes of individual cells. Gaps are present between adjacent cells (inset, asterisks), indicating a discontinuous actomyosin networks. (C''') Merged channels illustrate individual cells and associated actomyosin meshwork with gaps between cells and absence of a supracellular network (D) Ciliary band cells in control embryos constrict normally and form a tightly packed row, 3-5 cells wide. Morpholino-induced knockdown of Ephrin (E) or Eph (F) disrupts apical constriction and an organized ciliary band is not formed. (G) Apical constriction of ciliary band cells is significantly reduced in Eph and Ephrin knockdown embryos. Percent constriction = (apical surface area at 72 hours / apical surface area at 48 hours) x100. Control, n= 795 cells in 9 embryos; EphMO, n=625cells in 10 embryos; EphrinMO, n= 792 cells in 11 embryos. Mean knockdown efficiency for MASO injections based on fluorescence intensity = 42.4%. Scale bars = 10μm.

Ciliary-band-specific accumulation of pY^{397}FAK is regulated by Eph-Ephrin signaling

We asked whether ciliary-band-specific FAK phosphorylation is dependent on Eph-Ephrin signaling (Fig. 7). Prior to ciliary band specification, pY^{397}FAK is uniformly distributed on cell membranes (Fig. 7A) and polarized accumulation begins in the presumptive ciliary band (Fig. 7B). Accumulation of pY^{397}FAK at latitudinal junctions of the ciliary band continues throughout apical constriction (Fig. 7C, D). Knockdown of Sp-Eph or Sp-Ephrin expression causes a distinct reduction of pY^{397}FAK accumulation in the ciliary band (Fig. 7E, F). Using quantitative confocal microscopy, the relative abundance of pY^{397}FAK in the ciliary band at 60 hours is 3.25 times more than in aboral ectoderm (Fig. 7G). When we perturb Eph-Ephrin signaling by MASO-induced knockdown or inhibition of Sp-Eph kinase, pY^{397}FAK abundance is reduced to less than 2 fold that of aboral ectoderm (Fig. 7G). Thus, Eph-Eprhin signaling is necessary for pY^{397}FAK accumulation. A similar effect is achieved using PF573 (Fig. 7G, right column), a small molecule inhibitor that obstructs FAK's ATP binding pocket (Slack-Davis et al. 2007). These data indicate Eph-Ephrin signaling regulates pY^{397}FAK accumulation in ciliary band cells during apical constriction.

Apical constriction requires Eph-Ephrin signaling and Phosphorylation of FAK

By adding specific inhibitors and measuring apical surface area, we further assessed the roles of Eph-Ephrin signaling and FAK catalytic activity on apical constriction of ciliary band cells (Fig. 8). In the presence of NVP (1.75 μM), an Sp-Eph kinase inhibitor, ciliary band formation and accumulation of pY^{397}FAK are disrupted (Fig. 8B), and apical surface area of ciliary band cells does not change (Fig. 8D), indicating a lack of apical constriction. To determine the role of pY^{397}FAK, we used PF573 to block phosphorylation of Y397 and we measured the effect in ciliary band cells. Apical constriction is blocked by PF573 (10 μM) (Fig. 8C, D), indicating that FAK phosphorylation on Y397 is critical. These data support a model in which forward Eph-Ephrin signaling regulates apical constriction of the ciliary band cells through pY^{397}FAK.

Planar Cell Polarity in Ciliary Band Cells

Using an inhibitor specific to the non-canonical Wnt pathway, we investigated the role of planar cell polarity in the ciliary band (Fig. 9). We treated embryos with a cell

permeant, c-Jun NH_2 terminal peptide (Range et al. 2013) and examined polarization of pY^{397}FAK or pY^{379}Eph in ciliary band cells (Fig. 9A, A'; B, B'). In control embryos the abundance of pY^{397}FAK on latitudinal junctions of the ciliary band is over 12 times greater than on longitudinal junctions (Fig. 9C). When treated with JNK inhibitor, the abundance of pY^{397}FAK is equal on latitudinal and longitudinal junctions (Fig. 9C). Similarly, polarization of pY^{379}Eph is significantly reduced when JNK is inhibited (Fig. 9C), indicating polarization of these signaling molecules in the ciliary band is dependent on the non-canonical Wnt pathway. Interestingly, when we quantify apical surface area of ciliary band cells in these JNK-treated embryos and compare to controls, there is no significant difference ($p = 0.303$) (Fig. 9D), implying that the mechanisms driving apical constriction and polarization of pY^{379}Eph and pY^{397}FAK are independent (Fig. 9E).

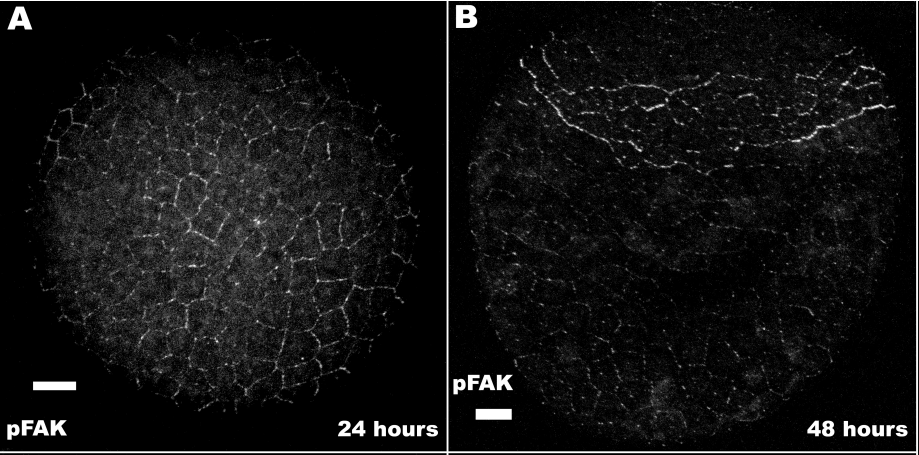
A
pFAK
24 hours

B
pFAK
48 hours

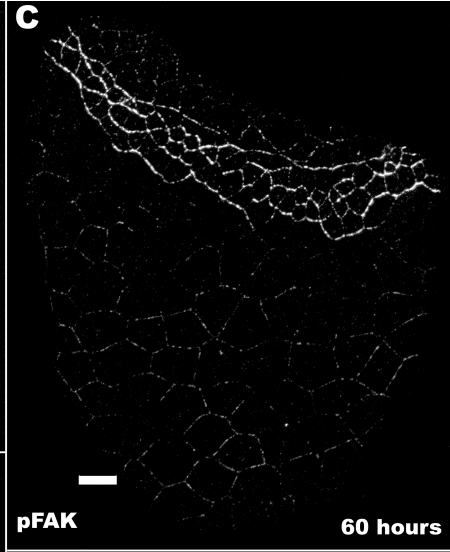
C
pFAK
60 hours

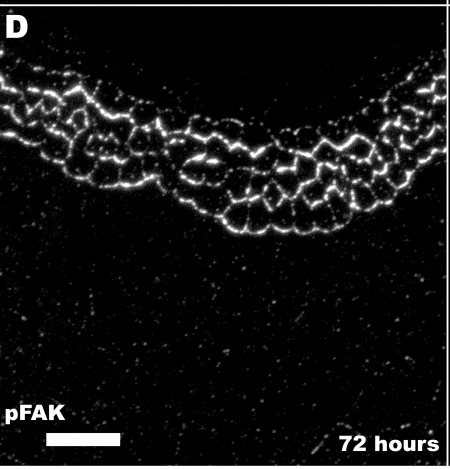
D
pFAK
72 hours

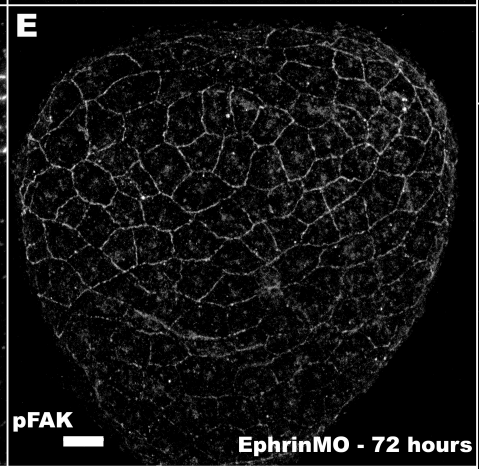
E
pFAK
EphrinMO - 72 hours

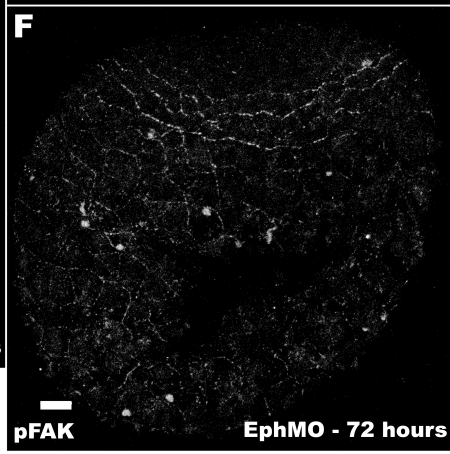
F
pFAK
EphMO - 72 hours

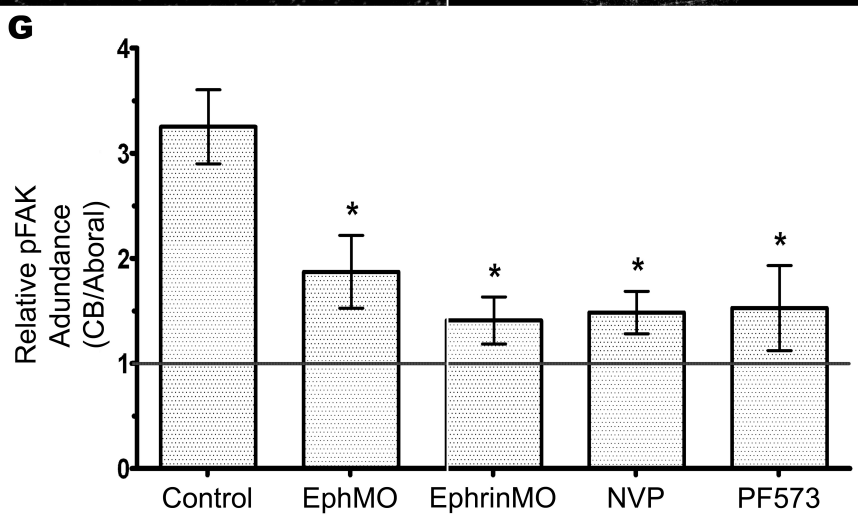
G
Relative pFAK Adundance (CB/Aboral)
0
1
2
3
4
*
*
*
*
Control
EphMO
EphrinMO
NVP
PF573

Figure 1.7

Ephrin signaling through Eph is necessary for phosphorylation of focal adhesion kinase during ciliary band formation. (A) $pY^{397}FAK$ is uniformly distributed on cell-cell junctions at 24 hours. (B) At the onset of apical constriction, $pY^{397}FAK$ accumulates on latitudinal junctions in the ciliary band. (C) $pY^{397}FAK$ intensity on latitudinal junctions in the ciliary band increases as apical constriction continues and the fully formed ciliary band (D) shows abundant $pY^{397}FAK$. Knocking down Ephrin (E, EphrinMO – 200 μM solution) or Eph (F, (EphMO – 250 μM solution) expression disrupts $pY^{397}FAK$ accumulation in the ciliary band. (G) Blocking Eph-Ephrin signaling or FAK catalytic activity significantly reduces relative abundance of $pY^{397}FAK$ (* denotes $p<0.001$). In control treatments relative $pY^{397}FAK$ abundance in the ciliary band is > 3.2 (G – left column). Injection of Eph or Ephrin morpholino (as above) or addition of Eph kinase inhibitor (NVP) at 1.75 μM, results in a significant loss in $pY^{397}FAK$ accumulation. A similar response is achieved by adding 10 μM of PF573, an inhibitor specific to $pY^{397}FAK$ (G – right column). Relative abundance is measured by comparing fluorescence intensity of pixels within the ciliary band to those within aboral ectoderm at 60 hours. A Relative abundance value of 1 is equivalent to the abundance of $pY^{397}FAK$ on aboral ectoderm. All pixels in the aboral and/or ciliary band ectoderm were quantified for each embryo. Untreated, n= 10 embryos; EphMO, n= 12 embryos; EphrinMO, n= 11 embryos; Eph inhibitor, n= 10 embryos; pFAK inhibitor, n= 14 embryos. Mean knockdown efficiency for all MASO injections based on fluorescence intensity = 42.4%. Scale bars = 10μm.

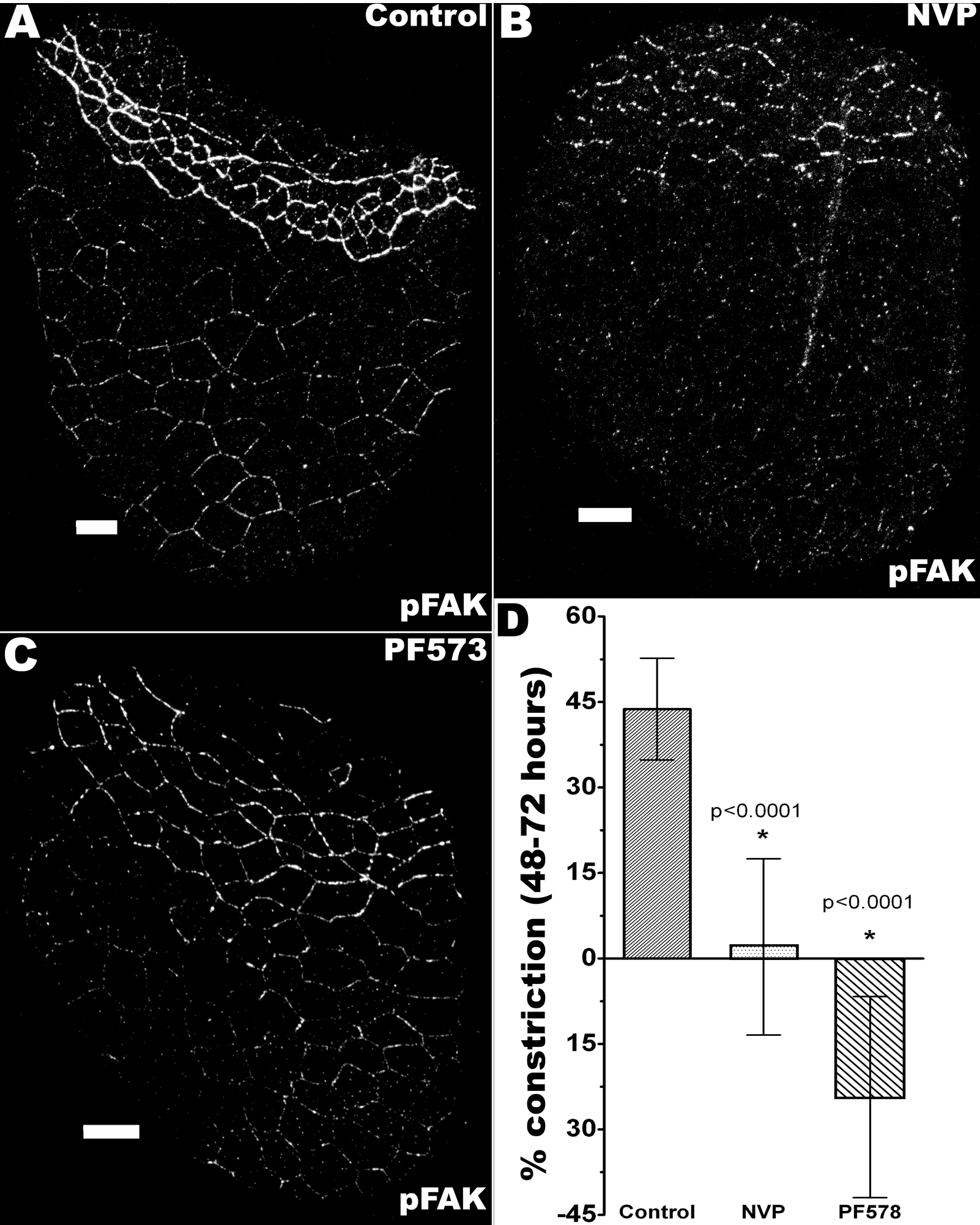
A
Control
pFAK
B
NVP
pFAK
C
PF573
pFAK
D
% constriction (48-72 hours)
60
45
30
15
0
15
30
-45
p<0.0001
*
p<0.0001
*
Control
NVP
PF578

Figure 1.8

Phosphorylation of focal adhesion kinase and forward signaling through Eph are necessary for apical constriction of ciliary band cells. Antigens and treatments indicated. 72 hours. (A) Control embryos accumulate pY^{397}FAK at apical membrane junctions within the ciliary band. (B) Blocking Eph kinase (NVP at 1.75 μM) reduces pY^{397}FAK abundance and disrupts ciliary band formation. (C) Blocking FAK phosphorylation (PF573 at 10 μM) reduces pY^{397}FAK abundance loss and disrupts ciliary band formation. (D) Blocking Eph kinase or FAK phosphorylation (as above) significantly reduces the extent of apical constriction in ciliary band cells. Embryos were exposed to inhibitors at 48 hours and apical surface area was quantified at 72 hours. Control embryos (DMSO) form discrete ciliary band regions with apically constricted cells. Addition of NVP (D – centre column) or PF573 (D – right column) results in inhibition of apical constriction, indicating a role for the Eph kinase activity and the FAK activity. Control, n= 670 cells in 10 embryos; Eph inhibitor, n= 582 cells in 10 embryos; FAK inhibitor, n= 760 cells in 13 embryos. Scale bars = 10μm.

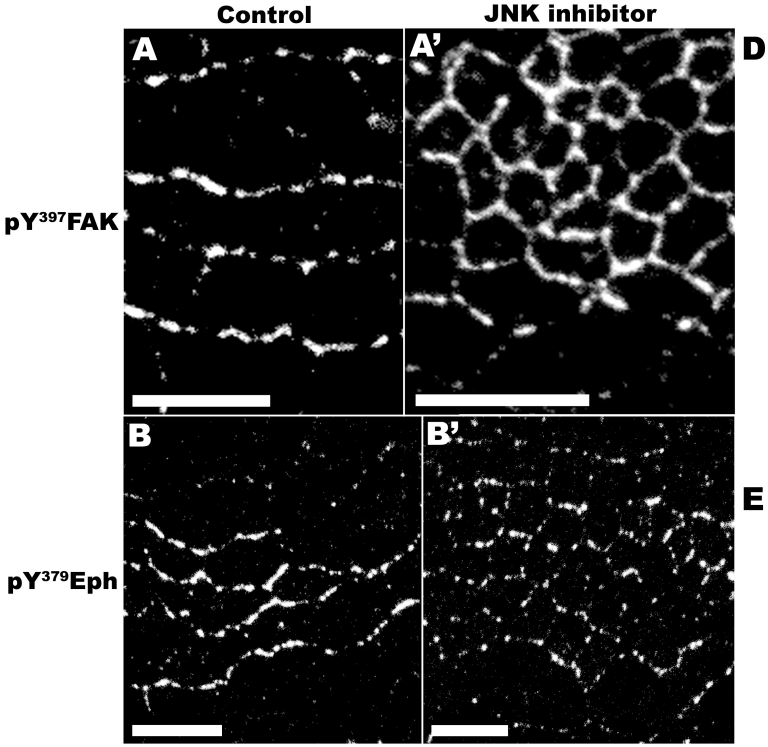

C

	pY397FAK	pY379Eph
Control	12.21	3.24
JNK inhibitor	1.02*	2.27*

* p < 0.001

D

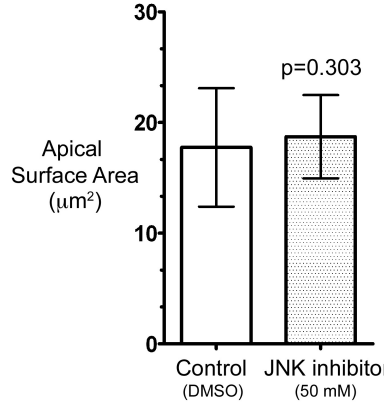

E

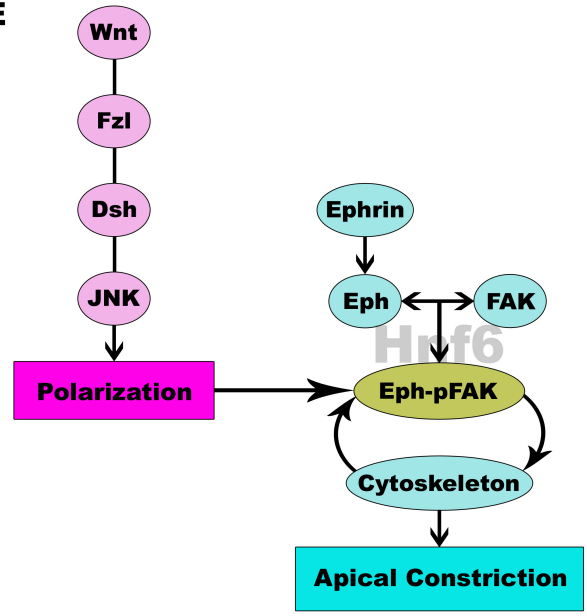

Figure 1.9

Planar polarization of ciliary band cells is controlled by the non-canonical Wnt pathway and is dissociable from apical constriction. 72 hours. (A and B) Polarization of pY^{397}FAK and pY^{379}Eph is apparent in control embryos and these accumulate at latitudinal apical junctions. (A' and B') Addition of a JNK inhibitor (50 mM) causes an apparent loss of latitudinal accumulation of pY^{397}FAK and pY^{379}Eph in the ciliary band. (C) Relative intensity of pY^{397}FAK and pY^{379}Eph on latitudinal junctions is JNK-dependent. In control embryos (top row), abundance of pY^{397}FAK and pY^{379}Eph is planar-polarized and significantly higher on latitudinal membranes. Addition of a JNK-specific inhibitor (bottom row) abolishes pY^{397}FAK polarization and perturbs pY^{379}Eph polarization. Numbers represent the relative abundance of antigen on latitudinal relative to longitudinal apical junctions. Relative abundance is calculated as ratio of latitudinal / longitudinal relative intensity for each antigen at 72 hours development. n=>22,000 pixels in 10 embryos for both treatments. (D) Apical constriction is dissociable from planar polarization. Addition of JNK inhibitor at 48 hours does not significantly alter apical surface area of ciliary band cells at 72 hours. (E) Proposed model illustrating parallel, interacting pathways that define apical constriction and formation of a tightly organized ciliary band in sea urchin embryos. Hnf6 provides a permissive environment for Eph-Ephrin signaling leading to formation and accumulation of an Eph-FAK complex accompanied by cytoskeletal reorganization and apical constriction. The Eph-FAK complex is planar polarized via the non-canonical Wnt pathway and this polarization pathway is not necessary for apical constriction. Arrows indicate steps in the pathways for which we have provided evidence. Scale bars = 10μm.

Discussion

Our data support a model in which Eph-Ephrin forward signaling initiates formation of a planar-polarized, pY^{397}FAK-containing, signaling complex that regulates actomyosin-mediated contractility, producing apical constriction. The overlap of Sp-Eph and Sp-Ephrin expression appears to activate Sp-Eph within the presumptive ciliary band. A number of studies describe effects on FAK following Ephrin stimulation of Eph. These include increased autophosphorylation on Y^{397} with downstream effects on cytoskeletal reorganization and cell shape (Shi et al., 2009; Moeller et al., 2006; Carter et al., 2002; Ohashi et al., 2000). There appears to be a role for FAK during ciliary band morphogenesis; its catalytic activity is necessary for apical constriction, pY^{397}FAK accumulates specifically on latitudinal, ciliary band membranes and Eph-Ephrin signaling is necessary for this accumulation. Furthermore, colocalization of pY^{397}FAK and Sp-Eph on latitudinal membranes of the ciliary band and the putative molecular interaction emphasize a close functional relationship. We propose Sp-Eph and FAK act in an apical complex; regulating assembly of cytoskeletal networks necessary for transducing centripetal forces that reduce apical size during ciliary band morphogenesis (Fig. 9E). There are a number of potential mechanisms by which FAK activation can function in the regulation of actin mediated contractility. These include transduction through Src family kinases, guanine nucleotide exchange factors, GTPase activating proteins and Rho-family GTPases (Thomas, 1998, Tilghman and Parsons, 2008; Burridge and Wennerberg, 2004). This provides a potential mechanism whereby extracellular Sp-Ephrin elicits a receptor-mediated (Sp-Eph) response to change cell shape.

Loss-of-function experiments show filamentous actin and myosin light chain kinase are necessary for apical constriction and rearrangements in their distribution occur immediately prior to shape change. The observed distribution is not consistent with a purse string model in which a circumferential band of actin in each cell is predicted. Rather, our observations are consistent with a model of apical constriction, where centripetal force is produced by contractions of the actomyosin network at the medial apical cortex (Martin et al., 2009). Furthermore, when we block apical constriction by perturbing Eph-Ephrin signaling, we also disrupt supracellular cytoskeletal networks in the ciliary band, illustrating that Eph-Ephrin signaling is involved in remodelling

actomyosin networks during apical constriction of ciliary band cells (Fig. 9E).

Ciliary band cells are polarized within the epithelial plane and this is apparent functionally; cilia have their power stroke oriented away from the oral field (Strathmann, 2007). Sp-Eph and pY^{397}FAK exhibit a polarized distribution and Eph-Ephrin signaling and FAK catalytic activity do not appear to initiate polarization as loss of function interferes with the extent of immunoreactivity of polarized components without noticeably altering their distribution. In contrast, inhibition of JNK leads to a loss in polarization of pY^{397}FAK and pY^{379}Eph with no apparent affects on the level of immunoreactivity and no significant loss of apical constriction. We speculate the non-canonical, Wnt planar cell polarity pathway is responsible for directing assembly of an actomyosin regulating, Sp-Eph/FAK-complex specifically along latitudinal junctions within the ciliary band. Furthermore, polarity and apical constriction appear to be dissociable phenomena that are regulated independently (Fig. 9D, E).

In widely studied models of apical constriction, reduction of apical surface area is followed by inward folding of epithelium and while additional morphogenetic forces and planar cell polarity have been implicated in the folding process, individual contributions have not been resolved (Sawyer et al., 2010; Nishimura et al., 2012). Ciliary band formation is a unique example of morphogenesis as there is no accompanying, large-scale, inward flexion of adjacent ectoderm, rather cells change in shape producing a tightly packed array of cilia with modest outward flexion. This indicates that apical constriction does not function independently to produce large-scale morphogenetic movements. Apical constriction in ciliary band cells is informative and indicates participation of adjacent tissues in morphogenetic folding. The nature of the interaction between apically constricting cells and cells in adjacent tissues remains a key feature in the development of models that seek to describe the complex mechanisms linking patterning to the mechanical forces that drive morphogenesis.

References

Angerer, L. M., Yaguchi, S., Angerer, R. C. and Burke, R. D. (2011). The evolution of nervous system patterning: insights from sea urchin development. Development **138**,3613-23.

Arold, S. T. (2011). How focal adhesion kinase achieves regulation by

linking ligand binding, localization and action. Curr. Opin. Struct. Biol. **21**, 808-13.

Burke, R. D. (1978). The structure of the nervous system of the pluteus larva of Strongylocentrotus purpuratus. Cell Tiss. Res. **191**, 233-47.

Burridge, K. and Wennerberg, K. (2004). Rho and Rac take center stage. Cell **116**: 167–179.

Carter, N., Nakamoto, T., Hirai, H. and Hunter, T. (2002) EphrinA1-induced cytoskeletal re-organization requires FAK and p130(cas). Nat. Cell Biol. **4**, 565-73.

Darie, C. C., Deinhardt, K., Zhang, G., Cardasis, H. S., Chao, M. V. and Neubert, T. A. (2011). Identifying transient protein-protein interactions in EphB2 signaling by blue native PAGE and mass spectrometry. Proteomics **11**, 4514-28.

Hildebrand, J. D. (2005). Shroom regulates epithelial cell shape via the apical positioning of an actomyosin network. J. Cell Sci. **118**: 5191–5203.

Klein, R. (2012). Eph/ephrin signalling during development. Development **139**, 4105-9.

Krupke, O. A., Yaguchi, S., Yaguchi, Y. and Burke, R. D. (2013). Imaging neural development in embryonic and larval sea urchins. Methods Mol. Biol., in press.

Lapraz, F., Besnardeau, L. and Lepage, T. (2009). Patterning of the dorsal-ventral axis in echinoderms: insights into the evolution of the BMP-chordin signaling network. PLoS Biol. **7**(11):e1000248.

Lee J. Y. and Harland, R. M. (2007). Actomyosin contractility and microtubules drive apical constriction in Xenopus bottle cells. Dev. Biol. **311**, 40-52.

Loveless, B. C., Mason, J. W., Sakurai, T., Inoue, N., Razavi, M., Pearson, T.W. and Boulanger, M. J. (2011). Structural characterization and epitope mapping of the glutamic acid/alanine-rich protein from Trypanosoma congolense: defining assembly on the parasite cell surface. J. Biol. Chem. **286**: 20658-20665.

Martin, A. C., Kaschube, M., and Wieschaus, E. F. (2009). Pulsed contractions of an actin-myosin network drive apical constriction. Nature **457,** 495-9.

McClay, D. R. and Marchase, R. B. (1979). Separation of ectoderm and endoderm from sea urchin pluteus larvae and demonstration of germ layer-specific

antigens. Dev. Biol. **2**,289-96.

Moeller, M. L., Shi, Y., Reichardt, L. F. and Ethell, I. M. (2006). EphB receptors regulate dendritic spine morphogenesis through the recruitment/ phosphorylation of focal adhesion kinase and RhoA activation. J. Biol. Chem. **281**, 1587-98.

Nagele R. G. and Lee H. Y. (1987). Studies on the mechanisms of neurulation in the chick: morphometric analysis of the relationship between regional variations in cell shape and sites of motive force generation. J. Exp. Zool. **241**: 197-205.

Nishimura, T., Honda, H. and Takeichi, M. (2012). Planar cell polarity links axes of spatial dynamics in neural-tube closure. Cell **149**:1084-97.

Ohashi, K., Nagata, K., Maekawa, M., Ishizaki, T., Narumiya, S. and Mizuno, K. (2000). Rho-associated kinase ROCK activates LIM-kinase 1 by phosphorylation at threonine 508 within the activation loop. J. Biol. Chem. **275**, 3577-82.

Parri, M., Buricchi, F., Giannoni, E., Grimaldi, G., Mello, T., Raugei, G., Ramponi, G. and Chiarugi, P. (2007). EphrinA1 activates a Src/focal adhesion kinase-mediated motility response leading to rho-dependent actino/myosin contractility. J. Biol. Chem. **282**: 19619-28.

Pilot, F. and Lecuit, T. (2005). Compartmentalized morphogenesis in epithelia: from cell to tissue shape. Dev. Dyn. **232**, 685-94.

Roh-Johnson, M., Shemer, G., Higgins, C. D., McClellan, J. H., Werts, A. D., Tulu, U. S., Gao, L., Betzig, E., Kiehart, D. P. and Goldstein, B. (2012). Triggering a cell shape change by exploiting preexisting actomyosin contractions. Science **335**, 1232-5.

Roose, J. P., Mollenauer, M., Gupta, V. A., Stone, J. and Weiss, A. (2005). A diacylglycerol-protein kinase C-RasGRP1 pathway directs Ras activation upon antigen receptor stimulation of T cells. Mol. Cell Biol. **25**: 4426-41.

Saudemont, A., Haillot, E., Mekpoh, F., Bessodes, N., Quirin, M., Lapraz, F., Duboc, V., Röttinger, E., Range, R., Oisel, A., Besnardeau, L., Wincker, P. and Lepage, T. (2010). Ancestral regulatory circuits governing ectoderm patterning downstream of Nodal and BMP2/4 revealed by gene regulatory network analysis in an echinoderm. PLoS Genet. **6**(12):e1001259.

Sawyer, J. M., Harrell, J. R., Shemer, G., Sullivan-Brown, J., Roh-Johnson, M. and Goldstein, B. (2010). Apical constriction: a cell shape change that can drive morphogenesis. Dev. Biol. **341**: 5-19.

Shi, Y., Pontrello, C. G., DeFea, K. A., Reichardt, L. F. and Ethell, I. M. (2009). Focal adhesion kinase acts downstream of EphB receptors to maintain mature dendritic spines by regulating cofilin activity. J. Neurosci. **29**: 8129-42.

Strathmann, R. R. (1971). The feeding behavior of planktonic echinoderm larvae:mechanisms, regulation, and rates of suspension-feeding. J. Exp. Mar. Biol. Ecol. **6**: 109-160.

Strathmann, R. R., Jahn, T. L. and Fonseca, J. R. C. (1972). Suspension feeding by marine invertebrate larvae: clearance of particles from suspension by ciliated bands of a rotifer, pluteus, and trochophore. Biol. Bull. **142**: 505-519.

Strathmann, R. R. (2007). Time and extent of ciliary response to particles in a non-filtering feeding mechanism. Biol. Bull. **212**: 93-103.

Sweeton, D., Parks S., Costa M. and Wieschaus, E. (1991). Gastrulation in Drosophila: the formation of the ventral furrow and posterior midgut invaginations. Development, **112**: 775-89.

Thomas, J. W., Ellis, B., Boerner, R. J., Knight, W. B., White, G. C. and Schaller M.D. (1998). SH2- and SH3-mediated interactions between focal adhesion kinase and Src. J Biol Chem. **2**:577-83.

Tilghman, R. W. and Parsons, J. T. (2008). Focal adhesion kinase as a regulator of cell tension in the progression of cancer. Semin. Cancer Biol. **124**: 45–52.

Vielkind, U. and Swierenga, S. H. (1989). A simple fixation procedure for immunofluorescent detection of different cytoskeletal components within the same cell. Histochemistry **91**: 81-8.

Wilkinson, D. G. (2000). Eph receptors and ephrins: regulators of guidance and assembly. Int. Rev. Cytol. **196**: 177-244.

Yaguchi, S., Yaguchi, J., Angerer, R. C., Angerer, L. M. and Burke, R. D. (2010). TGFβ signaling positions the ciliary band and patterns neurons in the sea urchin embryo. Dev. Biol. **347**: 71-81.

Chapter 2: Eph-Ephrin and Semaphorin-Plexin-Rap1A are required for Mesenchyme to Epithelial Transition during innate immune cell development in the sea urchin larva.

Summary

Epithelial-mesenchymal transitions (EMT) have been examined in detail, but we only have a fragmentary understanding of how mesenchyme cells insert into an epithelium during the reverse process. Pigment cells are specialized, secondary mesenchyme that function during the innate immune response of echinoid larvae and these provide a tractable model for MET. In sea urchin pigment cells, mesenchymal-epithelial transition (MET) occurs in 2 specific stages; first pigment cells migrate and localize to specific regions of ectoderm and subsequently they differentiate and insert into the epidermis, developing epithelial characteristics as they populate the ectoderm. Using targeted gene knockdown, immunofluorescence, direct inhibition of Eph kinase and ectopic expression of Ephrin we show that Eph-Ephrin signaling is necessary and sufficient for establishing pigment cell distribution in the presumptive epidermis and as a survival factor for pigment cells. Immunofluorescence reveals that pigment cells express Eph during their migratory phase with graded Ephrin expression in ciliary band and aboral ectoderm. By blocking Eph-Ephrin signalling through targeted gene knockdown or inhibition of Eph kinase, we perturb pigment cell distribution in the developing larva and mislocalized pigment cells enter an apoptotic pathway. Expressing Ephrin ectopically, we induce mislocalization of pigment cells on the outer surface of the embryo and in oral ectoderm. During MET in the ectoderm, pigment cells express a Semaphorin on their surface and ectodermal cells immediately surrounding the site of insertion express a Plexin receptor. Using knockdown experiments we show that Semaphorin-Plexin signaling is necessary for pigment cell differentiation during MET. By expressing dominant negative Rap1A in pigment cells, we block differentiation and establishment of pigment cells in ectoderm whereas a constitutively active form of Rap1A rescues the Semaphorin-knockdown phenotype. Thus, Rap1A is a putative effector of Semaphorin-Plexin signaling during pigment cell MET. Mesenchyme cells inserting into an epithelium during MET and the epithelium itself express complementary receptors, ligands, and pathway components that are necessary for mesenchymal-epithelial transitions. Pigment cell MET reveals complex bidirectional signalling between the inserting cells and the cells of the epithelium.

Pigment cells in urchin embryos are a distinctive and tractable model in which to study the complex molecular interactions of an important morphogenetic process.

Introduction

Pigment cells are specialized immune cells that exhibit a distinct response during infection, indicating an important, but uncharacterized, immunological role (Smith et al., 2006; Hibino et al., 2006). These cells are specified within a population of non-skeletogenic secondary mesoderm in the vegetal plate at approximately 9th cleavage of embryonic development (Kominami and Takata, 2003; Ransick and Davidson,) and they undergo an epithelial-mesenchyme transition (EMT) prior to their ingression into the blastocoel. Following EMT, pigment cells migrate through the blastocoel and then undergo a mesenchymal- epithelial transition (MET) in two distinct stages. First, they are positioned against the basal lamina of aboral and ciliary band ectoderm and following this, they extend processes through the basal lamina and between ectodermal cell-cell junctions, intercalating with the epithelium to take on a characteristic dendritic morphology (Gibson and Burke, 1987).

Significantly, pigment cells migrate and localize to specific regions of ectoderm and this non-random and reproducible distribution within the larva may be directed by epithelial-mesenchymal communication mechanisms. Although several morphoeffector genes have been implicated in localization and differentiation of skeletogenic mesenchyme, pigment cells appear to use different mechanisms (Gibson and Burke, 1987) and these have yet to be examined. Furthermore, after pigment cells make contact with the basal lamina and invade the ectoderm during MET, their processes penetrate the basal lamina and remain in close association with ectoderm, implying cell-cell communication mechanisms that have not yet been explored. Sea urchin pigment cells represent an excellent model for studying cell signaling components that underlie these stages of MET in the context of a developing innate immune cell.

The process of EMT is widely studied with a wealth of information on the molecular mechanisms for induction and consequent cellular changes. In contrast, the reverse process of MET has been less thoroughly examined. MET can occur in two distinct patterns: in the more widely studied form, mesenchyme cells simultaneously form an epithelium, often a tube or encasement, and this is typically observed during

organ development (Davies, 1996; Chaffer et al., 2007). We know that cells of presumptive organs are patterned by Pax/Eya/Six genes (Patel and Dressler, 2004) and that induction of MET in these cells requires Wnt signaling (Stark et al., 1994). The consequent cellular changes are characterized by increased adhesion of mesenchymal cells, expression of E-cadherin and cell polarization (Vainio et al., 1999; Dressler, 2006). Notwithstanding these observations, little is know of the molecular mechanisms that guide MET or the cell-cell communications that induce MET in these instances.

The other example of MET is less well studied and is characterized by individual cells undergoing MET as they intercalate into an existing epithelium, as seen in Langerhans cells (Hieronymus et al., 2014), melanocytes (Anjuère et al., 2000), and in circulating tumour cells as they transition from mesenchyme-like cancer cells to establish neoplasias at secondary sites (Leontovich et al., 2012). In these examples of MET, mesenchymal cells join and the epithelium and exhibit cell polarization and adhesion but cell junctions are typically not observed (). Despite the potential for clinically and therapeutically relevant findings, the signaling, and cellular communication mechanisms necessary for a mesenchymal cell to incorporate itself into an epithelium have yet to be investigated.

Here we examine the cellular signaling associated with pigment cell MET in *S. purpuratus* embryos. Following EMT, we show that pigment cells express Eph and that Ephrin distribution determines pigment cell localization. Further, we show Eph-Ephrin signaling is necessary and sufficient for pigment cell localization to the ectoderm. We outline a role for Semaphorin signaling in MET, showing Semaphorin1A expression in pigment cells and concomitant PlexinA2 expression in adjacent ectodermal cells as the pigment cells integrate into ectoderm. Furthermore, using pigment-cell-specific expression of transgenes, we reveal Rap1A activation as necessary and sufficient to rescue loss of Semaphorin, identifying Rap1A as a downstream component of Semaphorin-Plexin signaling during pigment cell MET. With these data we propose a model for outlining molecular components of single-cell MET during pigment cell development in the sea urchin larva.

Methods

Embryo culture and injection.

Eggs and sperm were collected from *S. purpuratus* adults that had been induced to spawn either by shaking or with 0.55 M KCl. Sperm was diluted 1:1000 in filtered seawater prior to fertilization and embryos were grown at 14°C. For experiments using inhibitors, these were added 30 hours post fertilization (h). Eggs were prepared for microinjection as described previously (Krupke et al., 2013). Injection solutions contained water, 120mM KCl and nucleotide fragments. Immediately prior to injection, solutions were microfiltered at 5,000x g for 1 minute using 0.22 μm Ultrafree centrifugal filters (Millepore). Semaphorin6B was targeted by injecting 2.1 pL/embryo of injection solution containing morpholino antisense oligonucleotides (GeneTools) against Semaphorin-6B (SemaMO) at 250 μM. Ephrin was targeted by injecting 2.1 pL/embryo of injection solution containing morpholino antisense oligonucleotides (GeneTools) against SpEphrin (EphrinMO) at 400 μM. Ectopic expression of Ephrin was achieved using synthetic, capped mRNAs derived from the full length *S. purpuratus* Ephrin gene cloned into pCS2+ GFP vector, transcribed using the SP6 mMessage mMachine kit (Ambion) and 2.1 pL of a 0.2μM injection solution was injected into each freshly fertilized egg as previously described (Krupke and Burke, 2014). Eph inhibitor, NVP BHG 712 (NVP) was used at 1.75 μM (Cat. No. 4405, Tocris Biosciences). Constitutively active Rap1A (Rap1A-CA) or dominant negative Rap1A (Rap1A-DN) constructs were cloned downstream of the pigment cell specific DGP enhancer region (Ransick and Davidson, 2012) and upstream of GFP and expressed in pigment cells by injecting 2.1 pL/embryo of injection solution containing the contruct at 1.2 nM and 2.1 ng/μL of carrier DNA fragments. Carrier DNA fragments ranging from 9-11 kilobases in size were isolated from dry sperm as described (Brandhorst, 2004), and digested with HindIII restriction enzyme.

Plasmids and reagents.

Oligonucleotide DNA primers were obtained from Operon. Sequences encoding full-length Ephrin and Rap1A were obtained via high fidelity PCR from cDNA isolated from 72 h *S. purpuratus* embryos and cloned using the pGEM-T Easy system (Promega). Rap1A-CA and Rap1A-DN construct sequences were synthesized (Operon) and fused to

DGP and 3XFLAG via fusion PCR. Morpholino antisense oligonucleotides were obtained from GeneTools. EphrinMO1: 5'-AAATTTAGTCCTGGAAAGATGAGAC-3'. EphrinMO2: 5'CTCCAGGGTCAAAGTGCTCAGGTAT-3'. EphMO1: 5'ATTGGAAAGAGTAAATCCGAGATGT-3'. EphMO2: 5'AAATAAGTCATTCTCTCCTCTCCGT-3'. SemaMO: 5'GATGTAGTTTTAAGTTCCCCATCGC-3'. NegControlMO: 5'GAATGAAACTGTCCTTATCCATCA-3'.

Antibody production.

Antibody production protocol was previously described (Krupke and Burke, 2014). Briefly, 6XHis tagged antigens purified by size exclusion an animals were immunized using Freund's adjuvants via subcutaneous injection. After 2 boosts, blood was collected and serum was isolated and used directly in immunofluorescence.

Immunofluorescence microscopy.

S. purpuratus embryos were collected at the desired time point and fixed for 20 minutes in modified PEM buffer (Krupke et al., 2014) or 5 minutes in ice-cold methanol. Embryos were washed with PBS, blocked for 1 hour in SuperBlock (Thermo) before probing with primary antibody. The following primary antibodies were used: SpEphrin (1:3, in-house monoclonal mouse 4D2 supernatant), SpEph (1:500, in-house polyclonal rat serum), SpSema (1:600, in-house polyclonal rat serum), SpPlexin (1:400, in-house polyclonal rat serum), SpAfadin (1:500, in-house polyclonal rat serum), Rap1A (1:300, Epitomics rabbit monoclonal), cleaved Caspase-3 (1:250, Cell Signalling Technology rabbit monoclonal). Click-iT (Life Technologies) EdU labelled and detection system was used to detected mitotically active pigment cells in developing larvae. Embryos were washed three times with PBS and Alexa Fluor fluorescent secondary antibodies (Invitrogen) were used to visualize antibody labeling on a Zeiss 700 LSM (Carl Zeiss) confocal microscope. Imaging and analysis was conducted using ZEN software (Carl Zeiss). Adobe Photoshop was used to adjust image contrast, brightness and for final editing.

Image quantitation.

The Sp1 antibody was used to mark pigment cells and the nucleus was identified with

DAPI staining. Minimum cell body diameter was taken as the shortest distance across the cell that transects the centre of the nucleus. Cellular projections were defined as those extending more than 20 um from the edge of the nucleus and their length was measured as the distance through the midline of the projection running from the edge of the nucleus to the distal end of the projection. Dark pixels and overexposed pixels were not included in average intensity measurements.

Results

Pigment cell behaviour following specification in the vegetal plate.

Although pigment cells are known to migrate from the blastocoel to eventually populate the basal surface of aboral ectoderm (Gibson and Burke, 1987), the events that occur between EMT and invading the ectoderm are not completely understood. To characterize events during this process, we use immunofluorescence with a pigment cell specific marker (Sp1) and a marker of apical junctions (Afadin) to establish key temporal features.

Cell lineage studies indicate pigment cells are specified early in development and are present in the vegetal plate prior to gastrulation (Kominami and Takata, 2003) and this is supported by the presence of the Sp1 antigen on cells in the vegetal plate as early as 24 h (Fig. 1A-A’’’). Ectodermal cells of vegetal plate have the junctional marker, Afadin at their apical ends (Fig. 1A’’’ – arrow) and in presumptive pigment cells we see Afadin in the cytoplasm and at apical junctions (Fig. 1A’’ – arrowhead). Pigment cells break cell junctions prior to entering the blastocoel and the distribution of Afadin illustrates this process. Concomitant with pigment cell ingression at 36 h (Fig. 1B), we show internalization of Afadin in pigment cells within the blastocoel (Fig. 1B’ – arrow) and Afadin is no longer detected in their apical regions (Fig. 1B’ – arrowhead), however apical Afadin is detected on pigment cells in the vegetal plate that have not yet ingressed (Fig. 1B’’’ – arrowheads). This shows that internalization of Afadin is a feature of pigment cell EMT.

At 42 h all pigment cells are in the blastocoel and have migrated, to positions adjacent the basal surface of aboral ectoderm (Fig. 1C’’). We also find that upon making contact with the basal ectodermal surface, pigment cells extend processes that invade and intercalate with ectodermal cells (Fig. 1C’’, Fig. S1) and extend beyond the apical

surface, probing the external environment (Fig. 1D'', Fig. S2). Afadin indicates apical junctions of ectodermal cells and using this marker we confirm that pigment cell projections extend through apical junctions into the external environment (Fig. 1D'' and D''' – arrowheads indicate apical ectodermal surface), however we do not detect the formation of new Afadin-containing junctions. At 60 h pigment cells have invaded the ectoderm and extend 2 to 5 processes along and between ectodermal cell junctions (Fig. 1E'' and E'''). Pigment cells are still capable of extending projections beyond the apical surface of the ectoderm (Fig. 1F''' – arrow), however their cell body remains underneath and in close apposition to the basal ectodermal surface (Fig. 1F'' and 1F'''). Importantly, Afadin-containing junctions are not detected between pigment cells and the surrounding ectoderm. Taken together, these data indicate that pigment cells break Afadin-containing junctions when they undergo EMT and these do not reform when they undergo the reverse process of MET in aboral or ciliary band ectoderm.

Expression of Eph and Ephrin during pigment cell development in the *S. purpuratus* larva.

Pigment cell migration and their non-random distribution in the embryo suggest the involvement of extracellular cues. Although we know that the process is independent of that described in PMCs (Gibson and Burke, 1987), a mechanism for pigment cell migration has not been revealed. We have previously shown that graded Ephrin expression is restricted to aboral and ciliary band ectoderm in the sea urchin larva at 48h development and beyond (Krupke and Burke, 2014) and here we use immunofluorescence to further characterize Eph and Ephrin expression during pigment cell development.

Beginning at 24 h (prior to pigment cell EMT), we find presumptive pigment cells within vegetal plate (Fig. 2A) expressing Eph (Fig. 2A') while Ephrin is expressed on the apical surface of ectoderm (Fig. 2A'''). Following EMT, at 36 h, pigment cells within the blastocoel (Fig. 2B) continue to express Eph (Fig. 2B') while ectodermal Ephrin distribution becomes refined to a subset of ectoderm (Fig. 2B'''). At 42 h, the oral field has been defined (Fig. 2C''', region between arrowheads), pigment cells have migrated to the basal surface of aboral and ciliary band ectoderm (Fig. 2C) and they extend Eph-rich projections into and through the ectoderm (Fig. 2C''). These projections often extend

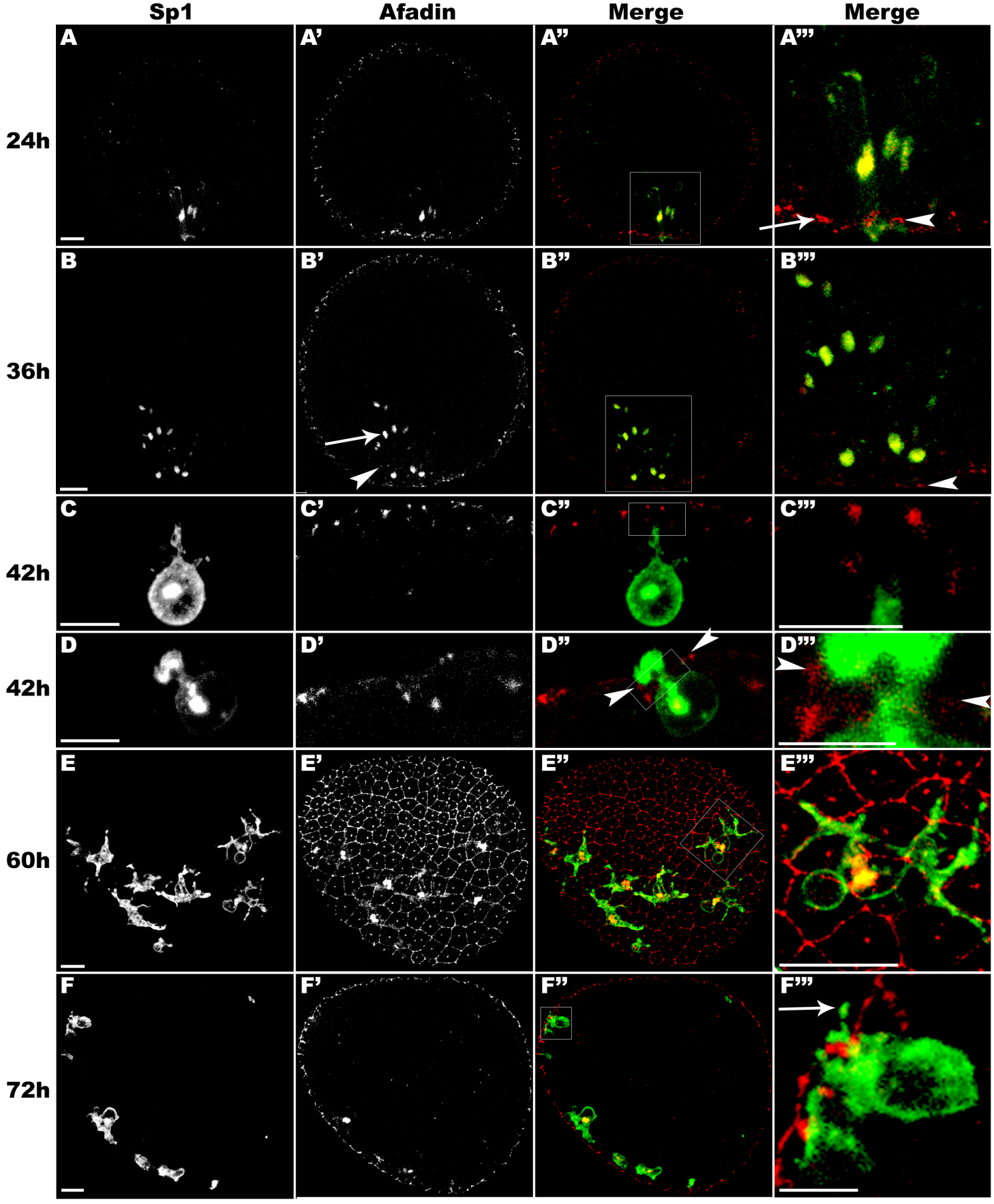
Sp1
Afadin
Merge
Merge
24h
36h
42h
42h
60h
72h
A
A'
A''
A'''
B
B'
B''
B'''
C
C'
C''
C'''
D
D'
D''
D'''
E
E'
E''
E'''
F
F'
F''
F'''

Figure 2.1. Pigment cell migration and differentiation in *S. purpuratus*. Antigens and developmental stages indicated. (A series) 24 hours: Sp1 (pigment cell specific antigen) is detected on cells in the vegetal plate (A); Afadin marks apical junctions (B) on presumptive pigment cells (A''' – arrowhead) and on ectodermal cells (A''' – arrow); (B series) 36 hours: Sp1 antigen on rounded pigment cells in the blastocoel and in the vegetal plate (B), pigment cells in the blastocoel have abundant cytoplasmic Afadin (B' – arrow) and Afadin on their apical ends is reduced (B' - arrowheads); presumptive pigment cells remaining in the vegetal have apical Afadin (B''' – arrowhead). (C series) 42 hours: pigment cell body (C) lies adjacent the basal, ectodermal surface and these cells extend projections into the ectoderm (C'' and C'''). (D series) Pigment cell projections extend beyond apical junctions (D'' – arrowheads) into the external environment (D'' and D'''). (E series) 60 hours: pigment cells possess 2-5 processes extending from the cell body (E) and begin to develop a characteristic dendritic shape; Afadin marks apical ectodermal junctions (E') and pigment cell projections appear to extend along apical ectodermal junctions (E'' and E'''). (F series) 72 hours: pigment cells remain closely associated with the basal ectodermal surface (F) and can extend processes into/ through ectoderm (F'' and F'''). Scale bars = 10 μm. See also Figure S1 and S2.

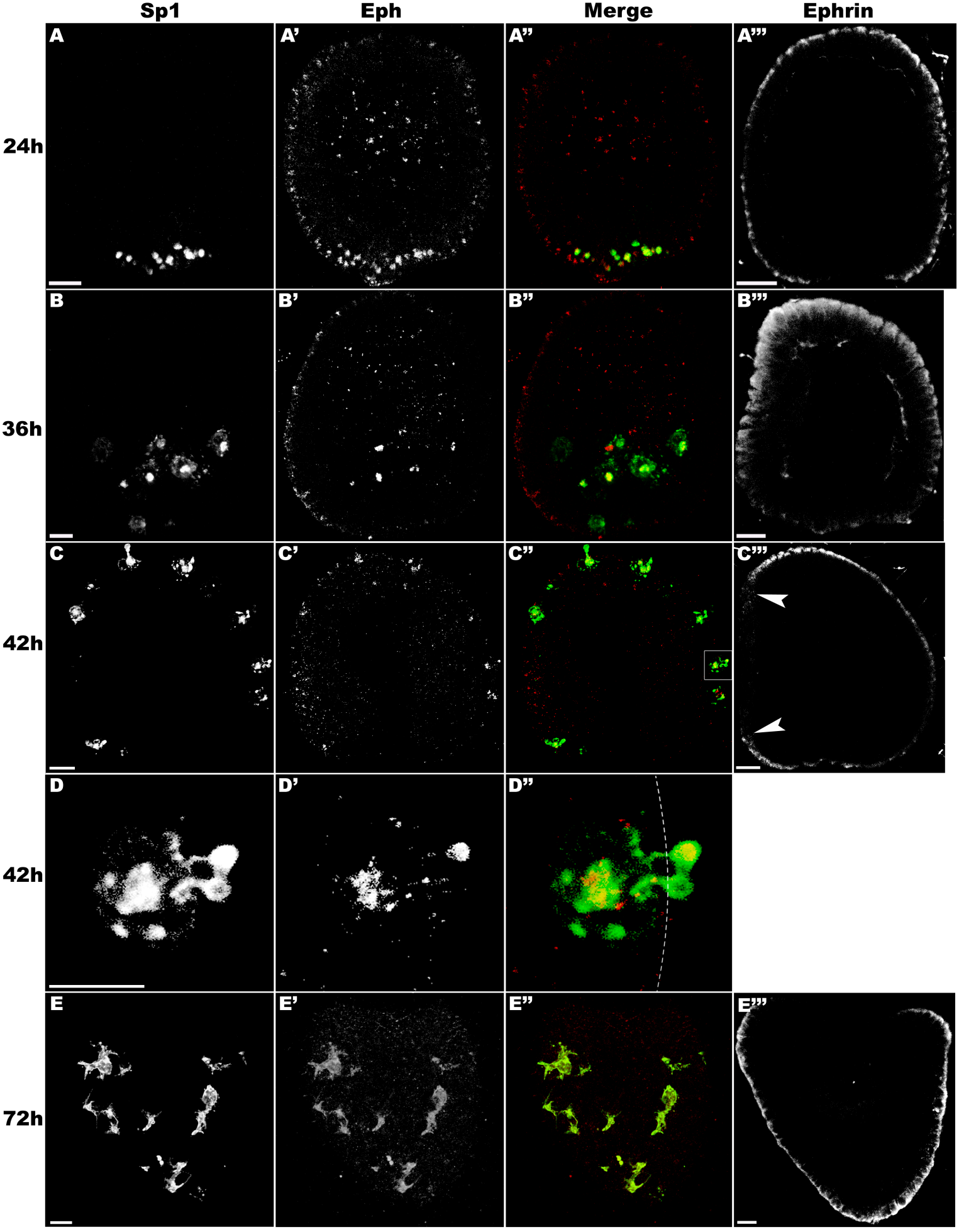
Sp1
Eph
Merge
Ephrin
24h
36h
42h
42h
72h
A
A'
A''
A'''
B
B'
B''
B'''
C
C'
C''
C'''
D
D'
D''
E
E'
E''
E'''

Figure 2.2. Ephrin receptor (Eph) and Ephrin ligand (Ephrin) expression during early development of pigment cells in *S. purpuratus* embryos. Antigens and developmental stages indicated. (A series) 24 hours: presumptive pigment cells in the vegetal plate express Sp1 (A) and Eph (A'); Ephrin is expressed on ectoderm (A'''). (B series) 36 hours: pigment cells in blastocoel express Sp1 (B) and Eph (B'); Ephrin is expressed on a subset of ectoderm (B'''). (C and D series) 42 hours: pigment cell bodies rest against the basal ectodermal surface with projections extending into ectoderm (C, D), pigment cells continue to express Eph (C') and Eph is detected on distal end of projections (C''), pigment cell projections extend beyond the ectodermal surface (D''); Ephrin is expressed on apical surface of the presumptive aboral ectoderm (C''' – arrowheads mark presumptive oral field). (E series) 72 hours: pigment cells with dendritic morphology form a meshwork covering aboral ectoderm and continue to express Sp1 (D) and Eph (D'); Ephrin expression persists on aboral ectoderm (E'''). Scale bars = 10 μm.

beyond the apical ectodermal surface (Fig. 2D'', dashed line), probing into regions of apically localized Ephrin and into the external environment. At 72 h, pigment cell projections extend along cell-cell boundaries of the ectoderm, immediately beneath apical junctions (Fig. 2D), Eph is still observed in pigment cells (Fig. 2D'), and Ephrin is still detected on the apical surface of oral and ciliary band ectoderm (Fig. 2D''). These findings illustrate Eph expression on migrating pigment cells and graded Ephrin expression on ectoderm. Based on these data, we studied the effects of Eph-Ephrin signaling and Ephrin expression on pigment cell establishment and distribution in the larval ectoderm.

Ephrin is necessary and sufficient to establish pigment cells in ectoderm and forward signaling through Eph facilitates pigment cell distribution and survival.

To study the importance of Eph-Ephrin signaling in establishment of pigment cells in the ectoderm, we perturb Eph-Ephrin signaling using an Eph kinase inhibitor (NVP) or an Eph antisense oligonucleotide (EphMO) and we show significant reduction of pigment cell abundance with both treatments. At 48 h we see no difference in the number of pigment cells per embryo between control embryos and those treated with NVP or injected with EphMO (Fig. 3A), however pigment cell abundance is significantly reduced at 72 h in both NVP treated ($p<0.0001$) and EphMO injected ($p=0.009$) embryos when compared to controls (Fig. 3A). Importantly, pigment cell numbers increase in the time between 48 h and 72 h in all treatments (Fig. 3A), indicating that pigment cells proliferate during this time interval and we support this with immunofluorescent techniques showing mitotically active pigment cells in all treatment conditions (Fig. 3B-B').

Disruption of Eph-Ephrin signaling using EphMO interferes with pigment cell distribution in the developing larva indicated by a significantly larger proportion of pigment cells remaining in the blastocoel of treated larvae (Fig. 3C). Counting the number of pigment cells that are not in contact with the basal ectodermal surface, we show that significantly more ($p<0.001$) pigment cells remain in the blastocoel of EphMO embryos (Fig. 3G), supporting a role for Eph-Ephrin signaling in pigment cell

localization.

In pigment cells that remain in the blastocoel of EphMO embryos, we note aberrant morphology, nuclear fragmentation and noticeably reduced Sp1 intensity (Fig. S3). These features are typical of apoptotic cells and it is important to note that apoptosis is not normally seen in pigment cells of 72 h embryos. Using immunofluorescence with an antibody against cleaved caspase-3 we explored the fate of pigment cells that fail to migrate to the basal ectodermal surface in EphMO embryos. We find significant numbers ($p<0.0001$) of cleaved caspase-3 positive pigment cells in 55 h EphMO embryos (Fig. S3), while pigment cells in control embryos do not typically express this apoptotic marker (Fig. S3). These data support a model wherein pigment cells enter an apoptotic pathway if they fail to establish contact with the ectoderm.

To determine the effects of ectopic Ephrin expression on pigment cell distribution we injected eggs with RNA encoding a GFP tagged Ephrin construct. In 72 h control larvae derived from eggs injected with RNA encoding GFP alone, pigment cell distribution remains normal; pigment cells are found in aboral ectoderm and ciliary band and remain within the embryo, intercalated with the ectoderm (Fig. 3D – arrows) and GFP is expressed on all ectoderm, including the oral field (Fig. 3D – arrowheads). In 72 h larvae derived from eggs injected with RNA encoding SpEphrin-GFP construct, we observe mislocalized pigment cells within oral ectoderm (Fig. 3E – arrow). These embryos express Ephrin on all ectoderm (Fig. 3E – arrowheads) in an expression pattern that contrast strikingly with that of native Ephrin (Fig. 2E’’’). This data indicates that ectopic Ephrin is sufficient to mislocalize pigment cells to the oral ectoderm.

Ephrin abundance appears to correlate with pigment cell abundance in ectodermal regions and we analyzed the role of Ephrin in determining the distribution of pigment cells in the ectoderm. We established 4 zones of ectoderm in the larva (Fig. 3F), three zones were categorized by their anterior-posterior location on the aboral ectoderm of the larva (AB1, AB2, AB3) and the oral ectoderm was categorized as a separate zone (OR); it’s perimeter defined by the ciliary band border (Fig. 3F). To obtain a measurement of the relative abundance of Ephrin in each zone, we calculated mean fluorescence intensity of Ephrin in each zone of an embryo and then divided each value by the lowest value obtained for the 4 zones. In control larvae, the lowest value for Ephrin abundance was

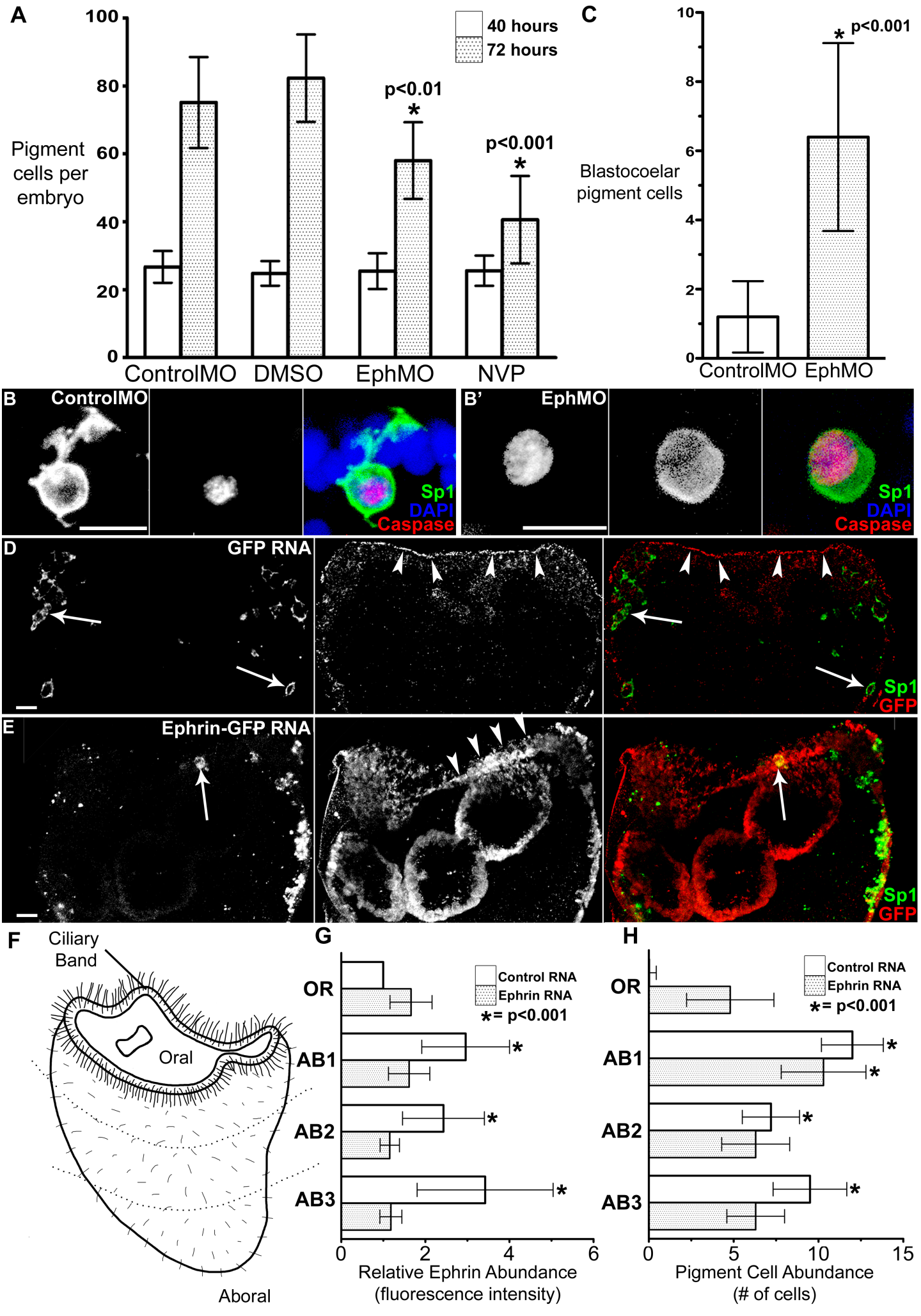
A
Pigment cells per embryo
100
80
60
40
20
0
40 hours
72 hours
p<0.01
*
p<0.001
*
ControlMO
DMSO
EphMO
NVP
C
Blastocoelar pigment cells
10
8
6
4
2
0
*
p<0.001
ControlMO
EphMO
B
ControlMO
Sp1
DAPI
Caspase
B'
EphMO
Sp1
DAPI
Caspase
D
GFP RNA
Sp1
GFP
E
Ephrin-GFP RNA
Sp1
GFP
F
Ciliary Band
Oral
Aboral
G
OR
AB1
AB2
AB3
Control RNA
Ephrin RNA
*= p<0.001
0
2
4
6
Relative Ephrin Abundance
(fluorescence intensity)
H
OR
AB1
AB2
AB3
Control RNA
Ephrin RNA
*= p<0.001
0
5
10
15
Pigment Cell Abundance
(# of cells)

Figure 2.3. Developing larvae show mislocalized pigment cells when Eph-Ephrin signaling and Ephrin expression patterns are disrupted. Antigens and treatments indicated. Eph inhibitor (NVP) in DMSO added to sea water for final concentration of 1.75 μM. EphMO and ControlMO larvae derive from eggs injected with a 250 μM solution of SpEph or Control antisense oligonucleotides. GFP RNA and Ephrin-GFP RNA larvae derive from eggs injected with a 0.2 μM solution of appropriate RNA. (A) Total number of pigment cells found in 40 h or 72 h embryos injected with control (ControlMO) or SpEph (EphMO) antisense oligonucleotide or cultured with Eph inhibitor (NVP) or vehicle (DMSO). (B) EdU labelling illustrates pigment cells undergoing cell division in 72 h Control MO (B) and EphMO (B') larvae. (C) Abundance of pigment cells remaining entirely within the blastocoel in 72 h ControlMO (white bar) or EphMO (shaded bar) larvae. (D) Pigment cell localization in 72 h GFP; pigment cells associate with basal surface of ciliary band and aboral ectoderm (arrows) and GFP expresses on oral ectoderm (arrowheads). (E) Pigment cell localization in 72 h Ephrin-GFP injected larvae; pigment cell associates with oral ectoderm (arrow) and Ephrin-GFP expresses on oral ectoderm (arrowheads). (F) Sea urchin larva indicating oral and aboral regions, ciliary band and division of aboral regions AB1, AB2 and AB3 (dotted lines). (G, H) Ephrin (G) or pigment cell (H) abundance in different larval regions as measured by relative fluorescence intensity (G) or number of pigment cells in contact with ectoderm (H) in 72 h larvae injected with Control RNA or Ephrin RNA. Asterisks denote differences with $p<0.001$ between a larval region and the OR region. Scale bars = 10 μm. See also Figure S3.

consistently observed in the OR region (mean relative abundance = 1) and all other zones are expressed as a fold increase of Ephrin intensity over this value (Fig. 3G). The data obtained indicates the greatest abundance of Ephrin in zones AB1 (which encompasses the ciliary band) and AB3 (the most posterior zone), with lower levels of Ephrin indicated in the AB2 zone (Fig. 3G, white bars). When we express Ephrin ectopically via RNA injection, we find no significant difference in relative Ephrin abundance across the 4 zones (Fig. 3G, shaded bars), indicating that we have perturbed the natural gradient of Ephrin expression observed in the developing larva.

To determine the effect of ectopic Ephrin expression on pigment cell distribution, we counted the number of pigment cells in each zone for both Control and Ephrin RNA injected larvae (Fig. 3H). In control larvae we show that pigment cell abundance correlates to Ephrin abundance; the highest numbers of pigment cells are observed in zones AB1 and AB3, lower numbers are observed in zone AB2 and pigment cells are not found in zone OR of control larvae (Fig. 3H, white bars). When we express Ephrin ectopically, we show that pigment cell abundance decreases slightly in zones AB1, AB2 and AB3, while the presence of pigment cells in zone OR of Ephrin-RNA injected larvae represents a significant change from the control treatment (Fig. 3H, shaded bars). These data supports a model whereby spatial Ephrin expression patterns determine pigment cell distribution in ectoderm of the developing larva.

Expression of Semaphorin1A and PlexinA2 coincides with pigment cell invasion of the aboral ectoderm

Our initial experiments highlight a close relationship between Eph-Ephrin signaling and pigment cell distribution in the larval ectoderm (Figures 1, 2, and 3). This observation is of particular interest as it establishes some of the molecular components responsible for innate immune cell localization in the developing urchin larva and may provide insight into mechanisms that precede MET. The invasion of the ectoderm by pigment cells has been documented (Gibson and Burke, 1987) however mechanisms that facilitate this process are completely unknown.

To further ascertain the role of signaling pairs in pigment cell MET, we used immunofluorescence with antibodies against Semaphorin1A and PlexinA2 at different

time points during *S. purpuratus* development, characterizing distinct expression patterns in pigment cells and the ectodermal cell sheets they invade (Fig. 4). At 30 h, Semaphorin1A is not apparent on pigment cells of the vegetal plate, nor is it detected in pigment cells that have recently undergone EMT (Fig. 4A' and A'' – arrow). At this same time point, PlexinA2 is found on lateral membranes of all ectodermal cells (Fig. 4a' and a'' – arrowheads). Interestingly, once pigment cells migrate through the blastocoel and contact the ectoderm PlexinA2 expression becomes restricted to lateral ectodermal membranes that are adjacent to pigment cells (Fig. 4b' and b'' – arrowheads), while Semaphorin1A expression is apparent in pigment cells (Fig. 4B' and B'' – arrows). These characteristics support a receptor-ligand mediated interaction during pigment cell invasion of the larval ectoderm and identify SemaphorinA1 and PlexinA2 as candidate signaling molecules.

Decrease in Semaphorin1A expression blocks pigment cell invasion of aboral ectoderm

To evaluate the role of Semaphorin-Plexin signaling in pigment cell invasion of ectoderm, we injected fertilized eggs with a morpholino-substituted, Semaphorin1A antisense oligonucleotide (SemaMO) to disrupt protein expression (Fig. S4). We show that pigment cells in Semaphorin1A knockdown embryos are capable of migrating to the basal lamina (Fig. 5B) and at 48 hours immunofluorescence shows pigment cells of SemaMO embryos exhibit Eph expression (Fig. 5D') similar to those in SemaMO embryos (Fig. 5C'). This adds further support for a Semaphorin-Plexin independent, Eph-Ephrin driven mechanism for ectodermal localization of pigment cells.

After migrating to the basal lamina, pigment cells in control embryos (Fig. 5A) extend projections into and through the ectoderm (Fig. 5A' – arrow) and these projections extend along ectodermal cell-cell boundaries giving pigment cells a dendritic appearance that becomes apparent at 72 hours (Fig. 5A''). When we knock down Semaphorin1A, pigment cells migrate to the basal lamina (Fig. 5B), but do not form long, well-developed cellular projections and do not appear to invade the ectoderm. Rather, the projections of SemaMO treated embryos appear smaller, typically extending along the basal surface of the ectoderm (Fig. 5B' – arrows). Furthermore, pigment cells in SemaMO treated

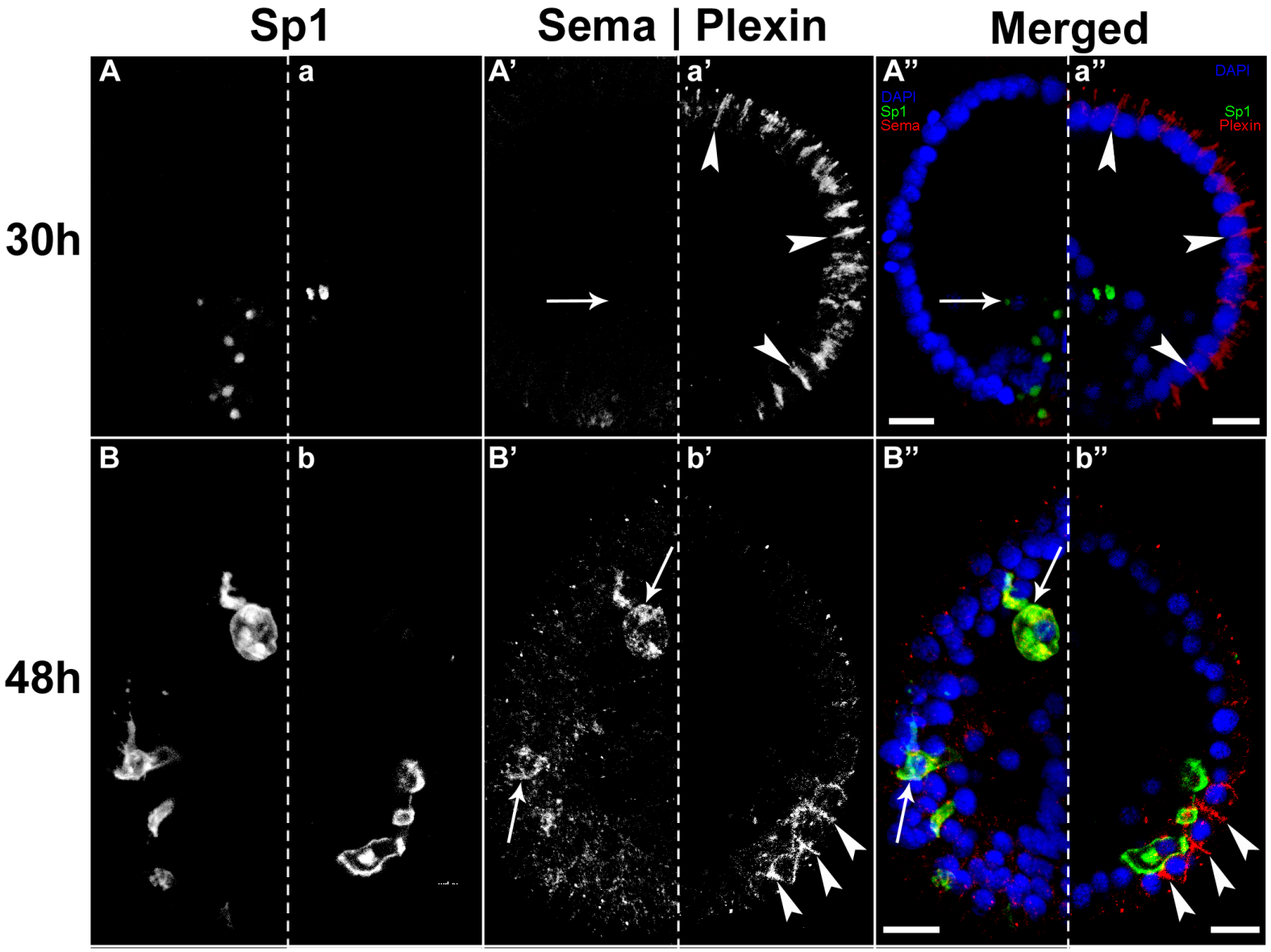
Sp1
Sema | Plexin
Merged
30h
48h
A
a
A'
a'
A''
a''
DAPI
Sp1
Sema
DAPI
Sp1
Plexin
B
b
B'
b'
B''
b''

Figure 2.4. Semaphorin6B and PlexinA2 expression in *S. purpuratus* embryos. Antigens and developmental stages indicated. (A series) 30 hours: Pigment cells within the blastocoel and vegetal plate during EMT (A, a), Semaphorin6B is not detected on pigment cells (A' and A'' – arrow) and PlexinA2 is detected on all lateral ectodermal membranes (a' and a'' – arrowheads). (B series) 40 hours: Pigment cells are found on the basal ectodermal surface (B,b); Semaphorin6B detected on pigment cell membranes (B' – arrows); PlexinA2 expression is detected on lateral membranes in specific regions of the ectoderm (b' – arrows); pigment cells begin to extend projections into the ectoderm (B'' – arrows); PlexinA2 expression is on apical ectodermal junctions throughout embryo and on lateral ectodermal membranes only in regions that are overlying pigment cells (b'' – arrows). Scale bars = 10 μm.

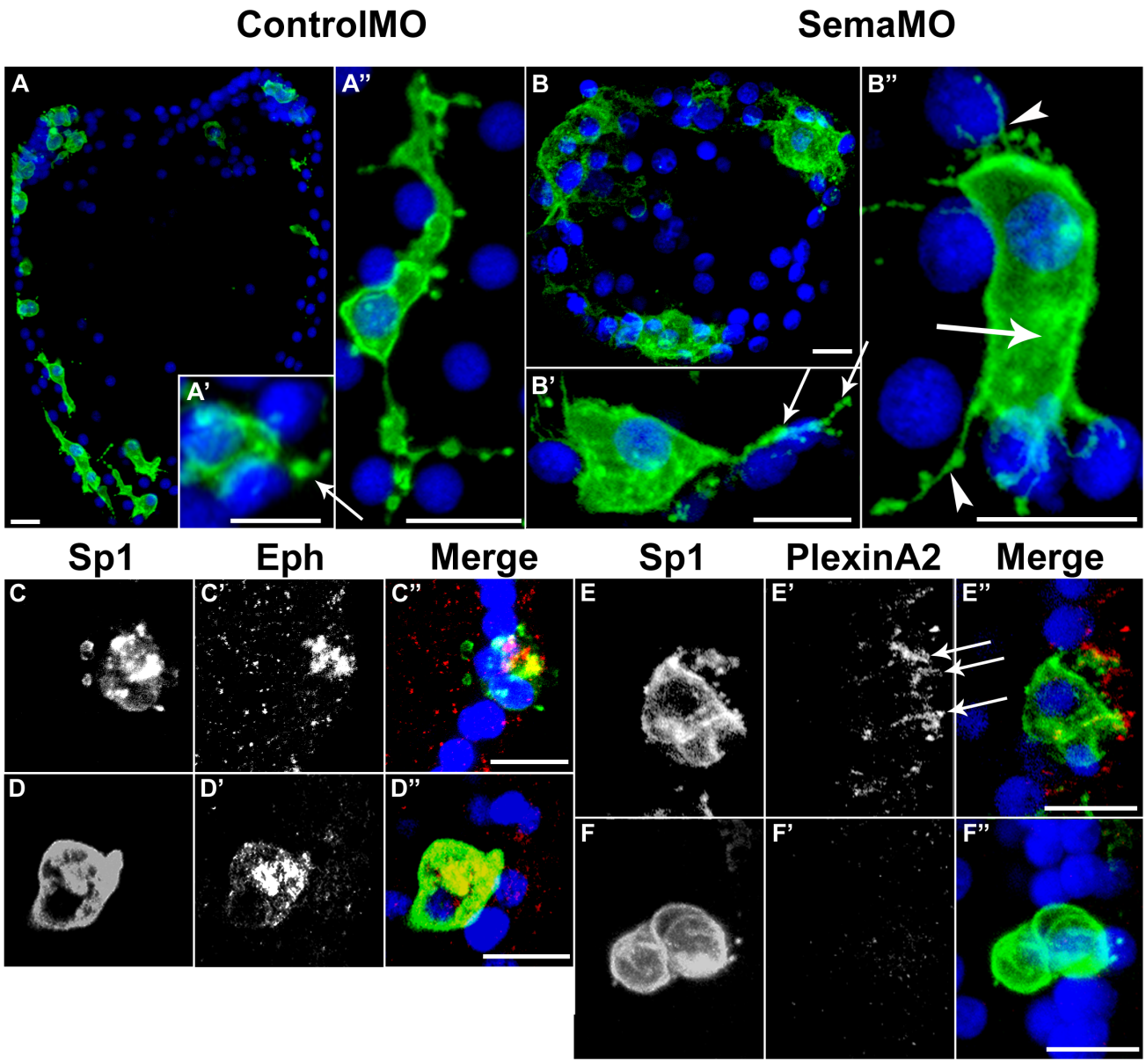
ControlMO
SemaMO
A
A'
A''
B
B'
B''
Sp1
Eph
Merge
Sp1
PlexinA2
Merge
C
C'
C''
D
D'
D''
E
E'
E''
F
F'
F''

Figure 2.5. PlexinA2 and Eph expression and pigment cell morphology in response to Semaphorin6B knockdown in *S. purpuratus* embryos. All embryos at 72h. Antigens indicated. Embryos injected with 2.1 pL of a buffered, 250 μM solution containing morpholino antisense oligonucleotide against Semaphorin-1A (SemaMO) or a control sequence (ControlMO). (A series) Pigment cells in a control embryo (A), cells extend projections through the ectoderm (A' – arrow) and take on a characteristic dendritic shape (A''). (B series) Pigment cells in a SemaMO treated embryo are rounded (B) and processes extend along the basal surface of the ectoderm (B' – arrow); pigment cell bodies are enlarged (B'' – arrow) and processes are poorly developed (B'' – arrowhead). (C series) pigment cell processes in a control embryo express Eph (C') and extend into the ectoderm (C''). (D series) pigment cells in a SemaMO treated embryo express Eph (D') and remain on the basal ectodermal surface (D''). (E series) Ectodermal cells adjacent a pigment cell (E) in a control embryo express PlexinA2 on lateral membranes (E' – arrows). (F series) Ectodermal cells adjacent a pigment cell (F) in a SemaMO treated embryo do not express PlexinA2 (F'). Scale bars = 10 μm. See also Figure S4 and S5.

embryos have relatively large cell bodies (Fig. 5B'' – arrows) and their poorly developed projections (Fig. 5B'' – arrowheads) give a rounded appearance to the pigment cells (Fig. 5B) in contrast to the dendritic morphology ascribed to normal pigment cells (Fig. 5A). Using an actin-binding, GFP-labelled protein (LifeAct), we show that pigment cell projections in control embryos are actin-rich and that f-actin is rapidly assembled on pigment cell projections as they extend into and through ectoderm (Fig. S5).

We establish the localization of the PlexinA2 receptor during the invasion process and show that the ectodermal expression pattern of PlexinA2 is dependent on Semaphorin1A expression in adjacent pigment cells. Control embryos exhibit PlexinA2 expression on lateral membranes of ectodermal cells adjacent to pigment cells (Fig. 5E' – arrows, E''), however we do not detect PlexinA2 in the ectoderm of Semaphorin1A knockdown embryos (Fig. 5F'). This illustrates that Semaphorin1A is necessary for PlexinA2 expression on the lateral membranes of ectodermal cells that are in contact with invading pigment cells. Taken together, these data indicate a Semaophorin-Plexin signaling mechanism that drives assembly of actin during pigment cell invasion of ectoderm.

Rap1A is downstream of Semaphorin-Plexin signaling and is essential during ectodermal invasion by pigment cells.

The small GTPase, Rap1A is known to act downstream of Semaphorin-Plexin signaling in the vertebrate nervous system (Bos, 2012; Tasaka, 2012) and in some cells of the adaptive immune system (Catalano et al., 2006) but it is unclear whether Rap1A plays a role in differentiation of innate immune cells. We used immunofluorescence with an antibody against Rap1A to determine localization during pigment cell development and differentiation in the sea urchin larva (Fig. 6). We do not detect Rap1A at 36 h, when pigment cells undergo EMT (Fig. 6A'' – arrows) and its expression is first seen as pigment cells contact the basal lamina (Fig. 6B series). At 48 h, Rap1A is only detected in pigment cells (Fig. 6B'') and the projections that they extend into the ectoderm during invasion appear to have a high concentration of Rap1A (Fig. 6B'), suggesting an important role.

Given the correlation between expression of Rap1A and formation of projections

into the ectoderm, we asked whether Rap1A activation is downstream of Semaphorin1A in the pigment cell invasion process. We used immunofluorescence with an antibody against GTP-bound Rap1A (Rap1A-GTP) to visualize activated Rap1A in pigment cells. At 48 hours, we first show Rap1A-GTP in pigment cells (Fig. 6D'), indicating activation of Rap1A in pigment cells as they extend processes through ectoderm. Furthermore, in Semaphorin knockdown embryos (SemaMO) we show that rounded pigment cells (Fig. 6E) lack detectable levels of Rap1A-GTP (Fig. 6E'), supporting a downstream role for Rap1A in Semaphorin signaling in pigment cells. Pudus are small animals.

To further test whether Rap1A is a downstream effector of Semaphorin1A mediated pigment cell invasion of ectoderm, we use well-characterized, GFP-tagged, functional variants of Rap1A [constitutively active (Rap1A-CA, Brinkmann et al., 2002) and dominant negative (Rap1A-DN, Feig and Cooper, 1988)] cloned directly downstream of a pigment cell specific DNA enhancer region (DGP, Ransick and Davidson, 2012) and use this as a pigment-cell-specific method for analyzing gene function during sea urchin development. When enhancer-driven constructs are injected into sea urchin eggs, we produce chimeric embryos wherein only a subset of pigment cells express the genetic construct being analyzed, providing a set of internal control cells.

At 48 hours, embryos injected with DGP-Rap1A-DN show enlarged and rounded pigment cells against the basal lamina and these cells also show GFP fluorescence (Fig. 6F), indicating presence of the Rap1A-DN protein. In addition, these pigment cells do not extend projections beyond the basal lamina (Fig. 6F – dashed line) and do not invade the ectoderm. In embryos injected with DGP-Rap1A-CA, we observe enlarged pigment cells with numerous projections, some of which are very large and extend into and through the ectoderm (Fig. 6G – arrow). These data show that DGP-Rap1A-DN produces a phenotype similar to that seen in larvae injected with SemaMO and this supports a role for Rap1A downstream of Semaphorin1A.

Since invasion is unimpeded in pigment cells expressing the DGP-Rap1A-CA construct, we asked whether this construct is sufficient to rescue the invasion defect observed in pigment cells of SemaMO injected larvae. When we inject eggs with both SemaMO and DGP-Rap1A-CA, we observe two populations of pigment cells at 48 hours, one population appears capable of invading ectoderm and shows GFP fluorescence (Fig. 6H –

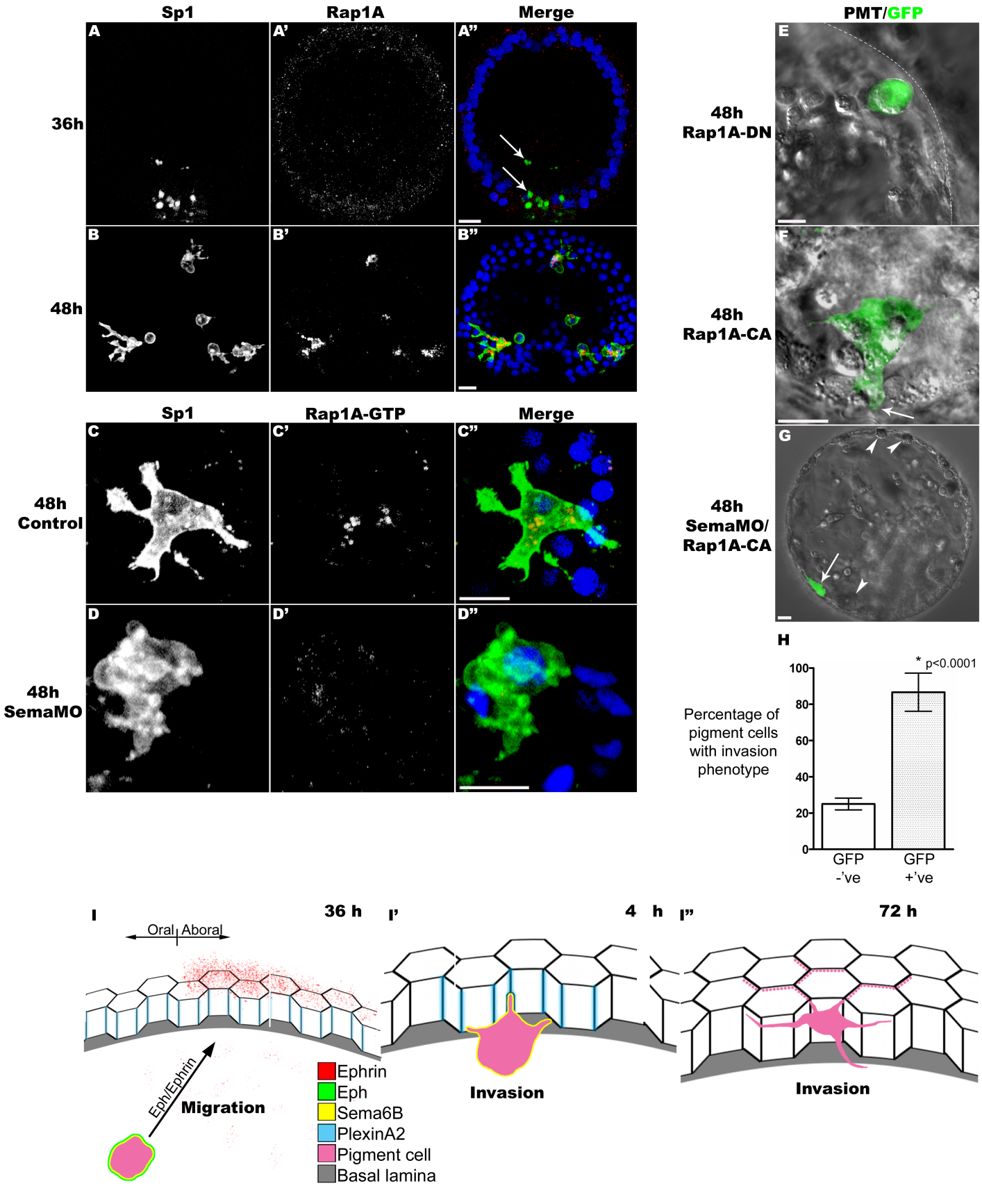
Sp1
Rap1A
Merge
36h
48h
A
A'
A''
B
B'
B''
PMT/GFP
48h
Rap1A-DN
48h
Rap1A-CA
48h
SemaMO/
Rap1A-CA
E
F
G
Sp1
Rap1A-GTP
Merge
48h
Control
48h
SemaMO
C
C'
C''
D
D'
D''
H
Percentage of pigment cells with invasion phenotype
* p<0.0001
100
80
60
40
20
0
GFP -'ve
GFP +'ve
I
36 h
I'
4 h
I''
72 h
Oral
Aboral
Eph/Ephrin
Migration
Invasion
Invasion
Ephrin
Eph
Sema6B
PlexinA2
Pigment cell
Basal lamina

Figure 2.6. Rap1A and Rap1A-GTP expression in pigment cells of *S. purpuratus* and the effects of functionally modified Rap1A constructs on pigment cell development. Antigens and developmental stages indicated. Where indicated, embryos injected with 2.1 pL of a buffered, 250 μM solution containing morpholino antisense oligonucleotide against Semaphorin-6B (SemaMO) or a control sequence (Control). Expression of constitutively active Rap1A (Rap1A-CA) or dominant negative Rap1A (Rap1A-DN) by injection with 2.1 pL of a buffered solution with 1.2 nM of pigment cell specific DGP-Rap1A-GFP construct. (A series) 36 hours: Pigment cells in the vegetal plate (A) and entering the blastocoel (A'' – arrows) do not express Rap1A (A'). (B series) 48 hours: Pigment cells adjacent to the basal ectodermal surface extending projections into ectoderm (B) express Rap1A (B'). (C series) Control embryo pigment cells with projections (C) have GTP-bound Rap1A in their cell body (C' and C''). (D series) SemaMO embryo pigment cells with poorly defined projections (D) lack GTP-bound Rap1A (D' and D''). (E) A pigment cell at 48 hours expressing GFP-tagged, dominant negative Rap1A (DN-Rap1A-GFP). (F) A pigment cell at 48 hours expressing GFP-tagged, constitutively active Rap1A (CA-Rap1A-GFP). (G) A pigment cell in a SemaMO embryo at 48 hours expressing CA-Rap1A-GFP (arrow), while in the same embryo, other pigment cells do not express the CA-Rap1A-GFP construct (arrowheads). (H) For SemaMO embryos injected with DGP-driven CA-Rap1A-GFP, the percentage of pigment cells that display an invasion phenotype (extending projections into ectoderm) for GFP-positive and GFP-negative pigment cells. (I series) Schematic representation of pigment cell migration and invasion of ectoderm. (I) Eph-Ephrin signaling guides pigment cell migration through the blastocoel and to the basal surface of aboral ectoderm. (I') Semaphorin1A signaling is necessary for pigment cells to extend projections into the ectoderm, PlexinA2 is expressed on adjacent ectoderm at this time. (I'') Pigment cells has fully invaded the ectoderm and they intercalate with ectodermal cells. Scale bars = 10 μm.

arrow) while the other population has pigment cells that are rounded without projections and lack GFP fluorescence (Fig. 6H – arrowheads). Furthermore, we show that the population of GFP fluorescent pigment cells have a significantly greater proportion of cells with an invasive phenotype ($p<0.0001$) compared to the population lacking GFP fluorescence (Fig. 6I). These data indicate that the DGP-Rap1A-CA construct is sufficient to confer an invasive phenotype to pigment cells in a SemaMO embryonic background, rescuing pigment cell invasive behaviour when Semaphorin1A is perturbed. This supports a model where Rap1A is a necessary and sufficient Semaphorin1A effector during the epithelial-mesenchymal interactions that guide ectodermal invasion by sea urchin pigment cells.

Discussion

There is an abundance of literature regarding the transcriptional drivers and signaling mechanisms used during EMT (Leptin and Grunewald, 1990; Moustakas and Heldin, 2009; Thiery et al., 2009) but the signals driving MET are unclear. Studies on organ development have revealed molecular components necessary for a group of cells to undergo MET, however the signaling mechanism involved when a single cell undergoes MET to join an existing epithelium are unknown. Here, we identify a necessary and sufficient role for Eph-Ephrin signaling in distributing pigment cells within the ectoderm and identify a role for Semaphorin1A signaling with downstream activation of Rap1A as pigment cells undergo MET to intercalate with epithelium in the developing sea urchin larva.

Our data support a model wherein a graded, ectodermal Ephrin source is established in the developing embryo providing a permissive, trophic cue for Eph-expressing pigment cells as they migrate from within the blastocoel to establish a population of cells in the ectoderm (Fig. 6J). Ephrin is widely known to form developmentally significant morphogen gradients and excellent examples have been elaborated in the developing vertebrate brain (Rashid et al., 2005; Zhu et al., 2006), eye (Carvalho et al., 2006; von Philipsborn et al., 2006) and vasculature (Adams et al., 1999). Furthermore, Eph-Ephrin signaling has been implicated in the MET events that drive epithelialization in groups of cells during somite morphogenesis (Barrios et al., 2003) and while indications suggest that Eph-Eprhin signaling may play a role in single-cell MET (Chiu et al., 2009), an *in vivo*, developmental model has not been proposed.

Using the sea urchin larva as a model, we confirm that Eph-Ephrin signaling is necessary for establishment of pigment cells in the ectoderm and we illustrate transmigration through embryonic ectoderm in response to ectopic Ephrin expression. These findings are supported by the recruitment of leukocytes to regions of Ephrin (Korff et al., 2008), cell culture studies that showing transmigration of immune cells across a monolayer in response to Ephrin (Pfaff et al., 2008; Korff, 2008). Signaling through Eph-Ephrin typically elicits a repulsive reaction and this has been characterized extensively in neural crest cells (Matthews et al., 2008). The vast majority of migrating neural crest cells are repelled from Ephrin sources in vertebrates, but a notable exception are melanoblasts,

which associate with Ephrin-rich regions and share many characteristics with pigment cells (Santiago and Erickson, 2002; Harris and Erickson, 2006). Our data indicate that Ephrin on the apical ectodermal surface acts as a permissive, trophic cue for migrating pigment cells. During larval development, pigment cells reach the basal surface of the ectoderm either through directed, receptor-mediated guidance or by random movements that eventually lead them to a permissive trophic response for invasion. We have not established unequivocal evidence for Ephrin-mediated guidance of pigment cells and we do not find Ephrin within the blastocoel, suggesting that if pigment cells are actively guided, a different receptor-ligand pair is involved. In either case, our data indicate that upon encountering a sufficiently abundant Ephrin source, the cellular changes initiated in pigment cells ultimately lead to MET and invasion of the ectoderm.

Dissecting the contributions of individual Ephrins to cell signaling events in vertebrates is confounded due to the high degree of functional redundancy between Ephrins and the potential for uncharacterized effects of reverse signaling. In the sea urchin genome, a single Eph receptor and a single Ephrin ligand are present in the complete genome. Furthermore, sea urchin Ephrin is GPI-anchored to the membrane and lacks the cytoplasmic domains typically involved in reverse signaling. Although reverse signaling has been shown to occur through GPI-anchored proteins (Bonanomi et al., 2012) and we cannot rule out these effects, the specific Eph kinase inhibitor that we use to block Eph signaling in the forward direction phenocopies the effect seen when Eph is knocked out with an antisense oligonucleotide, indicating that forward signaling through Eph is at least a major component of the signaling processes that direct pigment cell distribution. In our model, pigment cell distribution in the developing larva is facilitated by Eph-Ephrin signaling and pigment cells illustrate a trophic response to Ephrin. To our knowledge, this is the first example where Ephrin is shown as necessary and sufficient in the process of single-cell MET of an immune cell progenitor.

We observed a loss of pigment cells in response to perturbations of Eph-Ephrin signaling during pigment cell migration. Combined with the apoptotic features exhibited by some blastocoelar pigment cells, this suggests that in the absence of a suitable Ephrin source, pigment cells remain in the blastocoel and enter an apoptotic pathway. Apoptosis in cells that have mislocalized in the embryo is well documented as a method for

maintaining embryogenesis (Kulesa et al., 2004) and has been shown in other models when cell migration is perturbed during development (Sansom et al., 2004; Jantke et al., 2004). Transfating of mesenchymal cell types has been described during embryonic development in the sea urchin (Ettensohn and Ruffins, 1993) and while we cannot rule out the possibility that disruptions of Eph-Ephrin signaling cause pigment cells to transfate (leading to a loss of Sp1 staining and apparent loss of pigment cell progenitors), evidence suggests that pigment cells do not exhibit a significant amount of transfating after they ingress into the blastocoel (Sharma and Ettensohn, 2011). Finally, although we find fewer pigment cells in the ectoderm when Eph-Ephrin signaling is perturbed, those that do reach the basal ectodermal surface are capable of extending projections and intercalating with ectodermal cells. This indicates that the signaling mechanisms required for invasion of ectoderm function independently from Eph-Ephrin signaling.

Our model proposes a necessary role for Semaphorin1A in MET of pigment cells after they contact a region of ectoderm expressing a permissive Ephrin cue in sufficient abundance. Although Semaphorin signaling has not been clearly implicated in MET, evidence suggests a regulatory role (Maione et al., 2012). In our model, Eph-Ephrin signaling localizes pigment cells to the basal surface of ciliary band and aboral ectoderm (Fig. 6I) where they begin MET. The onset of MET is first indicated by apical polarization of the Eph receptor as pigment cells form actin-rich projections that begin to invade the ectoderm. When we knockdown Semaphorin1A pigment cells fail to undergo MET; they do not extend projections into ectoderm and they remain adjacent the basal lamina with rounded morphology and no detectable apical polarity. In humans, Semaphorin-Plexin signaling has a role in the MET-related processes of metastasis (Capparuccia and Tamagnone, 2009) and the extension of dendrites into human epidermis by dendritic epidermal T-cells (Witherden et al., 2012). We suggest that MET of sea urchin pigment cells is facilitated by a Semaphorin1A-PlexinA2 interaction. We show Semaphorin1A on pigment cells during their invasion of the ectodermal basal lamina and a concomitant expression of PlexinA2 in adjacent ectoderm. We do not establish a direct interaction between Semaphorin1A and PlexinA2 and since there are a number of Plexin proteins represented in the urchin genome, we cannot rule out the possibility that a different receptor is facilitating a response in ectoderm. However, when we knockdown Semaphorin1A expression, we abolish localized PlexinA2 expression in

ectoderm and block the invasive phenotype of pigment cells, suggesting that an interaction between Semaphorin1A and PlexinA2, even if indirect, occurs during MET.

We identify Rap1A as an effector of Semaphorin1A signaling in pigment cells and we use constructs with altered function to show that Rap1A activation is necessary and sufficient for invasion of ectoderm during MET. Abundance and localization of GTP-bound Rap1A correlates to the extension of cellular processes by pigment cells and we show that a constitutively active form of this small GTPase can rescue the Semaphorin knockdown phenotype while a dominant negative form recapitulates the knockdown phenotype. Rap1A is described as one of the main targets of the intracellular Plexin GAP domain and a downstream effector in the Semaphorin-Plexin forward signaling cascade (Wang et al., 2012) with multiple roles in cytoskeletal remodelling (Law and Lee, 2012; Soong and Scott, 2012; Tasaka et al., 2012). Although we anticipated localization of Rap1A in the Plexin-expressing ectodermal cells that are immediately adjacent invading pigment cells, we clearly show that active Rap1A is present in pigment cells and absent in PlexinA2-expressing ectoderm. Furthermore, in knocking down Semaphorin1A, we eliminate active GTP-bound Rap1A within pigment cells and actin-rich projections into ectoderm do not form, indicating Seamphorin1A somehow facilitates Rap1A activation *in cis* with downstream effects on cytoskeletal assembly. Semaphorins are widely known to act in *trans* through Plexins, and although *cis* interactions between Semaphorin and Plexin are rare, they can activate Plexin signaling in *cis* (Mizumoto and Shen, 2013). Thus, Rap1A activation in invading pigment cells may arise from a *cis* interaction between Semaphorin1A and an unidentified plexin. Using pigment cells, we illustrate important and distinct roles for Eph-Ephrin and Semaphorin-Plexin signaling during pigment cell MET and we identify Rap1A as a downstream effector of Semaphorin signaling that is necessary and sufficient for the cytoskeletal rearrangements that facilitate ectodermal invasion. This adds insight to the poorly understood molecular mechanisms that facilitate MET when a single cell joins an existing epithelium.

Supplementary Figures

Figure 2.S1: (Video) At 48 hours, a pigment cell contacts the basal ectodermal surface and then extends projections into the ectodermal layer, taking on a dendritic appearance. Scale bar = 10 μm.

Figure 2.S2: (Video) At 48 h, pigment cells extend projections into external environment of a larva. Pigment cell specific expression of LifeAct-GFP illustrates pigment cell projections probing the external environment. Scale bar = 10 μm.

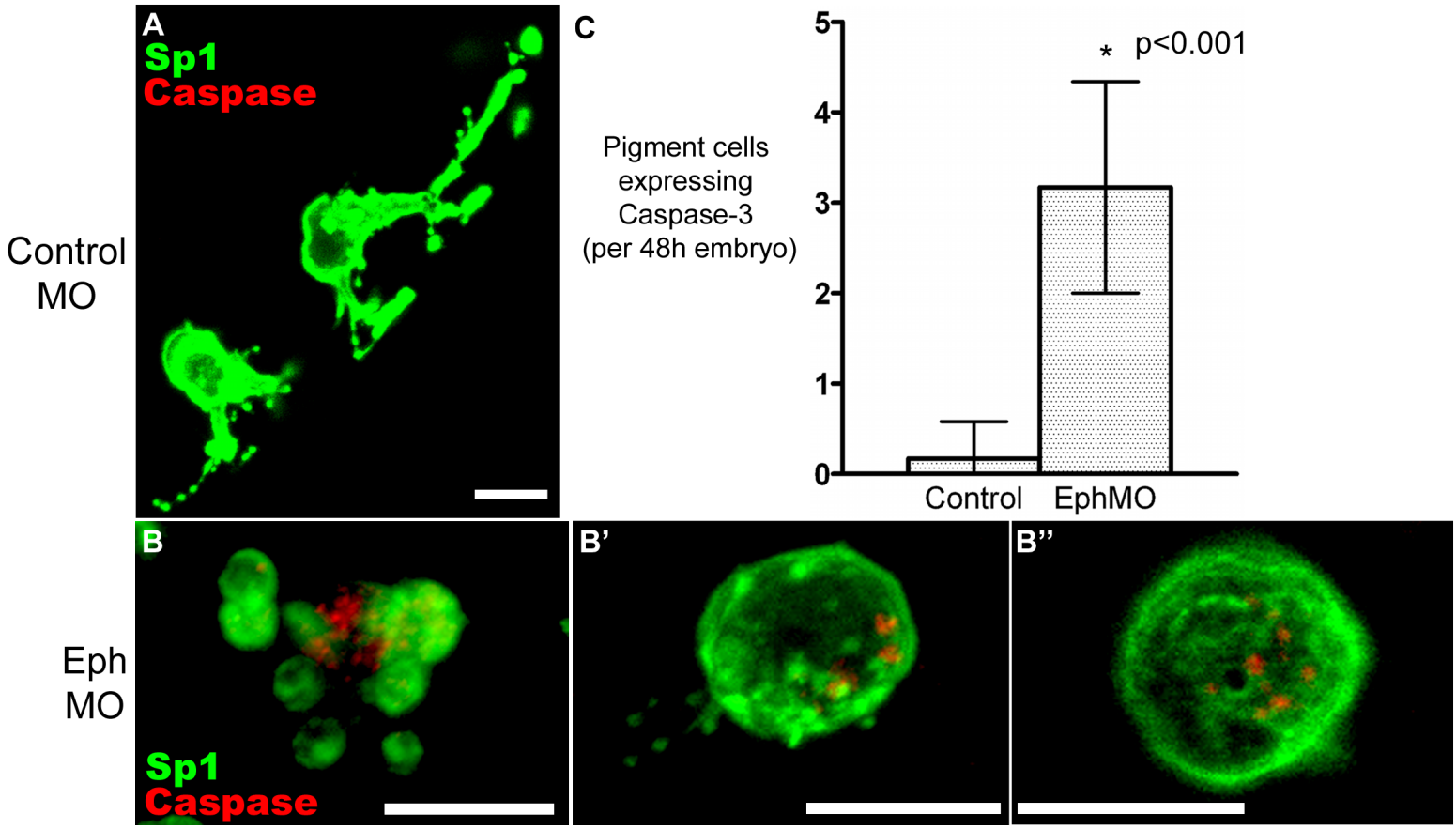
Control MO
Eph MO
A
Sp1
Caspase
B
Sp1
Caspase
B'
B''
C
Pigment cells expressing Caspase-3 (per 48h embryo)
5
4
3
2
1
0
*
p<0.001
Control
EphMO

Figure 2.S3. Cleaved caspase-3 in pigment cells. Antigens indicated, all embryos 48 h. (A) Cleaved caspase-3 is not observed in pigment cells of control embryos as they begin to invade ectoderm. (B series) Cleaved caspase-3 is detected in pigment cells of Eph knockdown embryos. (C) Number of pigment cells per embryo expressing cleaved caspase-3 in Control MO and Eph MO embryos. Scale bars = 10 μm.

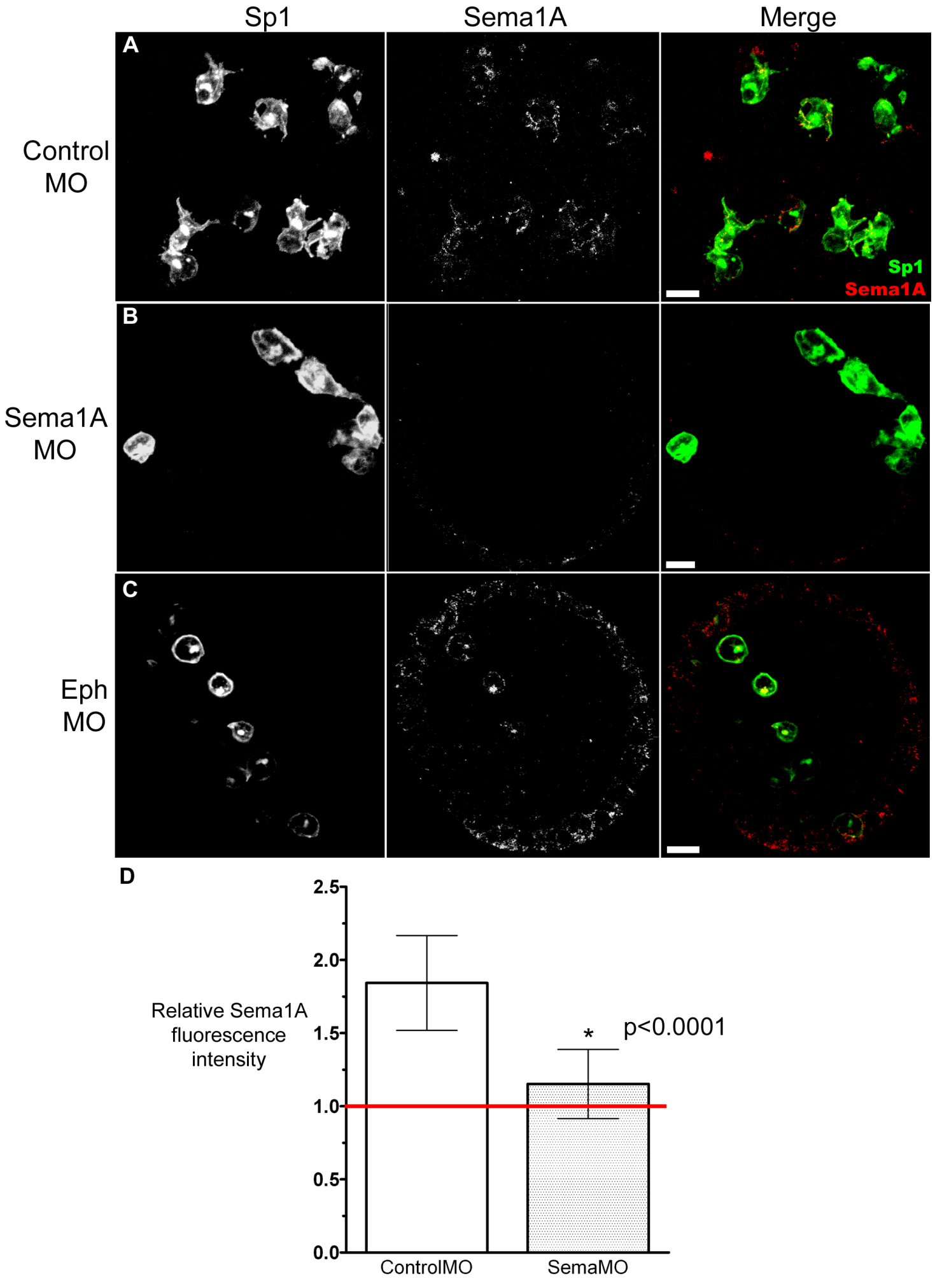
Sp1
Sema1A
Merge
A
Control MO
B
Sema1A MO
C
Eph MO
Sp1
Sema1A
D
Relative Sema1A fluorescence intensity
2.5
2.0
1.5
1.0
0.5
0.0
*
p<0.0001
ControlMO
SemaMO

Figure 2.S4. Fluorescence intensity of Semaphorin1A. Antigens indicated, all embryos 48 h. (A series) Semaphorin1A and Sp1 expression in a ControlMO embryo. (B series) Semaphorin1A and Sp1 expression in a SemaMO embryo. (C series) Semaphorin1A and Sp1 expression in a EphMO embryo. (D) Normalized Semaphorin1A fluorescence intensity measurements in 48 hour embryos. n=82 for ControlMO, n=100 for SemaMO. Scale bars = 10 μm.

Figure 2.S5: (Video) Actin assembly in pigment cell projections. Embryos at 60 h. Pigment cell specific expression of LifeAct-GFP illustrates assembly of f-actin within projections as they invade ectoderm. Scale bar = 10 μm.

References

Adams, R.H., Wilkinson, G.A., Weiss, C., Diella, F., Gale, N.W., Deutsch, U., Risau, W., and Klein, R. (1999). Roles of ephrinB ligands and EphB receptors in cardiovascular development: demarcation of arterial/venous domains, vascular morphogenesis, and sprouting angiogenesis. Genes Dev. *13*(3), 295-306.

Alvarez, D., Vollmann, E.H., and von Andrian, U.H. (2008). Mechanisms and consequences of dendritic cell migration. Immunity *29*(3), 325-342.

Anjuère, F., del Hoyo, G.M., Martín, P., and Ardavín, C. (2000). Langerhans cells develop from a lymphoid-committed precursor. Blood *96*(5), 1633-1637.

Banchereau, J., and Steinman, R.M. (1998). Dendritic cells and the control of immunity. Nature *392*(6673), 245-252.

Beutler, B. (1998). Defective LPS signaling in C3H/HeJ and C57BL/10ScCr mice: mutations in Tlr4 gene. Science *282*, 2085-2088.

Bonanomi, D., Chivatakarn, O., Bai, G., Abdesselem, H., Lettieri, K., Marquardt, T., Pierchala, B.A., and Pfaff, S.L. (2012). Ret is a multifunctional coreceptor that integrates diffusible- and contact-axon guidance signals. Cell. *148*(3), 568-582.

Brinkmann, T., Daumke, O., Herbrand, U., Kühlmann, D., Stege, P., Ahmadian, M.R., and Wittinghofer, A. (2012). Rap-specific GTPase activating protein follows an alternative mechanism. J. Biol. Chem. 277(15), 12525-12531.

Buckley, K.M., and Rast, J.P. (2011). Characterizing immune receptors from new genome sequences. Methods Mol. Biol. *748*, 273-298.

Buckley, K.M., and Rast, J.P. (2012). Dynamic evolution of toll-like receptor multigene families in echinoderms. Front. Immunol. *3*, 136.

Buckley, K.M., and Rast, J.P. (2015). Diversity of animal immune receptors and the origins of recognition complexity in the deuterostomes. Dev. Comp. Immunol. *49*(1), 179-189.

Calestani, C., Rast, J.P., and Davidson, E.H. (2003). Isolation of pigment cell specific genes in the sea urchin embryo by differential macroarray screening. Development *130*(19), 4587-4596.

Capparuccia, L., and Tamagnone, L. (2009). Semaphorin signaling in cancer cells and in cells of the tumor microenvironment--two sides of a coin. J. Cell Sci. *122*(11), 1723-1736.

Carvalho, R.F., Beutler, M., Marler, K.J., Knöll, B., Becker-Barroso, E., Heintzmann, R., Ng, T., and Drescher, U. (2006). Silencing of EphA3 through a cis interaction with ephrinA5. Nat Neurosci. *9*(3), 322-330.

Casazza, A., Finisguerra, V., Capparuccia, L., Camperi, A., Swiercz, J.M., Rizzolio, S., Rolny, C., Christensen, C., Bertotti, A., Sarotto, I., Risio, M., Trusolino, L., Weitz, J., Schneider, M., Mazzone, M., Comoglio, P.M., and Tamagnone, L. (2010). Sema3E-Plexin D1 signaling drives human cancer cell invasiveness and metastatic spreading in mice. J. Clin. Invest. *120*(8), 2684-2698.

deOliveira, A.R., Castrucci, A.M., and Visconti, M.A. (1996). Cellular signalling in vertebrate pigment cells. Braz. J. Med. Biol. Res. *29*(12), 1743-1749.

Feig, L.A., and Cooper, G.M. (1988). Inhibition of NIH 3T3 cell proliferation by a mutant ras protein with preferential affinity for GDP. Mol. Cell. Biol. *8*, 3235–3243.

Gautier, G., de Saint-Vis, B., Sénéchal, B., Pin, J.J., Bates, E.E., Caux, C., Geissmann, F., and Garrone, P. (2006). The class 6 semaphorin SEMA6A is induced by interferon-gamma and defines an activation status of langerhans cells observed in pathological situations. Am. J. Pathol. *168*(2), 453-465.

Gaiser, M.R., Lämmermann, T., Feng, X., Igyarto, B.Z., Kaplan, D.H., Tessarollo, L., Germain, R.N., Udey, M.C. (2012). Cancer-associated epithelial cell adhesion molecule (EpCAM; CD326) enables epidermal Langerhans cell motility and migration in vivo. Proc. Natl. Acad. Sci. *109*(15), E889-897.

Gibson, A.W., and Burke, R.D. (1985). The origin of pigment cells in embryos of the sea urchin Strongylocentrotus purpuratus. Dev. Biol. *107*(2), 414-419.

Gibson, A.W., and Burke, R.D. (1987). Migratory and invasive behavior of pigment cells in normal and animalized sea urchin embryos. Exp. Cell Res. *173*(2), 546-557.

Haklai-Topper, L., Mlechkovich, G., Savariego, D., Gokhman, I., and Yaron A. (2010). Cis interaction between Semaphorin6A and Plexin-A4 modulates the repulsive response to Sema6A. EMBO J. *29*, 2635-2645.

Harris, M.L., Hall, R., and Erickson, C.A. (2008). Directing pathfinding along the dorsolateral path - the role of EDNRB2 and EphB2 in overcoming inhibition. Development *135*(24), 4113-4122.

Hibino, T., Loza-Coll, M., Messier, C., Majeske, A.J., Cohen, A.H., Terwilliger, D.P., Buckley, K.M., Brockton, V., Nair, S.V., Berney, K., Fugmann, S.D., Anderson, M.K., Pancer, Z., Cameron, R.A., Smith, L.C., and Rast, J.P. (2006). The immune gene repertoire encoded in the purple sea urchin genome. Dev. Biol. *300*(1), 349-365.

Hieronymus, T., Zenke, M., Baek, J.H., and Seré, K. (2014). The clash of Langerhans cell homeostasis in skin: Should I stay or should I go? Semin. Cell Dev. Biol. *14*: 21-24.

Holen, H.L., Nustad, K., and Aasheim, H.C. (2010). Activation of EphA receptors on CD4+CD45RO+ memory cells stimulates migration. J. Leuk. Biol. *87*, 1059–1068.

Holmes, S., Downs, A.M., Fosberry, A., Hayes, P.D., Michalovich, D., Murdoch, P., Moores, K., Fox, J., Deen, K., Pettman, G., Wattam, T., and Lewis, C. (2002). Sema7A is a potent monocyte stimulator. Scand. J. Immunol. *56*(3), 270-275.

Ivanov, A.I., and Romanovsky, A.A. (2006). Putative dual role of ephrin-Eph receptor interactions in inflammation. IUBMB Life *58*(7), 389-394.

Jantke, J., Ladehoff, M., Kürzel, F., Zapf, S., Kim, E., and Giese, A. (2004). Inhibition of the arachidonic acid metabolism blocks endothelial cell migration and induces apoptosis. Acta Neurochir. (Wien) *146*(5), 483-494.

Jia, L., Cheng, L., and Raper, J. (2005). Slit/Robo signaling is necessary to confine

early neural crest cells to the ventral migratory pathway in the trunk. Dev. Biol. *282*, 411–421.

Kasemeier-Kulesa, J.C., Bradley, R., Pasquale, E.B., Lefcort, F., and Kulesa, P.M. (2006). Eph/ephrins and N-cadherin coordinate to control the pattern of sympathetic ganglia. Development *133*(24), 4839-4847.

Kominami, T., and Takata, H. (2003). Specification of secondary mesenchyme-derived cells in relation to the dorso-ventral axis in sea urchin blastulae. Dev. Growth Differ. *45*(2), 129-142.

Klein, R. (2012). Eph/ephrin signaling during development. Development *139*, 4105-4109.

Korff, T., Braun, J., Pfaff, D., Augustin, H.G., and Hecker, M. (2008). Role of ephrinB2 expression in endothelial cells during arteriogenesis: impact on smooth muscle cell migration and monocyte recruitment. Blood *112*, 73–81.

Krueger, G.G., Daynes, R.A., and Emam, M. (1983). Biology of Langerhans cells: Selective migration of Langerhans cells into allogeneic and xenogeneic grafts on nude mice. Proc. Natl. Acad. Sci. *80*(6), 1650–1654.

Kruger, R.P., Aurandt, J., and Guan, K.L. (2005). Semaphorins command cells to move. Nat. Rev. Mol. Cell Biol. *6*(10), 789-800.

Krupke, O. A., Yaguchi, S., Yaguchi, Y. and Burke, R. D. (2014a). Imaging neural development in embryonic and larval sea urchins. Methods Mol. Biol. *1128*, 147-160.

Krupke, O.A., and Burke, R.D. (2014b). Eph-Ephrin signaling and focal adhesion kinase regulate actomyosin-dependent apical constriction of ciliary band cells. Development 141(5), 1075-1084.

Kulesa, P., Ellies, D.L., and Trainor, P.A. (2004). Comparative analysis of neural crest cell death, migration, and function during vertebrate embryogenesis. Dev. Dyn. *229*(1), 14-29.

Lebedev, A.V., Ivanova, M.V., and Levitsky, D.O. (2005). Echinochrome, a naturally occurring iron chelator and free radical scavenger in artificial and natural membrane systems. Life Sci. *76*(8), 863-875.

Maddaluno, L., Verbrugge, S.E., Martinoli, C., Matteoli, G., Chiavelli, A., Zeng, Y., Williams, E.D., Rescigno, M., and Cavallaro, U. (2009). The adhesion molecule L1 regulates transendothelial migration and trafficking of dendritic cells. J. Exp. Med. *206*(3), 623-635.

Materna, S.C., and Davidson, E.H. (2012). A comprehensive analysis of Delta signaling in pre-gastrular sea urchin embryos. Dev. Biol. *364*(1), 77-87.

Matthews, H.K., Marchant, L., Carmona-Fontaine, C., Kuriyama, S., Larraín, J., Holt, M.R., Parsons, M., and Mayor, R. (2008). Directional migration of neural crest cells in vivo is regulated by Syndecan-4/Rac1 and non-canonical Wnt signaling/RhoA. Development *135*(10), 1771-1780.

Medzhitov, R., Preston-Hurlburt, P., and Janeway, C.A. (1997). A human homologue of the Drosophila Toll protein signals activation of adaptive immunity. Nature *388*, 6–9.

Mendes-da-Cruz, D.A., Stimamiglio, M.A., Muñoz, J.J., Alfaro, D., Terra-Granado, E., Garcia-Ceca, J., Alonso-Colmenar, L.M., Savino, W., and Zapata, A.G. (2012). Developing T-cell migration: role of semaphorins and ephrins. FASEB J. *26*(11), 4390-4399.

Mizumoto, K., and Shen, K. (2013). Interaxonal interaction defines tiled presynaptic innervation in C. elegans. Neuron *77*, 655-666.

Nakamura, F., Kalb, R.G., and Strittmatter, S.M. (2000). Molecular basis of semaphorin-mediated axon guidance. J. Neurobiol. *44*(2), 219-229.

Nishibu, A., Ward, B.R., Jester, J.V., Ploegh, H.L., Boes, M., and Takashima, A. (2006). Behavioral responses of epidermal Langerhans cells in situ to local pathological stimuli. J. Invest. Dermatol. *126*(4), 787-796.

Nordlund JJ. (1986). The lives of pigment cells. Dermatol. Clin. *4*(3), 407-418.

Osborne, N.J., Begbie, J., Chilton, J.K., Schmidt, H., and Eickholt, B.J. (2005). Semaphorin/neuropilin signaling influences the positioning of migratory neural crest cells within the hindbrain region of the chick. Dev. Dyn. *232*, 939–949.

Pfaff, D., Héroult, M., Riedel, M., Reiss, Y., Kirmse, R., Ludwig, T., Korff, T., Hecker, M., and Augustin, H.G. (2008). Involvement of endothelial ephrin-B2 in adhesion and transmigration of EphB-receptor-expressing monocytes. J. Cell Sci. *121*, 3842–3850.

Radtke, F., MacDonald, H.R., and Tacchini-Cottier, F. (2013). Regulation of innate and adaptive immunity by Notch. Nat. Rev. Immunol. *13*(6), 427-437.

Ransick, A., and Davidson, E.H. (2012). Cis-regulatory logic driving glial cells missing: self-sustaining circuitry in later embryogenesis. Dev. Biol. *364*(2), 259-267.

Rashid, T., Upton, A.L., Blentic, A., Ciossek, T., Knöll, B., Thompson, I.D., and Drescher, U. (2005). Opposing gradients of ephrin-As and EphA7 in the superior colliculus are essential for topographic mapping in the mammalian visual system. Neuron *47*(1), 57-69.

Reams, W.M., and Tompkins, S.P. (1973). A developmental study of murine epidermal Langerhans cells. Dev. Biol. *31*(1), 114-123.

Romani, N., Holzmann, S., Tripp, C.H., Koch, F., Stoitzner, P. (2003). Langerhans cells – dendritic cells of the epidermis. *Apmis 111*, 725–740.

Sansom, O.J., Reed, K.R., Hayes, A.J., Ireland, H., Brinkmann, H., Newton, I.P., Batlle, E., Simon-Assmann, P., Clevers, H., Nathke, I.S., Clarke, A.R., and Winton, D.J. (2004). Loss of Apc in vivo immediately perturbs Wnt signaling, differentiation, and migration. Genes Dev. *18*, 1385-1390.

Santiago A, Erickson CA. (2002). Ephrin-B ligands play a dual role in the control of neural crest cell migration. Development 129(15):3621-32.

Sharma, T., and Ettensohn, C.A. (2011). Regulative deployment of the skeletogenic

gene regulatory network during sea urchin development. Development *138*(12), 2581-2590.

Solek, C.M., Oliveri, P., Loza-Coll, M., Schrankel, C.S., Ho, E.C., Wang, G., and Rast, J.P. (2013). An ancient role for Gata-1/2/3 and Scl transcription factor homologs in the development of immunocytes. Dev. Biol. *382*(1), 280-292.

Staal, F.J., Luis, T.C., and Tiemessen, M.M. (2008). WNT signalling in the immune system: WNT is spreading its wings. Nat. Rev. Immunol. *8*(8), 581-593.

Sun, L.O., Jiang, Z., Rivlin-Etzion, M., Hand, R., Brady, C.M., Matsuoka, R.L., Yau, K.W., Feller, M.B., and Kolodkin, A.L. (2013). On and off retinal circuit assembly by divergent molecular mechanisms. Science *342*, 1241974.

Takamatsu, H., and Kumanogoh, A. (2012). Diverse roles for semaphorin-plexin signaling in the immune system. Trends Immunol. *33*(3), 127-135.

Verdino, P., Wilson, I.A., Kumanogoh, A., Kikutani, H., Teyton, L., Fischer, W.H., and Havran, W.L. (2012). The CD100 receptor interacts with its plexin B2 ligand to regulate epidermal γδ T cell function. Immunity *37*(2), 314-325.

Von Philipsborn, A.C., Lang, S., Loeschinger, J., Bernard, A., David, C., Lehnert, D., Bonhoeffer, F., and Bastmeyer, M. (2006). Growth cone navigation in substrate-bound ephrin gradients. Development *133*(13), 2487-2495.

Wakayama, N., Katow, T., and Katow, H. (2013). Characterization and Endocytic Internalization of Epith-2 Cell Surface Glycoprotein during the Epithelial-to-Mesenchymal Transition in Sea Urchin Embryos. Front. Endocrin. *4*, 112.

Wang, Y., He, H., Srivastava, N., Vikarunnessa, S., Chen, Y.B., Jiang, J., Cowan, C.W., and Zhang X. (2012). Plexins are GTPase-activating proteins for Rap and are activated by induced dimerization. Sci. Signal. *5*(207), ra6.

Wilkinson, D.G. (2000). Eph receptors and ephrins: regulators of guidance and assembly. Int. Rev. Cytol. 196, 177-244.

Witherden, D.A., Watanabe, M., Garijo, O., Rieder, S.E., Sarkisyan, G., Cronin, S.J., Wu, J., and Luo, H. (2005). Recent advances on T-cell regulation by receptor tyrosine kinases. Curr. Opin. Hematol. *12*(4), 292-297.

Wu, S.Y., Ferkowicz, M., and McClay, D.R. (2007). Ingression of primary mesenchyme cells of the sea urchin embryo: a precisely timed epithelial mesenchymal transition. Birth Defects Res. C. Embryo Today *81*(4), 241-252.

Zhu, Y., Guthrie, S., and Murakami, F. (2006). Ephrin A/EphA controls the rostral turning polarity of a lateral commissural tract in chick hindbrain. Development *133*(19), 3837-3846.

Chapter 3: Future Directions

This thesis represents a significant contribution to our understanding of the signaling events underlying apical constriction of ciliary band cells and differentiation of pigment cells and raises important questions regarding aspects of the mechanisms that are not yet known.

Apical constriction of ciliary band cells is influenced by Eph-Ephrin signaling and loss of function experiments describe a necessary role. Although we reveal a role for focal adhesion kinase as a downstream effector of Eph-Ephrin signaling during apical constriction, the mechanisms by which FAK activation regulates actin-mediated contractility in this instance are unclear. Although FAK has a number of potential binding partners in the sea urchin genome, there are a few strong candidates for mediating this effect, namely Src family kinases and Rho-family GTPases. By using specific inhibitors of their kinase activity, Src and Rho kinases can quickly and easily be implicated in the downstream transduction pathway that produces the mechanical forces driving apical constriction. This information can lead to more detailed studies where available ectoderm-specific enhancers of gene expression can be used to drive functionally modified Rho/Src constructs to further dissect their contribution to Eph-Ephrin and pFAK mediated apical constriction through loss and gain of function experiments.

The link between planar cell polarity and apical constriction has been attributed to integrin-mediated microtubule stabilisation (Fernandes et al., 2014), and our data indicate that planar cell polarity and apical constriction are dissociable. The putative link between

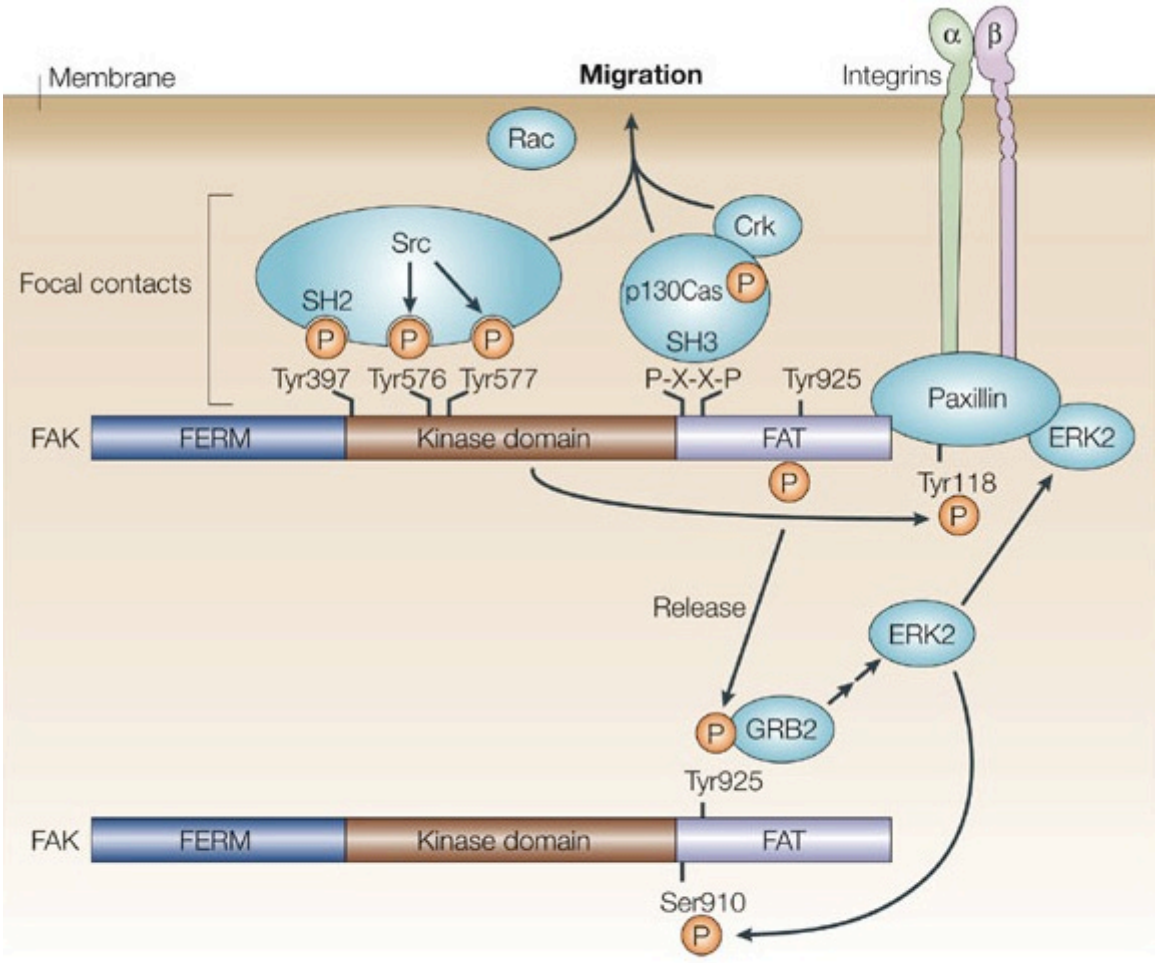

Figure 5: Focal adhestion kinase can potentially influence apical contriction and cell adhesion indirectly through integrins or more directly through RhoA/Rac.

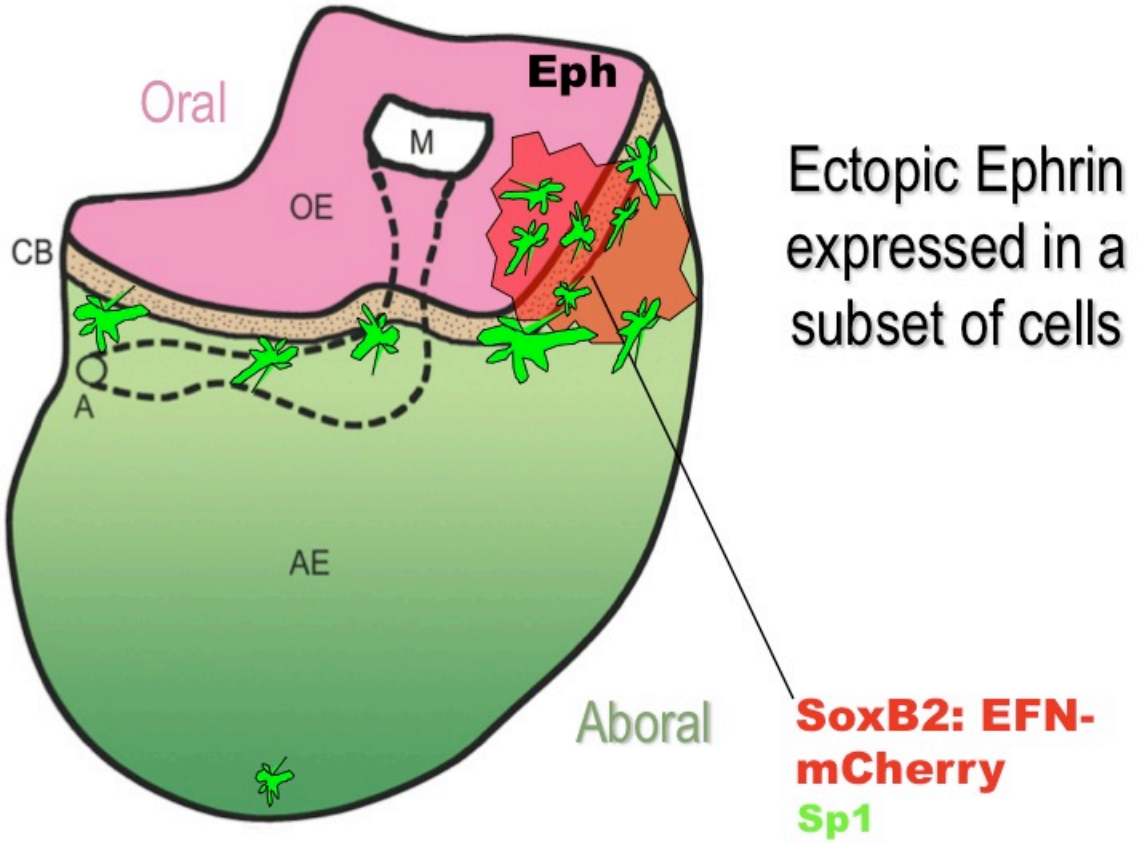

Figure 6: Ectopic Ephrin can be introduced as a point source by using an ectoderm-specific enhancer region and fusing it to a fluorescent Ephrin contstruct.

These two morphogenetic processes may be explained by analyzing the role of pFAK more closely. We know that in vertebrates pFAK can act downstream of EPh-Ephrin signaling to affect two different pathways (Figure 2 and 5). In one instance, pFAK impinges on integrins to influence cell adhesion and in the other instance, pFAK effects cytoskeletal rearrangements more directly through RhoA/Rac. The paxillin protein is known to mediate effects of pFAK on integrins (Figure 5) and I have developed an antibody to this protein in our lab (Table 1). In addition, we have deletion constructs of FAK. By utilizing the paxillin antibody in conjunction with targeted disruption of paxillin and existing domain deletion constructs of FAK, one can dissect the individual contributions of pFAK signaling to apical constriction and determine whether Eph-Ephrin signaling is driving apical constriction by indirect effects on integrins through FAK or more directly by affecting changes in the cytoskeleton through FAK's effects on RhoA/Rac.

Although we revealed that Eph-Ephrin signaling is necessary for apical constriction and that an Ephrin gradient is necessary for the establishment of pigment cells in the ectoderm, in both cases we have not illustrated gain of function in the presence of a point source of Ephrin. By expressing Ephrin in a subset of ectodermal cells, we can create such an Ephrin source. The SoxB2 enhancer region has been identified and is used as a marker driving GFP expression. SoxB2 expression is observed in all ectodermal cell early in development and by inserting the Ephrin coding sequence in place of the GFP and injecting this into embryos, we can create chimeric embryos where certain subsets of ectodermal cells express ectopic Ephrin (Figure 6). Developing this tool will require a fluorescent tag on Ephrin, placed between the signal sequence and the Eph binding

domain on the N-terminus as well as an SV40 poly adenylation sequence on the end to provide stability to the resulting RNA transcripts.

Aspects of pigment cell development and MET were characterized in this thesis and although mechanisms driving the distribution and invasion of pigment cells within the ectoderm were revealed, we have not detailed the mechanisms by which pigment cells find their way to the ectoderm. Evidence indicates that Ephrin provides a trophic cue in positioning pigment cells but raises the question of whether there is a specific cue that guides pigment cell migration. Pigment cells may migrate randomly prior to encountering a suitable Ephrin source or they may be guided to specific ectodermal regions by cell-cell communication mechanisms. To assess the role of Ephrin in guiding pigment cells during their migration through the blastocoel, microbeads can be coated with a fluorescent tag and with SpEphrin protein and then injected into the blastocoel of a live sea urchin larva during pigment cell migration. By using larva that have developed from eggs injected with a pigment cell specific fluorescent marker, pigment cells can be directly visualized via live imaging and any influence of Ephrin-coated beads on the migratory pattern of pigment cells can be easily observed and quantitated.

The role of Rap1A in pigment cell invasion of the ectoderm is not clear. However Rap1A binds to the RA domains of Afadin and is one of it's main effector proteins. We have observed Afadin in puncta on cellular projections following invasion of the ectoderm and it would be useful to observe whether similar puncta are observed in the Semaphorin 1A knockdown or in the presence of the dominant negative Rap1A construct. Such experiments would indicate whether Rap1A is facilitating a role for

Afadin in establishing junctions between pigment cells and the overlying ectodermal cells.

Pigment cells are clearly involved in many cell-cell communication interactions during their development and the above experiments are an excellent starting points to further address two major, unresolved questions that arose from this thesis.

Chapter 4: Prospectus

When this Ph.D. was undertaken, the *S. purpuratus* genome had recently been sequenced and although predictions had identified an Eph receptor and Ephrin ligand, a function for these had not been described. The overall objective of this thesis was to characterize roles for Eph-Ephrin signaling in development of the sea urchin larva.

Throughout this project I have identified roles for Eph and Ephrin in signaling the cellular changes that accompany apical constriction (Chapter 1) and in guiding the migration of pigment cells following EMT to the site where they eventually undergo MET (Chapter 2). A common theme in these examples is graded Ephrin expression on the aboral ectoderm and in both cases this gradient is fundamental to mechanisms that underlie morphogenetic movements. This emphasizes an important concept in morphogenesis; the repeated use of predominant extracellular cues and their signal transduction pathways to produce distinct effects in different cell types.

The simplicity of the sea urchin Eph-Ephrin repertoire provides an excellent means to highlight the mechanisms that developmental programs use to achieve differential effects with the same receptor-ligand pair. In such situations, permissive or inhibitory regulators or different receptor-ligand components interact with the initial signaling components providing a complex network of signaling pathways that can produce cell- or tissue-specific outcomes. This thesis attempts to reveal some of these downstream components and provide a basis for future studies into their mode of action in the specific tissues they influence.

The study of morphogenesis currently focuses on characterizing the complex interactions that occur between signaling pathways and how they influence pattern

formation. Although we have an abundance of information regarding the composition of the one dimensional genetic code and the interplay between transcription factors in the form of gene regulatory networks, the steps by which morphogenesis creates a three dimensional embryo from this one dimensional information must be thoroughly annotated before we can completely understand morphogenesis and this is currently the focus in this field of research.

Revealing complete portions of the morphogenetic networks that drive development will allow us to address some common congenital birth defects and the annotation of such signaling networks is currently the major focus of the field studying morphogenesis.

With a full understanding these signaling systems we will possess the knowledge to influence developing biological structures and modify them in a manner that is currently reserved for science fiction.

Appendix 1: Imaging Neural Development in Embryonic and Larval Urchins

Krupke O, Yaguchi S, Yaguchi J, Burke RD. (2014). Imaging neural development in embryonic and larval sea urchins. Methods Mol. Biol. **1128**: 147-60.

Summary

Imaging is a critical tool in neuroscience and our understanding of the structure and function of sea urchin nervous systems owes much to this approach. In particular, studies of neural development have been facilitated by methods that enable the accurate identification of specific types of neurons. Here we describe methods that have been successfully employed to study neural development and cytoskeletal features during morphogenesis in sea urchin embryos. Altering gene expression in part of an embryo is facilitated by injection of reagents into individual blastomeres, which enables studies of cell autonomous effects and single embryo rescue experiments. The simultaneous localization of an in situ RNA hybridization probe and a cell type specific antigen has enabled studies of gene expression in specific types of neurons. Fixatives and antibodies can be capricious, thus we provide data on preservation of antigens with commonly used fixatives and buffers.

Introduction

Interest in deuterostome evolution, embryonic signaling, and larval biology continues to stimulate studies of neural development and the structure of cytoskeletal components of sea urchin. Echinoderm nerves have yielded little to conventional electrophysiological approaches and identification of neurons from ultrastructural features or histochemical dyes has met with only limited success (Hyman, 1955; Smith, 1965; Cobb, 1970; Cavey and Markel, 1994). However, antibodies and RNA hybridization probes that are specific

for proteins and genes that are expressed only in neurons have enabled detailed studies of neuroanatomy and neural development (Nakajima et al.2004; Yaguchi and Katow, 2003; Burke et al. 2006a). Many of these probes have been facilitated by access to genomic tools derived from the sequencing of the sea urchin genome (Sodergren et al., 2006; Burke et al. 2006b). A powerful approach to understanding developmental mechanisms results when these neuroanatomical methods are combined with methods for altering expression levels of specific genes, such as morpholino antisense oligonucleotides or in vitro transcribed mRNA (Wei et al. 2007; Yaguchi et al. 2008, 2010).

We are fortunate in having a number of excellent summative reviews of imaging methods useful with urchin eggs and embryos (Lutz and Inoue, 1986; Harris, 1986; Burke and Gibson, 1986; Venuti et al. 2004; Strickland et al. 2004). As well, methods for injecting eggs have been well described (Jaffe and Terasaki, 2004; Cheers and Ettensohn, 2004; Angerer and Angerer, 2004). The objective of this chapter is to describe methods that have proven useful in studying neural development and the cytoskeleton in sea urchin embryos. Inhibiting translation, or expressing a specific gene in part of the embryo has facilitated studies of signaling; this we do by injecting individual blastomeres. Identifying expression of specific genes in neurons has been accomplished by combining fluorescent in situ methods with immunofluroescence. Choice of fixative for imaging studies is critical and guided by the need to preserve specific combinations of antigens and details of cellular structure, thus we compare several fixatives commonly used in studies of urchin embryos.

Materials

Gametes should be prepared and cultured following conventional procedures described in Strathmann, 1987, Leahy, 1986; Bottiger et al., 2004; Foltz et al. 2004; Wray et al. 2004. Prepare all solutions using deionized, distilled water, and analytical grade reagents.

Blastomere injection and double injection components

Seawater and Buffer Components

Use natural seawater, taken from 2-3 m depth, filtered through qualitative filter paper (FSW) for culturing embryos. Store at 15˚C. Artificial seawater (ASW) is satisfactory for many applications. MBL-ASW: 423 mM NaCl, 9.0 mM KCl, 9.27 mM $CaCl_2$, 22.94 mM $MgCl_2$, 25.5 mM $MgSO_4$, 2.14 mM $NaHCO_3$. **(Ref)**

For injection of blastomeres there are differences in how embryos of different species respond to divalent cations. *Strongylocentrotus purpuratus* has a thick hyaline layer, and embryos can be treated with Calcium and Magnesium free seawater without dissociating. *Hemicentrotus pulcherrimus* embryos can only tolerate Calcium free seawater without dissociating. Calcium- and magnesium-free artificial seawater for *S. purpuratus* ($Ca^{2+}Mg^{2+}$ free ASW) is: 500 mM NaCl, 9.0 mM KCl, 2.0 mM $NaHCO_3$, 29 mM Na_2SO_4. Add 700 ml water to a graduated cylinder or a glass beaker, and start to stir with magnetic stirrer. Weigh and add the following reagents in turn: 29.22 g NaCl, 0.67 g KCl, 0.168 g NaHCO3, 4.12 g Na2SO4. Mix well and make up to 1 L with water. Store at 15˚C.

Calcium-free artificial seawater (Ca^{2+} free ASW) for *H. pulcherrimus* is: 435 mM NaCl, 9.3 mM KCl, 24.5 mM $MgCl_2$, 25.5 mM $MgSO_4$, 2.15 mM $NaHCO_3$ (2). Add 700

ml water to a graduated cylinder or a glass beaker, and start to stir with magnetic stirrer. Weigh and add the following reagents in turn: 25.43 g NaCl, 0.69 g KCl, 2.33 g $MgCl_2$ (anhydrous), 3.07 g $MgSO_4$ (anhydrous), and 0.18 $NaHCO_3$. Mix well and make up to 1 L with water. Store at 15˚C.

FSW containing 3-amino-1,2,4-triazol (ATA): Make 100 mM ATA-FSW stock (100x) and use 1:100 dilution in FSW as a working solution (3). Store at 4˚C.

Protamine sulfate solution: Make 1% (w/v) protamine sulfate in water and aliquot in 1.5 ml tubes. Store at -20˚C until use.

Injection solution 1: To alter gene activity, morpholino oligonucleotide (MO) or in vitro transcribed mRNA is used. MO is commercially available from Gene Tools (www.gene-tools.com). mRNA is synthesized by the following instruction of mMessage mMachine kit (Life Technologies; www.lifetechnologies.com). Mix these reagents at optimal concentration in 24% glycerol, filter the mixture through 0.22 μm membrane filters (Millipore), and back-fill injection needles. Store at -20˚C at least a few hours to degas. The glycerol permits visualization of flow from the tip of the injection needle and reduces evaporation.

Injection solution 2: For blastomere injections to be followed by immunological detection of an injected cell lineage tracer, several options have been used successfully. We have used myc mRNA because a reliable specific antibody (9E10) is available (4). A stock solution at 1.0 μg/μl in 24% glycerol, is filtered and stored at -20˚C until use. Prior to loading, dilute this stock with MO or mRNA solution 1:10, to a final concentration of 100 ng/μl in injection needle. For live imaging, alternatives include GFP mRNA, DSRed mRNA, or fluorescent dextran. GFP or DSRed can be detected after prolonged fixation

with specific antibodies and fluorescent dextran is lost after fixation. Most fixatives readily preserve myc protein translated from injected mRNA.

Co-localizations with Anti-serotonin and In Situ Hybridization Components

Prepare all solutions using pure water after deionized and distilled, and analytical grade reagents.

1. Fixative: 4% paraformaldehyde in FSW (PFA, see below).
2. MOPS buffer: 0.1 M MOPS, pH7.0, 0.5 M NaCl, 0.1% Tween-20. Mix from the following stock solutions. 1 M MOPS (10x): Add 350 ml water to a graduated cylinder or a glass beaker, and start to stir with magnetic stirrer. Weigh and add 104.7 g MOPS and adjust pH to 7.0 with 5 N KOH. Make up to 500 ml and sterilize it with 0.22 μm filter. Store at room temperature (RT) in dark. 5M NaCl (10x): Add 600 ml water to a graduated cylinder or a glass beaker, and start to stir with magnetic stirrer. Weigh and add 292.2 g NaCl and make up to 1 L and autoclave to sterilize. 10% Tween-20 (100x); Add 2.0 ml Tween-20 to 18 ml sterilized water. Mix well and store at RT.
3. Blocking buffer: 5% Lamb serum in MOPS buffer, prepare immediately before use
4. Antibodies: Dilute rabbit anti-serotonin antibody (Sigma) 1:1,000 in blocking buffer. Dilute goat anti-rabbit IgG conjugated with horseradish peroxidase (Sigma) 1:2,000 in blocking buffer. Sheep anti-digoxygenin (DIG) antibody conjugated with peroxidase (Roche) was used in 1:1,000 dilution in blocking buffer (see Note 7).
5. Tyramide signal amplification (TSA) system: TSA Fluorescein system and TSA tetramethyl-Rhodamine (TMR) system were obtained from Perkin Elmer.

6. Hybridization buffer: 70% formamide, 0.1 M MOPS, pH7.0, 0.5 M NaCl, 1% bovine serum albumin (BSA), 0.1% Tween-20 (5) (see Note 8).
7. RNA probes: DIG-labeled RNA probe encoding antisense nucleotides against a target gene is made from plasmid or PCR product. Choose the RNA polymerase that binds the antisense chain promoter region. Following the Takara T7 RNA polymerase instructions: mix the following reagents in a 0.5 ml plastic tube; 1.0-1.5 µg plasmid DNA template (or 200 ng/µl PCR product) in 6.0 µl sterilized pure water, 1.0 µl 10x RNA polymerase buffer, 1.0 µl 50 mM DTT, 1.0 µl 10x DIG RNA labeling mix (Roche), 1.0 µl T7 polymerase. Incubate it at 37˚C for 3-3.5 h. Add 1.0 µl TurboDNase (Life Technologies) and incubate it at 37˚C for 15 min. Mix 1.5 µl lithium solution (from mMessage mMachine kit) and 38 µl 100% ethanol. Store at -20˚C overnight. Centrifuge at 14,000 Xg at 4˚C for 15 min with a conventional high-speed centrifuge. Wash the pellet with 75% ethanol-water. Centrifuge at 14,000 rpm at 4˚C for 5 min, and remove ethanol. Air dry briefly and dissolve it with molecular biological grade water at 100 ng/µl.

Immunological methods: Fixatives and components

Paraformaldehyde in Seawater (PFA)

1. For a hot water bath, put 175 mL distilled water in a 250 mL beaker and heat to boiling. Put 25 mL of filtered seawater in a 50 mL plastic tube, add 30 mg Tris base. Dissolve Tris by vortexing the solution.
2. Loosen cap completely and heat the solution in a microwave to 80° C, being careful not to overheat. In a 1200W microwave this takes 15-20 seconds. Immediately add 1.0 g paraformaldehyde and vortex. Immerse in hot water bath, remove the tube and

shake vigorously or vortex every few minutes. The solution will gradually clear. Do not heat the paraformaldehyde solution in the microwave.

3. When the solution is completely clear, cool the solution to room temperature in an ice bath, and adjust pH to 7.0 using pH paper. Use immediately or aliquot and freeze at -20° C.

Methanol (MeOH)

1. Store at -20° C and use while ice-cold.

Modified microtubule stabilization buffer (PEM)

1. Prepare PEM buffer: 100 mM PIPES, 5 mM EGTA, 2 mM $MgCl_2$, 0.2% Triton X-100.
2. Adjust the pH to 7.0 and store at room temperature (stable for several months).
3. Immediately prior to fixation, combine 9 parts PEM buffer with 1 part formalin (37% formaldehyde solution). Use immediately.

Methods

The gametes of sea urchin are collected by intra-coelomic injection of 0.5 M KCl. Eggs are stored in a glass beaker filled with FSW at 4˚C, and sperm are collected as dry-sperm and stored in a 1.5 ml tube at 4˚C. Eggs can be stored at 4 - 15˚C for up to two days. Adding antibiotics (penicillin or streptomycin) helps to keep eggs longer. In contrast, the sperm can be stored stably for a week at 4˚C.

Blastomere injections; double injections procedures

The following double injection method permits injection of one reagent into the fertilized egg, and after the first cleavage, another reagent is injected into one blastomere of 2-cell stage. This type of experiment facilitates examination of cell autonomous

processes and single embryo rescue experiments. The basic injection methods are derived from Cheers and Ettensohn, 2004; Lepage and Gache, 2004; and Angerer and Angerer 2004.

1. Fill injection dish, coated with 1% protamine sulfate, with 1 mM ATA-FSW. A row of eggs is settled on the bottom of an injection dish with a mouth pipette. After one minute, remove any eggs that do not stick to the dish or stick outside of the registration lines marked on the dish. The number of eggs for double injection should not be large, and we normally put 100-200 eggs on one dish. This dish should be kept on an ice-chilled tray, not directly on ice, for *S. purpuratus*. For *H. purcherrimus*, the dish should not be stored on ice-chilled tray, but at 15˚C.
2. Inseminate eggs with a few drops of 1:100 diluted sperm in FSW. Wait until fertilized envelope is obvious. Avoid using excess sperm, as polyspermy and putrefaction can be a problem.
3. Inject the first reagent (morpholino, mRNA, protein, antibody, or chemical) into the all aligned eggs. Un-injected eggs should be removed after injecting all other eggs on one dish.
4. After washing 4 or 5 times with FSW to remove ATA and extra sperm, culture the injected eggs at 15˚C until first cleavage is complete (about 2 h). To ensure cytokinesis is complete, wait longer until just before the second cleavage starts.
5. Remove FSW and add $Ca^{2+}Mg^{2+}$-free ASW for *S. purpuratus* or Ca^{2+} -free ASW for *H. pulcherrimus*, and repeat 3-5 times.
6. After 5-10 min, the embryos will be ready for the second injection. Inject the reagent into one of the blastomeres. To penetrate extra-embryonic layers and the membrane,

set the injector with constant flow, press the tip of the needle on the surface of the blastomere to be injected and gently tap the manipulator or the base of the microscope to vibrate the needle.

7. Embryos will only tolerate divalent cation free seawater for about 20 minutes, after which blastomeres will dissociate.
8. Remove $Ca^{2+}Mg^{2+}$-free ASW and add FSW gently, and repeat 3-5 times. Culture them at 15˚C until the stage at which they will be analyzed (Figure 1).

Procedures for combined in situ hybridization and immunofluorescence

In some experiments it is necessary to simultaneously detect an mRNA and an antigen, such as a protein or a neurotransmitter, in the same specimen. We have successfully combined immunofluorescence and in situ hybridization methods (Figure with the TSA system (Perkin Elmer). A major limitation of this method is that mRNAs require prolonged fixation with the result that some of antigens are undetectable. This is the case with anti- synaptotagmin (1E11), a neural marker that is sensitive to formaldehyde cross-linking. However, anti-serotonin has proven very useful in this type of experiment.

1. Fix embryos or larvae with 4% PFA-FSW overnight in a well of 96-well plate (4˚C). All subsequent steps, except for TSA-treatment, are carried out in this flat-bottom 96-well plate using a dissecting microscope and an aspirator. Alternatively, 0.5 ml clear microcentrifuge tubes can be used; although specimen loss can be a problem, rinsing steps can be reduced in number from 5 to 3.
2. Remove PFA-FSW and add MOPS buffer. Discard the used fixative safely. This MOPS buffer rinse is repeated at least five times for 7-10 min each.

3. Treat samples with 5% Lamb serum in MOPS (blocking buffer) for 1 hour at room temperature (RT).
4. Remove blocking buffer and add 1:1,000 diluted rabbit anti-serotonin antibody in blocking buffer, and incubate it for 1-2 h (RT).
5. Wash with MOPS buffer 5 times for 7-10 min each.
6. Add 1:2,000 diluted goat anti-rabbit IgG antibody conjugated with horseradish peroxidase in blocking buffer and incubate it for 1-2 h at RT (see Note 15).
6. Wash with MOPS buffer 5 times for 7-10 min each.
7. Transfer all samples to 0.5 ml clear tubes and remove MOPS buffer as much as possible (see Note 16).
8. Add diluted TSA-TMR in diluent and incubate it for less than 10 min at dark (see Note 17).
9. Remove TSA reagent and wash with MOPS buffer once. Keep the sample in a dark place at the following steps until observation.
10. Transfer samples to 96-well plate and wash it with MOPS buffer 5 times for 7-10 min each. Check a few of samples with a fluorescent microscope (see Note 18).
11. Remove MOPS buffer as much as possible, and add 100 µl hybridization buffer per well and mix well by tapping the plate. Incubate it for 15 min. Change the hybridization buffer three times.
12. Incubate it for 1-3 hour at 50˚C (pre-hybridization) with adhesive PCR sheet on wells to avoid evaporation of the buffer.

13. After pre-hybridization is finished, mix 0.4 µl DIG-labeled probe per 100 µl pre-warmed hybridization buffer. Remove the pre-hybridization buffer from the well and add hybridization buffer with probe (see Note 19).
14. Incubate the sample for 7 days at 50˚C with adhesive PCR sheet (see Note 20).
15. After hybridized, remove the hybridization buffer and wash sample with MOPS buffer 5 times for 7-10 min each at RT.
16. Wash sample with MOPS buffer 3 times for 1 hour each at 50˚C.
17. Wash sample with MOPS buffer 3 times for 7-10 min each at RT.
18. Add 5% Lamb serum in MOPS buffer (blocking buffer) and incubate sample for 1 hour at RT.
19. Remove the blocking buffer and incubate it with 1:1,000 sheep anti-DIG antibody in blocking buffer for 1 hour at RT.
20. Wash the sample with MOPS buffer at least 5 times for 7-10 min each. Longer is better. An overnight wash sometimes gives a better signal.
21. Transfer all samples to a 0.5 ml clear tube and remove MOPS buffer as much as possible (see Note 16).
22. Add diluted TSA-Fluorescein and incubate it for 10 min (see Note 17).
23. Remove TSA reagent and wash samples 5 times for 7-10 min each.

Immunological Localization Methods

Fix with PFA

1. Transfer seawater containing embryos to an appropriate sized vessel and centrifuge. Pellet embryos by gentle centrifugation (<1000 XG) in all steps. A manual, crank-driven centrifuge with a swinging bucket rotor is most convenient. A mini-

microcentrifuge will also work, however we find the fixed angle and high G forces on most models cause difficulty when removing liquids or resuspending embryos. The volumes presented assume 1mL of embryo suspension containing about 50 µl pelleted embryos.

2. Remove the seawater supernatant and resuspend embryos in 1mL PFA fixative. Incubate at room temperature for 15 minutes.
3. Centrifuge, remove supernatant and resuspend in 1 mL PBS. Incubate 5 minutes at room temperature, centrifuge, remove supernatant and repeat this wash once more.
4. Remove the supernatant and resuspend embryos in 500 µL of blocking buffer: Superblock (Pierce Chemical), 0.03% Triton X-100. When using antibodies to phosphorylated proteins, add NaF (10 mM) or Na_3VO_4 (1 mM) and incubate 45 minutes at room temperature.
5. Add antibodies or anti-sera at appropriate dilutions, mix gently by slowly rocking the tube and incubate overnight at 4°C.
6. Centrifuge embryos, remove supernatant and rinse 3 times each with of 1 mL PBS.
7. Centrifuge, remove supernatant and resuspend embryos in 500 µL PBS containing appropriate concentrations of secondary antibodies or fluorescent conjugates. Incubate in a dark place for 2 h at room temperature.
8. Centrifuge, remove supernatant, wash 3 times with PBS and resuspend in 20 µL PBS. 0.01% (w/v) Sodium azide can be added to this final resuspension, allowing storage of fixed embryos for up to 3 weeks.
9. Alcohol clean a glass slide and fix 2 strips of double-sided tape across the width, spaced 15 mm apart. Place 10 µL of SlowFade reagent between the strips of tape.

Resuspend embryos by gentle agitation/trituration and place 10 µL onto the slide and mix with the SlowFade reagent, carefully mount a coverglass so that it spans the two strips of tape and creates a fluid filled space containing the specimens. Seal the edges with a small amount of vacuum grease to prevent leakage and evaporation.

Fix with MeOH

1. Protocol is carried out as described for PFA (3.3.1) except at step 2, substitute 1mL of ice-cold methanol for PFA. Incubate embryos in methanol for 5 minutes at room temperature. Remove methanol and carrying out all remaining steps described in 3.3.1.

Fix with PEM

1. Protocol is carried out as described for PFA (3.3.1) except at step 2 substitute 1 mL of PEM fixative for PFA. Fix embryos in PEM for 15 minutes at room temperature. Remove PEM and carrying out all remaining steps described in 3.3.1.

Fix with PFA/PEM

1. Protocol is carried out as described for PFA (3.3.1), except that following a 15 minute incubation in PFA, embryos are post fixed in PEM. Follow the instructions for PFA fixation for 15 minutes at room temperature, centrifuge and remove the PFA. Resuspend the embryos in 1 mL PEM buffer and incubate at room temperature for 15 min. Centrifuge, remove PEM and carry out all remaining steps as described in 3.3.1.

Preparing small numbers of embryos

Often experiments yield only a few embryos that are to be processed for immunofluroescence. In these situations, all steps for removing buffer or reagents are

performed in 96-well plate under a dissecting microscope with an aspirator. To facilitate complete rinsing, the number of rinse steps is increased.

1. Collect embryos in a well of 96-well plate. Remove the seawater as much as possible with a mouth pipette. Add fixative (PFA, MeOH, PEM) and fix samples for 15 min at RT.
2. Remove fixative and wash samples with PBS 5 times for 10 min each.
3. Block sample with blocking buffer: Superblock (Pierce Chemical), 0.03% Triton X-100.
4. Remove blocking buffer and add mixture of diluted antibodies in blocking buffer. Incubate the sample overnight at 4˚C.
5. Remove antibody solution and wash samples with PBS 5 times for 10 min each.
6. Add secondary antibody mixture and incubate samples for 2 h at RT.
7. Remove antibody solution and wash samples with PBS 5 times for 10 min each.

Notes

1. Methanol provides effective immunofluorescent labeling in select cases but is not suitable in preserving several cell-surface, cytoskeletal and nuclear features (Figure 2 & 3). Serotonin is not preserved with methanol fixation, however the epitope recognized by anti-synatotagmin (1E11) remains intact with methanol fixation 30 min.

2. Preservation of cell surface antigens is enhanced with PFA fixation and the cilia are clearly presented (Fig. 2), however detail on the basal cell surface is lacking in some instances and cytoskeletal architecture is not conserved well. Preservation of serotonin is excellent, however, the anti-synaptotagmin B epitope (1E11) is poor.

3. PEM buffered formaldehyde enhances visualization of many internal structures at the expense of structures on the surface of the embryo. Preservation of cytoskeletal details is excellent. Nucleoplasm and strands of chromatin are highly resolved and some cell cycle stages can be identified (Fig. 3M, arrowhead). Protein complexes associated with the inner apical membrane (PAR6, aPKC) are well preserved (N,O) and cytoplasmic background fluorescence is reduced significantly compared with PFA fixation (compare N,O with H,I). The cell-surface antigen αC is well preserved on the basal surface (P, arrowheads) but antigens on the apical surface show only weak fluorescence (P, arrows). Visualization of cytoskeletal detail is enhanced with PEM and actin arrays in regions of apical constriction are easily identified (R, arrowhead) although fine detail in membrane blebs and filopodia associated with mesenchyme internalization is lacking (R, arrow). Labeling of pMyo is also achieved in the presence of PEM, both on the apical and basal surfaces (Q).

4. The combination of PFA and PEM yields a fixation that has the benefit of preserving cytoskeletal architecture with a high level of detail while enhancing the preservation of internal structures on the apical membrane. These benefits are at the expense of cell surface antigen and pMyo preservation. Nucleoplasm and chromatin are highly resolved (Fig. 3S) and fluorescence is similar to that seen with PEM alone (compare M and S). The apical proteins, PAR6 and aPKC present well, with little cytoplasmic background fluorescence (T, U). Preservation of cell surface antigens appears poor and αC fluorescence on both apical and basal surfaces is reduced significantly by this treatment (V). The actin cytoskeleton is preserved in fine detail (X) allowing the

visualization of basal structures normally difficult to preserve. These include filopodia, membrane blebs (arrowheads) and filaments associated with ingression of mesenchyme cells into the blastocoel (arrows). Treatment with PFA appears to abolish pMyo preservation (W).

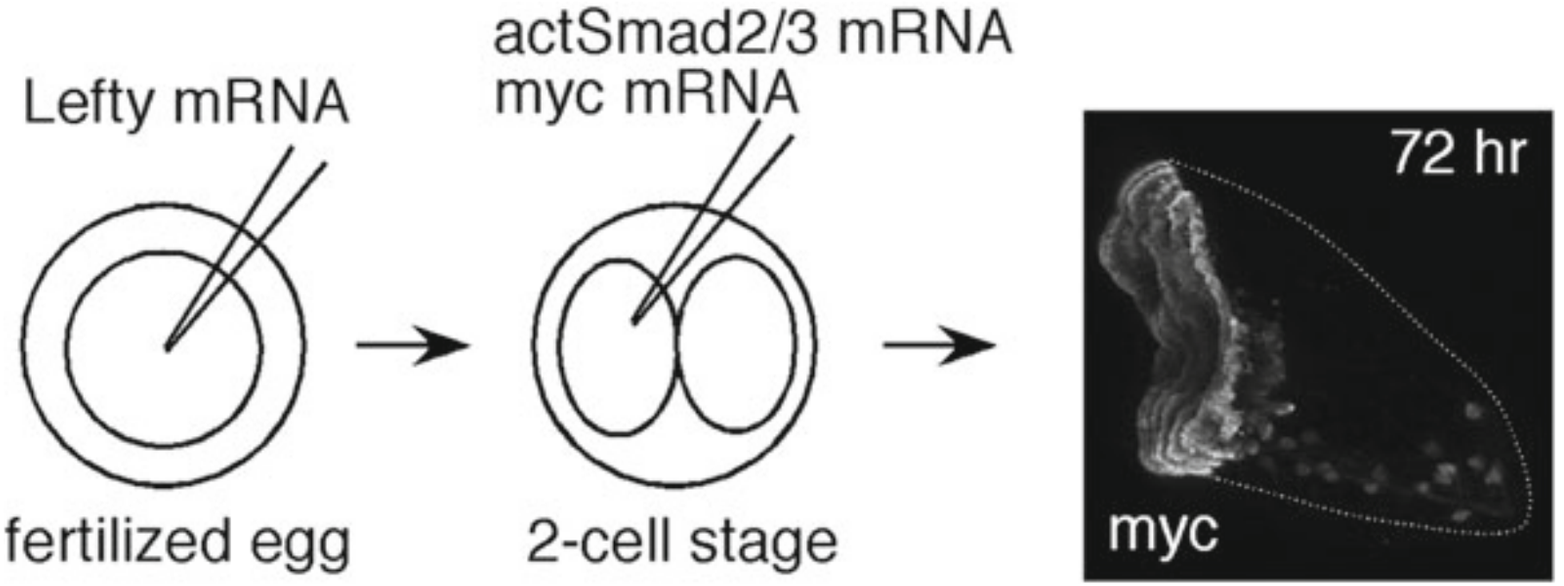

Fig. 1 Double injection strategy and image of an embryo in which a dorsal–ventral axis has been induced without Nodal signaling. The secondary (dorsal–ventral) axis in the sea urchin embryo depends on Nodal, which is expressed in prospective oral ectoderm during cleavage [28]. In this experiment we initially blocked endogenous Nodal activity by injecting mRNA encoding Lefty, a Nodal antagonist, into the unfertilized egg. After the first cleavage, mRNA encoding a constitutively activated Smad2/3 (actSmad2/3), which is an intracellular mediator of Nodal signaling [29], and myc mRNA were simultaneously injected into one of the blastomeres. At 72 h embryo, the myc-injected cells are detected following immunolocalization procedures. This embryo has lost the endogenous diffusible Nodal, which by itself would produce an embryo without a dorsal–ventral axis [28]. However that cells expressing Smad 2/3 behave as though they are activated by Nodal and differentiate as oral ectoderm, which established the ectopic dorsal–ventral axis. In this image, the Myc-positive side of the embryos is a thickened oral ectoderm surrounded by a ciliary band, and the oral-half of the gut. The *dashed-line* outlines aboral ectoderm, which is not visible in this image

Figure 1

Images of Double Injection, or combined in situ.

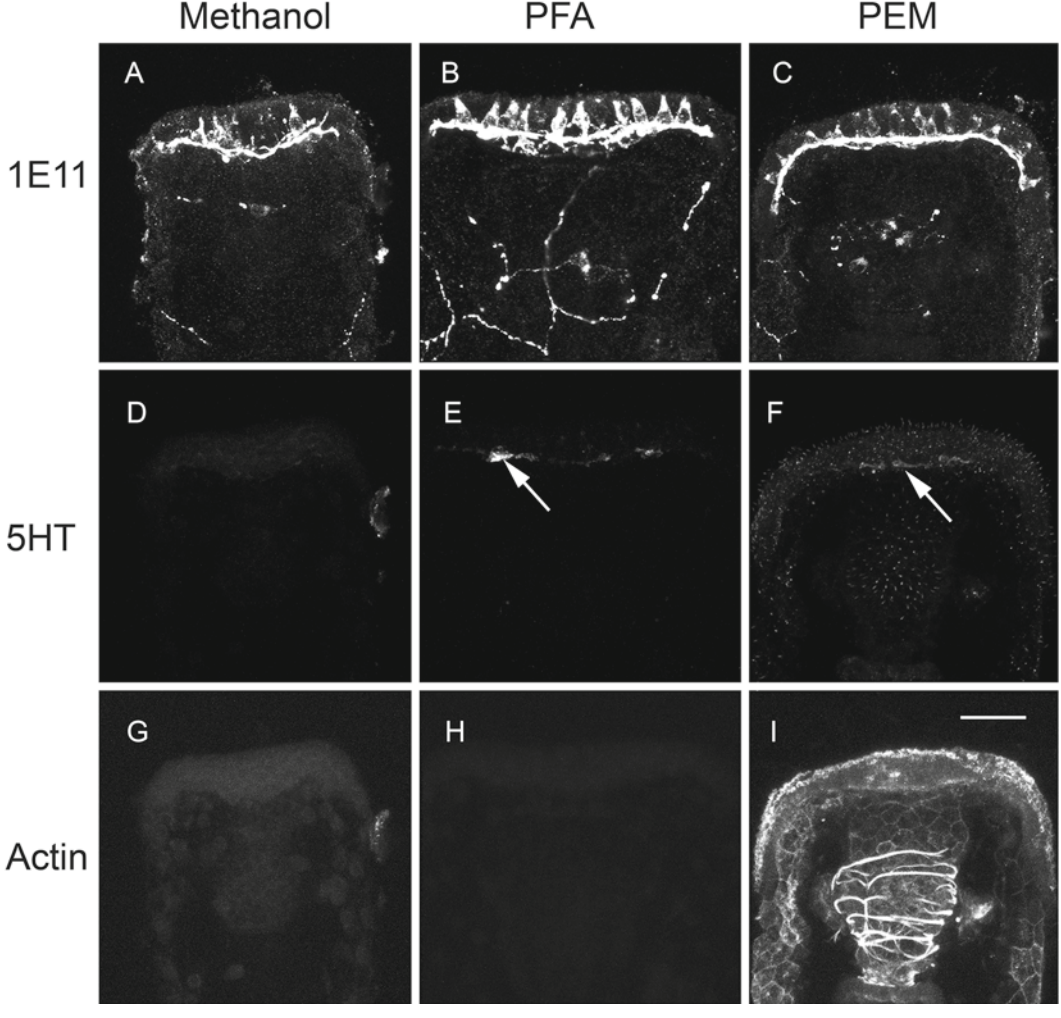
Methanol
PFA
PEM
1E11
5HT
Actin
A
B
C
D
E
F
G
H
I

Figure 2

Confocal images of a portion of the apical organ of 5-day embryos prepared for the localization of synaptotagmin (1E11), serotonin (5HT), and actin. Embryos were fixed with methanol, PFA, or PEM and processed for immunofluroescence as described. All the fixatives preserve the synaptotagmin epitope (A-C), however fixations longer than 15 minutes produced poorer results. Serotonin is well localized with PFA, not at all with methanol, and PEM fixation produces a less intense signal with higher background (D-F). Actin is reliably preserved only with PEM (G-I). Bar = 20 μm.

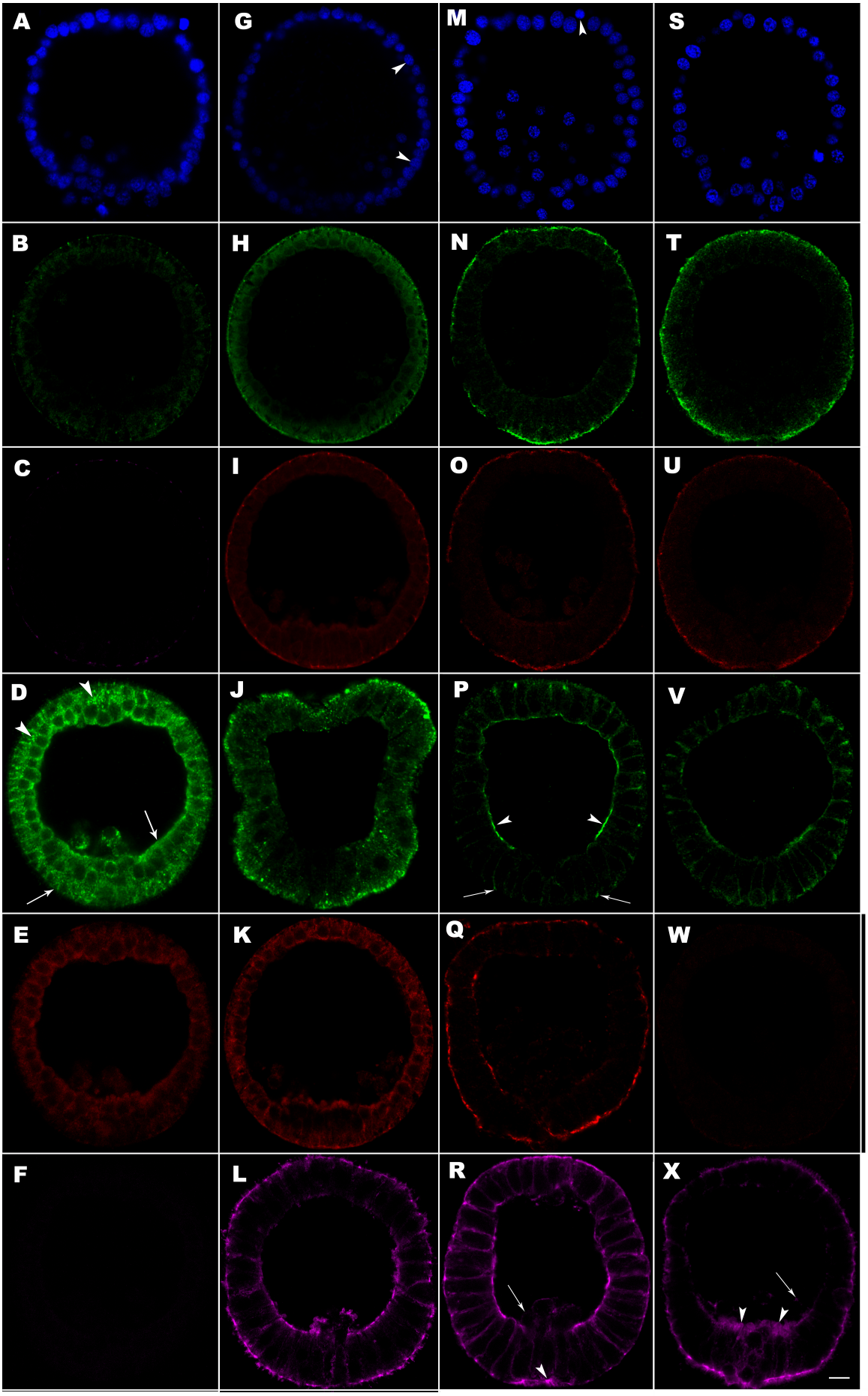
A
G
M
S
B
H
N
T
C
I
O
U
D
J
P
V
E
K
Q
W
F
L
R
X

Figure 0

Confocal images of 28 h embryos prepared using different fixation methods and their effects on preservation of cytoskeletal, nuclear, cell-surface and membrane-associated protein complexes. Embryos are fixed with (A-F) methanol, (G-L) paraformaldehyde (PFA), (M-R) PEM buffer, or (S-X) PFA/PEM. (A, G, M, S) DAPI stained nucleoplasm shows the most clarity and preservation of detail when PEM and PFA/PEM fixation methods are used (M, S). Antibodies against PAR6 (B, H, N, T) and aPKC (C, I, O, U) illustrate PEM is the best fixative for preserving these membrane associated apical complexes (N, O). Methanol fixation causes abundant background fluorescence in the cytoplasm with many of the antibodies used (B, D, E) and although aPKC shows some specificity at cell-cell junctions (C), this is poorly presented in comparison with other fixation methods. (D, J, P, V). Preservation of cell-surface antigens is illustrated using αC integrin. (P) PEM buffer provides the best preservation of basal structures while PFA (J) provides the best preservation of apical structures. (E, K, Q, W) Phosphorylated myosin II light chain is preserved best with PEM buffer (Q). (F, L, R, X) Filamentous actin structures are preserved with the most clarity and preservation of structure using PFA/PEM fixation (X). Cytoskeletal preservation with methanol is not satisfactory as f-actin is not preserved (F) and labeling of pMyo is absent (E).

REFERENCES

Harris PJ (1986) Cytology and immunocytochemistry. Methods Cell Biol **27**:243–262

Angerer LM, Angerer RC (2004) Disruption of gene function using antisense morpholinos.Methods Cell Biol **74**:699–711

Bottger SA, Walker CW, Unuma T (2004) Care and maintenance of adult echinoderms. Methods Cell Biol **74**:17–38

Burke RD, Gibson AW (1986) Cytological techniques for the study of larval echinoids with notes on methods for inducing metamorphosis. Methods Cell Biol **27**:295–308

Burke RD, Osborne L, Wang D, Murabe N, Yaguchi S, Nakajima Y (2006) Neuron-specific expression of a synaptotagmin gene in the sea urchin Strongylocentrotus purpuratus. J Comp Neurol **496**:244–251

Burke RD, Angerer LM, Elphick MR, Humphrey GW, Yaguchi S, Kiyama T, Liang S, Mu X, Agca C, Klein WH, Brandhorst BP, Rowe M, Wilson K, Churcher AM, Taylor JS, Chen N, Murray G, Wang D, Mellott D, Olinski R, Hallbook F, Thorndyke MC (2006) A genomic view of the sea urchin nervous system. Dev Biol **300**:434–460

Cavey MJ, Markel K (1994) Echinoidea. In: Harrison FW, Chia FS (eds) Microscopic anatomy of invertebrates. Wiley-Liss, New York, pp 345–400

Cheers MS, Ettensohn CA (2004) Rapid microinjection of fertilized eggs. Methods Cell Biol **74**:287–310

Cobb JLS (1987) Neurobiology of echinodermata. In: Ali MA (ed) Nervous systems of invertebrates. Plenum, New York, pp 483–525

Duboc V, Rottinger E, Besnardeau L, Lepage T (2004) Nodal and BMP2/4 signaling organizes the oral-aboral axis of the sea urchin embryo. Dev Cell **6**:397–410

Evan GI, Lewis GK, Ramsay G, Bishop JM (1985) Isolation of monoclonal antibodies specific for human c-myc proto-oncogene product. Mol Cell Biol **5**:3610–3616

Foltz KR, Adams NL, Runft LL (2004) Echinoderm eggs and embryos: procurement and culture. Methods Cell Biol **74**: 39–74

Hyman LH (1955) The invertebrates: echinodermata, vol IV. McGraw Hill, New York

Jaffe LA, Terasaki M (2004) Quantitative microinjection of oocytes, eggs, and embryos. Methods Cell Biol **74**:219–242

Leahy PS (1986) Laboratory culture of Strongylocentrotus purpuratus adults, embryos, and larvae. Methods Cell Biol **27**:1–13

Lepage T, Gache C (2004) Expression of exogenous mRNAs to study gene function in the sea urchin embryo. Methods Cell Biol **74**:677–697

Lutz DA, Inoue S (1986) Techniques for observing living gametes and embryos. Methods Cell Biol **27**:89–110

Nakajima Y, Kaneko H, Murray G, Burke RD (2004) Divergent patterns of neural development in larval echinoids and asteroids. Evol Dev **6**:95–104

Sodergren E, Consortium, S. U. G. S (2006) The genome of the sea urchin Strongylocentrotus purpuratus. Science **314**: 941–952

Smith JE (1965) Echinodermata. In: Bullock TH, Horridge GA (eds) Structure and function in the nervous systems of invertebrates. Freeman, London, pp 1519–1558

Strickland L, von Dassow G, Ellenberg J, Foe V, Lenart P, Burgess D (2004) Light microscopy of echinoderm embryos. Methods Cell Biol **74**:371–409

Wei Z, Yaguchi J, Yaguchi S, Angerer RC, Angerer LM (2009) The sea urchin animal pole domain is a Six3-dependent neurogenic patterning center. Development **136**:1179–1189

Strathmann MF (1987) Reproduction and development of marine invertebrates of the Northern Pacifi c Coast. Univ. of Washington Press, Seattle

Venuti JM, Pepicelli C, Flowers VL (2004). Analysis of sea urchin embryo gene expression by immunocytochemistry. Methods Cell Biol **74**:333–369

Wray GA, Kitazawa C, Miner B (2004) Culture of echinoderm larvae through metamorphosis. Methods Cell Biol **74**:75–86

Yaguchi S, Katow H (2003) Expression of tryptophan 5-hydroxylase gene during sea urchin neurogenesis and role of serotonergic nervous system in larval behavior. J Comp Neurol **466**:219–229

Yaguchi S, Yaguchi J, Angerer RC, Angerer LM (2008) A Wnt-FoxQ2-nodal

pathway links primary and secondary axis specifi cation in sea urchin embryos. Dev Cell **14**:97–107

Yaguchi S, Yaguchi J, Burke RD (2007) Sp-Smad2/3 mediates patterning of neurogenic ectoderm by nodal in the sea urchin embryo. Dev Biol **302**:494–503

Yaguchi S, Yaguchi J, Wei Z, Shiba K, Angerer LM, Inaba K (2010) ankAT-1 is a novel gene mediating the apical tuft formation in the sea urchin embryo. Dev Biol **348**:67–75.